Evaluation of the Environmental Viability of Direct Injection Schemes for Ocean Carbon Sequestration

by

Peter Hampus Israelsson

Submitted to the Engineering Systems Division
in partial fulfillment of the requirements for the degree of

Master of Science in Technology and Policy

at the

MASSACHUSETTS INSTITUTE OF TECHNOLOGY

February 2008

Author ....

Engineering Systems Division
October 15, 2007

Certified by ....

E. Eric Adams
Senior Research Engineer, Civil and Environmental Engineering
Thesis Supervisor

Accepted by ....

Dava J. Newman
Professor of Aeronautics and Astronautics and Engineering Systems
Director, Technology and Policy Program

Evaluation of the Environmental Viability of Direct Injection Schemes for Ocean Carbon Sequestration

by

Peter Hampus Israelsson

Abstract

This thesis evaluates the expected impact of several promising schemes for ocean carbon sequestration by direct injection of CO_2, and serves as an update to the assessment by Auerbach *et al.* (1997) and Caulfield *et al.* (1997) of water quality impacts and the induced mortality to zooplankton. The present work extends the methodology used in the earlier studies, incorporates recent acute CO_2 toxicity data on marine organisms, and considers three revised discharge approaches: a point release of negatively buoyant CO_2 hydrate particles from a moving ship; a long, bottom-mounted diffuser discharging buoyant liquid CO_2 droplets; and a stationary point release of hydrate particles forming a sinking plume. Results suggest that it is possible with present technology to engineer discharge configurations which achieve sufficient dilution to largely avoid acute impacts. Sub-lethal and ecosystem effects are discussed qualitatively, but not analyzed quantitatively. The analysis suggests that, as a temporary climate change mitigation strategy, ocean carbon sequestration by direct injection should not be dismissed on the basis of environmental impact alone. With minor modification, this thesis will also serve as the final chapter of the author's Ph.D. thesis to be submitted in 2008 to the MIT Department of Civil and Environmental Engineering.

Thesis Supervisor: E. Eric Adams
Title: Senior Research Engineer, Civil and Environmental Engineering

Acknowledgments

Contents

List of Figures

11

12

14

List of Tables

Chapter 1

Introduction

Carbon capture and storage (CCS) is increasingly being mentioned as one of the major options available to help reduce the build-up of greenhouse gases in the atmosphere [95, 55]. The ocean is potentially the largest carbon sink, and has the distinction that it is already being "used" under business as usual (BAU) operation: the net carbon flux from the atmosphere to the ocean is about one-third of the anthropogenic emission to the atmosphere, and over time more than two-thirds of the carbon we emit to the atmosphere will eventually wind up in the ocean. As a result of this practice, the surface ocean has already experienced a depression of about 0.1 pH units, which carries concern over impacts to coral and other near surface biota [55].

The logic behind direct ocean storage is that some of the CO_2 that we now put in the atmosphere could be input directly to the ocean, thus eliminating its deleterious effects on climate. One general strategy calls for isolating the CO_2, e.g., in a deep lake where its negative buoyancy would reduce the exchange of CO_2 with the overlying water column. The CO_2 could also react with seawater to form solid CO_2 hydrates, which would further inhibit mass exchange. However, even with a hydrate covering, diffusion from the lake surface to the overlying water column would render such storage temporary [36, 48]. The other strategic endpoint, and the one considered herein, is to dilute the CO_2 by dispersing if over the largest possible volume such that the excess pCO_2 concentrations, and the changes in pH, will be as small as possible.

In order that the sequestration be effective (i.e., that the CO_2 be retained in the ocean for as long as possible before being exchanged with the atmosphere), injection would need to be into intermediate and deep ocean depths, and away from areas of strong upwelling. Numerical simulations with ocean general circulation models suggest that most CO_2 injected at a depth of 3000 m over a range of representative sites would be retained for more than 500 years [93, 55].

Clearly direct ocean injection is only worth considering if the impacts to organisms residing at intermediate and deep depths are substantially less than the avoided climatic impacts, plus impacts to near surface marine biota, that would accrue under BAU. Such environmental impacts constitute the *general objective* of this study. There are several other attributes of direct ocean injection. It has already been mentioned that the storage is temporary. However, while several centuries is certainly short by geological time scales, it should be long enough to help us find alternatives to fossil fuels. Second, while the ocean is not infinite, it is large. Over 500 GTC could theoretically be dispersed uniformly over the entire ocean, without depressing the average pH by more than 0.1 units [55] presumably causing a small effect that is comparable to that currently experienced by near surface waters [8]. As a point of reference, Pacala and Socolow [95] identify 175 GTC as the emissions needed to be avoided over the next 50 years in order to stabilize atmospheric concentrations below 500 ppm. Of course, the engineering task of dispersing the CO_2 uniformly is far from trivial. Finally, injection would be transparent. Unlike geological storage, where the CO_2 is hidden underground, the concentration of CO_2 injected into the ocean would gradually increase in ways that could be easily monitored. If an environmentally acceptable endpoint can be established, relatively simple monitoring can be used to determine when this endpoint is met.

From the above discussion it seems clear that any policy that includes direct ocean injection should be linked to a policy of substantially and quickly reducing CO_2 emissions. Policy implications of ocean injection are discussed further in the concluding chapter.

Marine impacts associated with direct injection can be categorized in several ways.

First is the type of organism, which include fish, plankton, benthic organisms and micro-organisms. Our interest is mainly on plankton, because they can generally not avoid a plume, and because they generally reside within the water column where the exposure is greatest. Data also suggest that they are the most sensitive. Marine impacts can also be categorized in terms of degree and extent of impact, including acute impacts (mortality), sub-lethal impacts (e.g., reproductive effects), and ecosystem effects. Our interest, here, is mainly on acute effects, partly because these are the most dramatic, and also because they are easiest to measure. Some discussion of sub-lethal and ecosystems impacts is provided in Chapters 2 and 5.

Auerbach *et al.* (1997, [5]) examined available data on the acute impacts to planktonic marine organisms exposed to low pH. As part of this analysis they developed a procedure to integrate constant-concentration laboratory assay data with variable-concentration field exposures. In a companion study, Caulfied *et al.* (1997, [19]) simulated the time-variable concentrations seen by passive organisms that were transported through plumes resulting from several scenarios for direct ocean injection. Using the approach of Auerbach *et al.* [5], they identified regions of expected mortality for each scenario.

The bioassay data used by Auerbach *et al.* [5] were collected largely to explore the impacts of acidic wastes in the coastal zone, and not CO_2 discharge in the deep ocean. However, within the past decade a large number of studies have been conducted to directly examine the biological impacts associated with ocean sequestration. Additional work has also been conducted to optimize injection scenarios to reduce CO_2 concentrations. The *specific objective* of the current research is to review these more recent studies and to re-evaluate impacts using the approach of Auerbach *et al.* [5] and Caulfield *et al.* [19]. Accordingly, Chapter 2 summarizes available data concerning acute impacts to marine organisms, and Chapter 3 describes the modeling approach used herein, which is adapted from the work of Auerbach *et al.* [5], Caulfield *et al.* [19], and several other studies. Chapter 4 presents and interprets the predicted impact for the modeled discharge scenarios. Lastly, Chapter 5 summarizes the conclusions, provides recommendations for future investigation, and discusses policy implications.

Chapter 2

CO_2 Toxicity Studies

Auerbach *et al.* [5] and Caulfield *et al.* [19] provided quantitative estimates of the acute biological impact of a CO_2 injection into a marine environment. These studies were based on compiled toxicity data on the mortality of marine organisms, mainly zooplankton, due to a decrease in pH. Because none of these toxicity studies used CO_2 as the acidifying agent, the relevance of these data to carbon sequestration depends on the extent to which the mortality due to a CO_2 release is caused by the accompanying decrease in pH. Numerous studies over the past decade suggest that mortality for a given level of pH reduction is significantly enhanced when CO_2 is the acidifying agent, thus implying that hypercapnia is a more important effect than the accompanying acidosis.

Another shortcoming of the data available to Auerbach *et al.* [5] and Caulfield *et al.* [19] is that they were limited to organisms that inhabit the upper ocean. Recent studies suggest that the CO_2 tolerance of organisms in the upper ocean may be less than that of organisms in the deep ocean. Given that most ocean sequestration scenarios involve discharging CO_2 into the deep ocean, this is an important distinction.

Before proceeding it is important to briefly describe the analytical framework that will be used so that it is clear to the reader what type of data are needed. The *isomortality* approach developed by Auerbach is a way of adding up the exposure history of an organism (e.g., a zooplankter) and translate it into an acute impact.

This is accomplished by constructing isomortality curves, i.e., lines of equal mortality, such as the ones shown in Figure 2-1, and using the exposure history to map out a cumulative harm trajectory in exposure time - stress level space (see Chapter 3 for details). Such curves can be mapped out using mortality statistics such as LC values, i.e., a concentration that is lethal to a certain percentage of the test population within a fixed exposure time (e.g., LC_{50} for 50% mortality), or equivalently LT values, i.e., an exposure time at which a fixed concentration will be lethal to a certain percentage of the test population (see [37, 117] for an overview). Thus, the primary goal of the following literature review is to identify sources of acute toxicity data for as many species as possible, which can then be used to construct revised isomortality functions. In addition, the review will attempt to synthesize the current state of knowledge regarding the acute response of various organisms such that the isomortality analysis can be adjusted and evaluated accordingly.

2.1 pH toxicity studies

The existing dataset on the mortality of marine organisms in the presence of lowered pH due to an acidifying agent other than CO_2 is reviewed first. This consists mainly of the dataset compiled by Auerbach *et al.* [5] and a more recent study by Yamada and Ikeda [144].

Auerbach *et al.* (1997)

The following studies were included in Auerbach *et al.* [5]:

- Bamber (1987, [6]) studied the pH mortality of young carpet-shell clams.

- Bamber (1990, [7]) studied the pH mortality of three commercial bivalve mollusc species.

- Brownell [12] studied the pH mortality of the larvae of 8 marine fish species.

- Calabrese and Davis [14] looked at the pH tolerance of embryos and larvae of two commercial bivalve mollusc species.
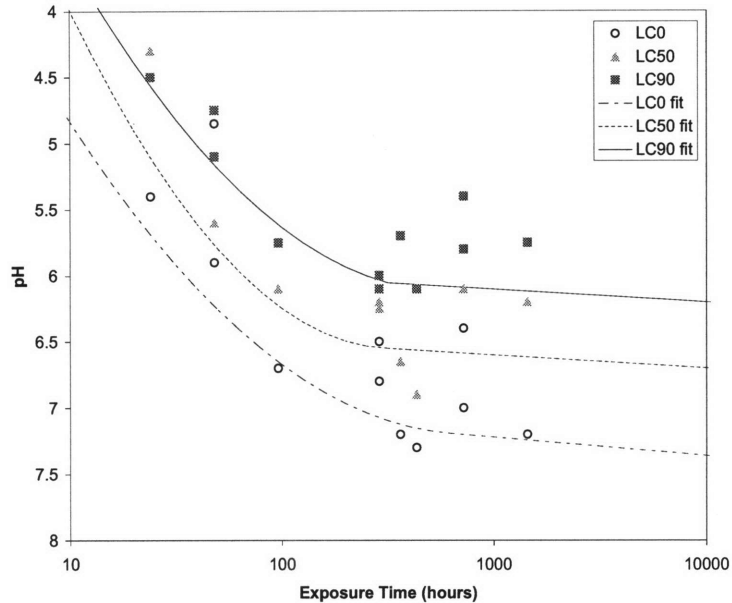
Figure 2-1: pH mortality data for the combined dataset of Auerbach *et al.* [5] for a variety of marine zooplankton and benthic species. Also shown are the isomortality lines developed by [5] from these data.

- Grice *et al.* [46] looked at the mortality and reproductive effects of three zooplankton when exposed to acid waste of varying pH levels.

- Rose *et al.* [105] looked at the pH mortality of a marine copepod.

- Portmann [99] studied the pH mortality of brown shrimp.

Auerbach [4] provides little explanation as to how he extracted and condensed the data to arrive at a "representative" dataset. It is however clear that the dataset presented does not consist solely of the raw data but is rather a subset that has been manipulated to some extent. For example, some mortality data were adjusted based on observed decreases in reproductive rates. For the present purpose, we will simply take his compiled data as given. Looking ahead, these data will not be used in the present analysis since more appropriate (CO_2-induced mortality) data now exist. Figure 2-1 shows the data extracted by Auerbach along with the isomortality curves developed from these data.

Yamada and Ikeda (1999)

Given the fact that the mortality dataset that existed at the time of Auerbach was restricted to shallow-water organisms, Yamada and Ikeda [144] looked at the pH sensitivity of 10 marine zooplankton. Plotted in Figure 2-2 is a comparison of the Auerbach *et al.* [5] dataset and the data collected by Yamada and Ikeda [144]. The combined dataset is compared to CO_2-induced toxicity data later in this chapter, which shows that marine organism are more sensitive to CO_2 than pH depression alone. This unfortunately makes the dataset plotted in Figure 2-2 of limited value to the present analysis.
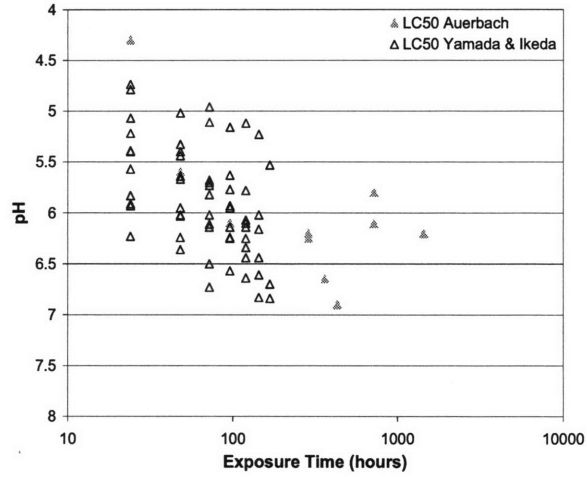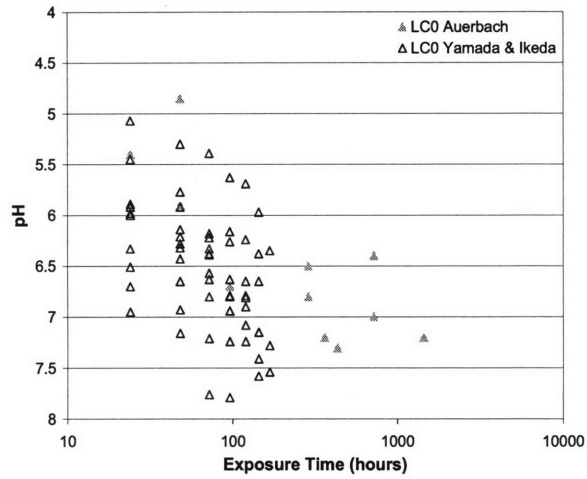
Figure 2-2: pH mortality data from the Auerbach [4] combined dataset (filled symbols) and the Yamada and Ikeda [144] dataset (open symbols): LC_0 (top) and LC_{50} (bottom).

2.2 CO_2 toxicity studies of fish

The fish studies are divided into two groups: adult and developmental. The developmental group includes eggs, larvae, and juvenile/young fish. Although the set of fish articles reviewed below are restricted to those with original data, there exist a number of in-depth review articles on the biological effects of CO_2 on fish. In particular, Ishimatsu *et al.* [58, 60] synthesized much (but not all) of the data presented below on fish (developmental and adult stages) and offered insight into the state of knowledge on the effects of hypercapnia on fish.

2.2.1 CO_2 toxicity studies of adult fish

Four main studies of lethal hypercapnia on adult fish were found: Grøttum and Sigholt [47]; Lee *et al.* [78]; Hayashi *et al.* (2004a, [51]); and Hayashi *et al.* (2004b, [50]). In addition, there are some data in Takeda and Itazawa [123]. These studies were not limited to overall mortality of marine fish species; in each case various indicators of blood composition were measured in an effort to understand the physiological response of the fish to lethal and sub-lethal exposures. Of the four main studies, all except Grøttum and Sigholt [47] were motivated by carbon sequestration. The CO_2 exposures tested were similar in each case, with a maximum pCO_2 of nearly 8 kPa.

There have been many studies of sub-lethal effects of CO_2 on fish; Grøttum and Sigholt [47] refer to this body of work as comprehensive and recommend [52] for an overview. For example, sub-lethal exposures have been studied in freshwater species such as carp [26, 146, 122, 145], tench [65], channel catfish [13], brown bullhead [44], European eel [30, 84], white sturgeon [27, 28], and multiple species of rainbow trout [114, 16, 64, 96, 98, 63, 10, 97]. Examples of marine species for which sublethal hypercapnic effects have been studied include Pacific spiny dogfish [29, 25, 83], *Conger conger* (a marine teleost) [130], the seawater salmon [96], Atlantic salmon [38, 39], spotted wolffish [41], larger spotted dogfish [102], spotted skate [45] and cod [77]. Additional references may be found in the literature review provided by Kita and Ohsumi [71].

The studies of lethal effects are described briefly below. In each case, crude estimates of LC_{50} values have been generated whenever possible by simple linear interpolation between the reported mortalities. This approach was used for the adult fish dataset in favor of a more rigorous method (e.g., [37, 117]) for two reasons. First, the data are sparse with generally few partial kills making curve fitting problematic, and second, these values are not used further in the present study in any isomortality-type analysis. The resulting data for all adult fish species are combined and discussed at the end of this section.

Grøttum and Sigholt (1996)

Motivated by the potential buildup of CO_2 that may occur during commercial farming of European seabass (*Dicentrarchus labrax*, a pelagic teleost [106]), Grøttum and Sigholt [47] studied the acute toxicity of carbon dioxide on this species, measuring mortality as well as plasma ion levels. 14 adult fish were placed in each of 7 flow-through tanks and were exposed to different steady concentrations of CO_2 for a period of 120 hours. The maximum pCO_2 studied was 62.3 mmHg (8.31 kPa), and pH values were also reported for each pCO_2 studied. LC_{50} values were reported for 48, 72, 96, and 120 hour exposures, and the mortality curve for the 120 hour exposure was given. The study also reports plasma Cl^-, Na^+, and lactate concentrations.

Lee *et al.* (2003)

Lee *et al.* [78] studied the lethal and sub-lethal effects of CO_2 on yellowtail (*Seriola quinqueradiata*, a pelagic teleost [50]). 5 and 6 yellowtail were exposed to a steady pCO_2 of 7 mmHg (0.93 kPa) and 38 mmHg (5.07 kPa), respectively, for a period of 72 hours. Most of the discussion in the study is devoted to the cardiorespiratory and blood-gas responses of the fish, based on data such as heartrate, cardiac output, blood pressure and pH, and blood levels of O_2, CO_2, lactate, hematocrit, and bicarbonate. The authors tentatively conclude that cardiac failure is the primary cause of mortality induced by high CO_2 concentrations.

Hayashi et al. (2004a)

Hayashi et al. (2004a, [51]) compared the responses of Japanese flounder (*Paralichthys olivaceous*, a benthic teleost [50]) to high CO_2 exposure with the response to acidification using sulfuric acid. The goal of the study was to determine whether the toxicity of aquatic hypercapnia is due to the CO_2 exposure or to the accompanying decrease in ambient pH. Of the 11 flounder included in the study, 6 were exposed to seawater equilibrated with an air mixture containing 5% CO_2, and the remaining 5 were exposed to seawater to which 1 N H_2SO_4 had been added. The resulting pH in both cases was 6.18 (2 pH units lower than the unaltered seawater). Although the authors did not report the resulting aqueous pCO_2 value, it is reported as 4.95 kPa in Hayashi et al. (2004b, [50]) using the same experimental setup. The differences in mortality for the two groups is dramatic: all of the fish in the CO_2 group died between 3 and 48 hours of exposure, while none of the fish in the H_2SO_4 group died after 72 hours of exposure. A similar difference was noted in the response of arterial pH, hematocrit, pCO_2, and plasma ion concentrations (HCO_3^-, Cl^-, Na^+, and K^+).

Hayashi et al. (2004b)

The same authors as in the preceding article publish additional data in Hayashi et al. (2004b, [50]), focusing only on toxicity due to hypercapnia. Three fish species were studied: Japanese flounder (*Paralichthys olivaceous*), yellowtail (*Seriola quinqueradiata*), and starspotted dogfish (*Mustelus manazo*, a demersal elasmobranch). All three species were subjected to seawater equilibrated with an air mixture containing 1, 3, and 5% CO_2, and the dogfish were also exposed to an air mixture containing 7% CO_2 (the exposures correspond to pCO_2 values of 0.99, 2.97, 4.95, and 6.96 kPa, respectively). The pH of the unaltered seawater was 8.18, and the 1, 3, 5, and 7% exposures resulted in pHs of 7.01, 6.41, 6.18, and 6.02, respectively. The mortality results were:

- For the 18 Japanese flounder tested, there was no mortality for the 1 and 3% CO_2 cases after 48 and 72 hours of exposure, respectively. For the 5% CO_2 case, mortality was 17, 33, and 100% at 8, 24, and 48 hours of exposure, respectively.

- For the 15 yellowtail tested, there was no mortality for the 1 and 3% CO_2 cases after 72 hours of exposure. For the 5% CO_2 case, mortality was 20 and 100% after 3 and 8 hours of exposure, respectively.

- For the 20 dogfish tested, there was no mortality for the 1, 3, and 5% CO_2 cases after 72 hours of exposure. For the 7% CO_2 case, mortality was 20% at 72 hours.

Thus, the data indicate that the CO_2 toxicity is in this case species specific; the yellowtail were more susceptible than the Japanese flounder, and the starspotted dogfish had considerably higher resistance than the other two species.

Physiological parameters measured during the study included arterial pH, hematocrit, pCO_2, and plasma ion concentrations (HCO_3^-, Cl^-, Na^+, and K^+). The authors found a difference between the acid-base regulatory mechanism in the two teleosts and the elasmobranch, and also concluded that the observed acid-base regulation mechanisms differ from the generally accepted model for marine fish. The physiological response factors are discussed at length in [50].

It should be noted that these data are also presented in a review articles by Ishimatsu *et al.* ([60, 58]), which contains some additional discussion of sub-lethal effects.

Takeda and Itazawa (1983)

Takeda and Itazawa [123] studied methods for sedating fish for the purpose of live transport. One of these methods involved bubbling CO_2 and O_2 through water throughout the transport. Two species were tested, carp and porgie (scientific names not given in English; the article is in Japanese). This sedation approach proved feasible for carp but not for porgies as the latter group exhibited mortality at the pCO_2 required to induce sedation. Mortality statistics are reported for exposure periods of 4, 8, and 22 hours, with pCO_2 values ranging from 4 to 104 mmHg (0.53 - 13.9 kPa) and pH values ranging from 5.72 to 7.48. Exposure pCO_2 and pH were reported as observed ranges as opposed to specific values, making the data less precise

than the other studies on adult fish. According to Hayashi *et al.* (2004b, [50]) the porgie species is actually red sea bream (*Pagrus major*), which is assumed to be correct in the present study.

Combined adult fish dataset

Figure 2-3 shows all of the adult fish LC_{50} data together as a function of pCO_2 and pH. Based on the data from [51], hypercapnia appears to be a stronger stressor than the accompanying decrease in pH. However, the other studies did not consider mortality due to pH depression by another acid, and thus only one datapoint on the hypercapnia vs. acidosis issue is available from the adult fish dataset. The issue will instead be addressed in the developmental stage fish and copepod datasets. The adult fish data are compared to the other data later in this chapter.
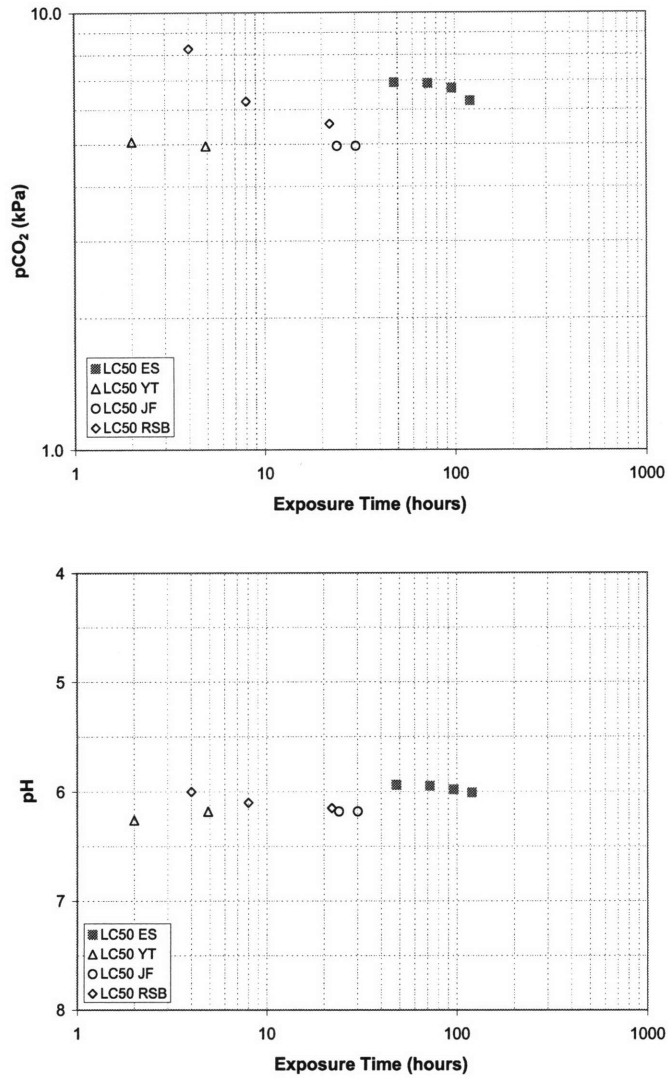
Figure 2-3: Mortality data for adult fish as a function of pCO₂ (top) and pH (bottom). Dataset includes European seabass (*Dicentrarchus labrax*, squares [47]); Japanese flounder (*Paralichthys olivaceus*, circles [51, 50]); yellowtail (*Seriola quinqueradiata*, triangles [78, 50]); and red sea bream (*Pagrus major*, diamonds [123]). Reported values are shown as filled symbols; estimated values are shown as open symbols.

The adult fish dataset is augmented with two studies relevant to evaluating the expected acute effects of CO_2 discharges on fish, Tamburri et al. [126] and Vetter and Smith [134]. Both studies attempted to observe the effect of high in situ pCO_2 on nektonic animals (i.e., species that can swim enough to overcome the ambient current), and in particular to determine whether or not they avoided regions of high pCO_2. Although the species studied were not all fish, their findings are included here because fish are the only nektonic organisms considered in the literature review. Tamburri et al. [126] attracted benthic macrofauna to beakers on the seafloor by releasing an odor solution and, once enough animals had gathered, the odor solution was passed through CO_2 hydrate to enrich the seawater. Avoidance of the plume was not observed for fish or invertebrates; fish swam through the plume in a zigzag fashion following the odor regardless of whether or not the elevated pCO_2 had been introduced. One species of fish, a hagfish, was observed to repeatedly enter the beaker and become anaesthetized, and then eventually recover and swim away. Acute toxicity was not observed even though the pH was lowered by about 2 pH units; respiratory distress was, however, noted in some species. Overall the authors conclude that fish and invertebrates do not avoid high CO_2 regions, and speculate that the induced mortality by CO_2 discharges could be significantly enhanced if nektonic scavengers seek out dead animals in high CO_2 regions and perish themselves. These findings were contradicted by the observations of Vetter and Smith [134] on the behavior of amphipods and synaphobranchid eels (the latter being a member of the fish family) near a natural hydrothermal vent discharging seawater with high pCO_2. They observed avoidance of baited traps near the vent, relative to a control site with additional baited traps, indicating avoidance for all species in the region. They did, however, note significant narcotic effects to amphipods placed in the vent which they attributed to high pCO_2. Once removed from the vent, the amphipods recovered. Overall, their observations did not support the creation of a mortality sink in the vicinity of a CO_2 discharge. Thus, the data are inconclusive regarding whether or not fish and other nektonic creatures would avoid or seek out CO_2 discharges.

2.2.2 CO$_2$ toxicity studies of developmental stage fish

Four articles with original data on the tolerance of developmental stage fish to high levels of CO$_2$ were found, all by the same lead author: Kikkawa *et al.* (2003, [68]), Kikkawa *et al.* (2004, [69]), Kikkawa *et al.* (2006a, [70]), and Kikkawa *et al.* (2006b, [67]).

Kikkawa *et al.* (2003)

Kikkawa *et al.* (2003, [68]) compared the mortality of red sea bream (*Pagrus major*) eggs and larvae due to hypercapnia with the mortality due to an equivalent level of acidification using another acid. In the acidification portion of the study, pH levels of 6.2 and 5.9 were achieved by adding varying amounts of 1 N HCl to seawater. In the hypercapnia portion of the study, these same pH levels were achieved by equilibrating seawater with air mixtures containing 5 and 10% CO$_2$, corresponding to pCO$_2$ values of 4.95 and 9.90 kPa, respectively. The eggs (embryos) used in the study were at the stage where auditory vesicles form (21 hours after fertilization) and were subjected to a 6-hour exposure time; the larvae were at the preflexion stage (10-12 days after hatching) and were given a 24-hour exposure time.

The differences in mortality between the strong acid and CO$_2$ exposures were dramatic for both eggs and larvae. For eggs, the HCl and CO$_2$ exposure cases resulted in mortalities of 3.6 and 85.8% for a pH of 6.2, and 0.9 and 97.4% for a pH of 5.9, respectively. For larvae, the HCl and CO$_2$ exposure cases resulted in mortalities of 1.6 and 61.2% for a pH of 6.2, and 5.0 and 100% for a pH of 5.9, respectively. These findings are consistent with the findings of Hayashi *et al.* [51] for adult Japanese flounder, for which hypercapnia and not the accompanying acidification was the cause of toxicity.

Kikkawa *et al.* (2004)

By far the largest dataset on the CO$_2$ toxicity of developmental fish comes from Kikkawa *et al.* (2004, [69]). In total four species were studied: red sea bream (*Pagrus*
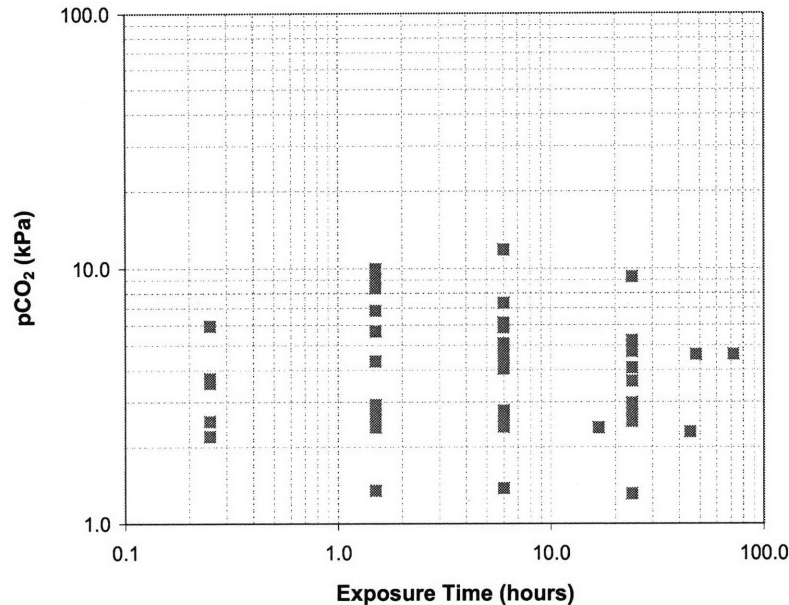
Figure 2-4: Reported CO_2 LC_{50} data from Kikkawa *et al.* (2004, [69]) for developmental stages of red sea bream (*Pagrus major*), Japanese sillago (*Sillago japonica*), Japanese flounder (*Paralichthys oliaceus*), and eastern tuna (*Euthymnus affinis*). All developmental stages that were tested are combined in the figure.

major), Japanese sillago (also known as Japanese whiting, *Sillago japonica*), Japanese flounder (also known as bastard halibut, *Paralichthys oliaceus*), and eastern tuna (*Euthymnus affinis*). For red sea bream and Japanese sillago, developmental stages tested included egg (cleavage and embryo), larva (preflexion, flexion, and postflexion), and juvenile. For Japanese flounder, egg (cleavage) and young were tested; for eastern tuna, only the egg (cleavage) stage was tested. Exposure tests for three of the species generally lasted 24 hours; Japanese flounder tests went as long as 72 hours. In most cases mortality data were collected after 15 minutes, 90 minutes, 6 hours, and 24 hours. Exposure concentrations were for the most part in the 1-10 kPa range, except for the more CO_2 tolerant eastern tuna where they reached nearly 15 kPa. The authors reported LC_{50} concentrations in each case, as well as the mortality curves for the red sea bream and Japanese sillago experiments.

Taken as a whole, the combined dataset from this study (see Figure 2-4) does not

reveal a clear trend. The data are more revealing when plotted by species and by developmental stage, as shown in Figure 2-5. Note that in the case of red sea bream and Japanese sillago, the eggs at cleavage stage and the juvenile fish are most sensitive to hypercapnia. The Japanese flounder egg data are similar to these, and the young data suggest a slightly higher tolerance, but this could also be due to slightly older fish (young flounder vs juvenile bream/sillago). The eastern tuna egg data show a higher CO_2 tolerance, as noted by [69].
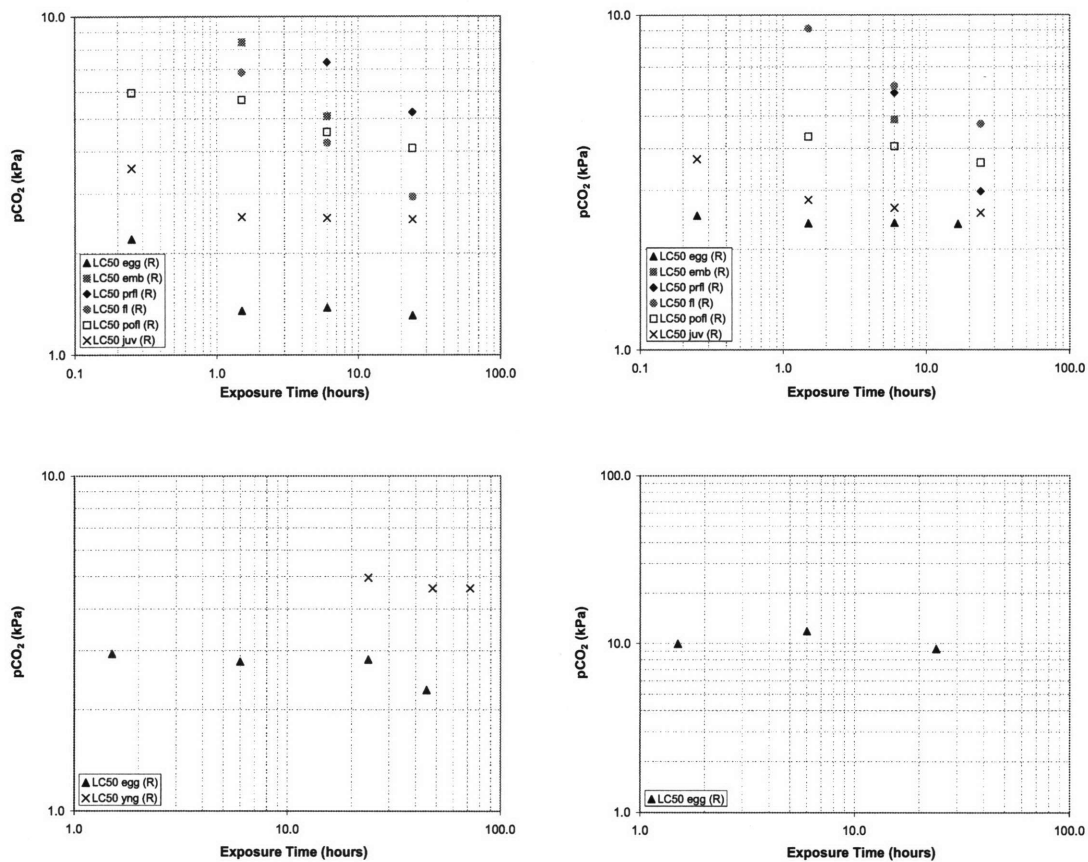
Figure 2-5: Kikkawa *et al.* (2004, [69]) CO_2 LC_{50} data by development stage for red sea bream (*Pagrus major*, top left); Japanese sillago (*Sillago japonica*, top right); Japanese flounder (*Paralichthys oliaceus*, bottom left); and eastern tuna (*Euthymnus affinis*, bottom right - note the different vertical scale). Symbols refer to different stages: filled triangles = egg (cleavage); filled squares = egg (embryo); filled diamonds = preflexion larva; filled circle = flexion larva; open squares = postflexion larva; x = juvenile (juv) or young (yng). All values were reported by the authors.

Kikkawa *et al.* (2006a)

Building on previous results, Kikkawa *et al.* (2006a, [70]) investigated how the CO_2 toxicity of juvenile Japanese sillago (*Sillago japonica*) differs when the exposure concentration is time variable. As a baseline, Kikkawa *et al.* conducted a series of 18-hour experiments in which fish were immediately placed in seawater equilibrated with air mixtures containing 1, 3, 5, 7, and 9% fCO_2 (approximately 1, 3, 5, 7, and 9 kPa). This *one-step exposure* approach is the same as in all CO_2 mortality studies previously described. Kikkawa *et al.* then conducted a set of four *step-wise exposures* in which fish were exposed to CO_2 levels that were gradually increased in a series of discrete steps from 1% and 7-10% fCO_2, and then suddenly reintroduced into natural (normocapnic) seawater. The resulting CO_2 toxicity was markedly different, and two general observations were made. First, in all cases the mortality at peak CO_2 concentration was reduced when the exposure was gradual rather than sudden. For example, while mortality was near 100% after 15 minutes of the one-step 7% and 9% fCO_2 exposures, mortality in the first step-wise experiment was not observed until the maximum 9% fCO_2 was reached (6 hours into the experiment) and at 18 hours the mortality was only 67%. Second, the fish were very sensitive to a sudden drop of CO_2 concentration; of the fish that survived the peak CO_2 concentration, 100% died within 15 minutes of exposure to normocapnic seawater in three of the four experiments and 76.7% died in the last experiment.

The step-wise exposure data from [70] are not plotted as they are not compatible with one-step exposure data. However, the step-wise exposure findings cast doubt over the validity of the Auerbach *et al.* [5] isomortality approach as it pertains to fish and are considered later in this analysis.

Kikkawa *et al.* (2006b)

The general findings of [70] were confirmed in Kikkawa *et al.* (2006b, [67]), where tomato clownfish embryos (*Amphipron frenatus*) were subjected to one-step and two-step exposures. One-step exposures of 14.3, 9.6, 6.8, 4.8, and 2.9 kPa were adminis-

tered for experiment durations of 6, 24, 48, 72, and 96 hours. For these experiments, an LC_{50} of 14.3 kPa, 10.3 kPa, and 7.0 kPa was reported for 48, 72, and 96 hour exposures. During the two-step exposure experiments, where embryos were first placed for 48 hours in one concentration and then moved suddenly to a second concentration for another 48 hours, a substantial difference in response was observed. When going from 2.9 kPa to normocapnic water, the mortality after 96 hours was about 40%, compared to 0% for a constant one-step exposure. Likewise, mortality is about 75% after 96 hours when going from 4.8 kPa to normocapnia, compared to 5-35% for a one-step exposure of 4.8 kPa for 96 hours. Thus, embryos of tomato clownfish exhibit a sensitivity to sudden changes in pCO_2 akin to that observed for juvenile Japanese sillago in Kikkawa *et al.* (2006(a), [70]), albeit to a lesser degree. The adaptive ability observed in [70], whereby fish survived longer when gradually exposed to higher concentrations in multiple steps, was not observed here.

Combined developmental fish dataset

The combined CO_2 mortality dataset for developmental fish is plotted in Figure 2-6, where the red sea bream data of [68], the Japanese sillago data of [70], and the tomato clownfish data of [67] have been added to the data from [69]. The large variability across developmental stages is apparent in the red sea bream and Japanese sillago data, and it is interesting to note that in these case the cleavage stage eggs and the juvenile fish show the highest sensitivity.
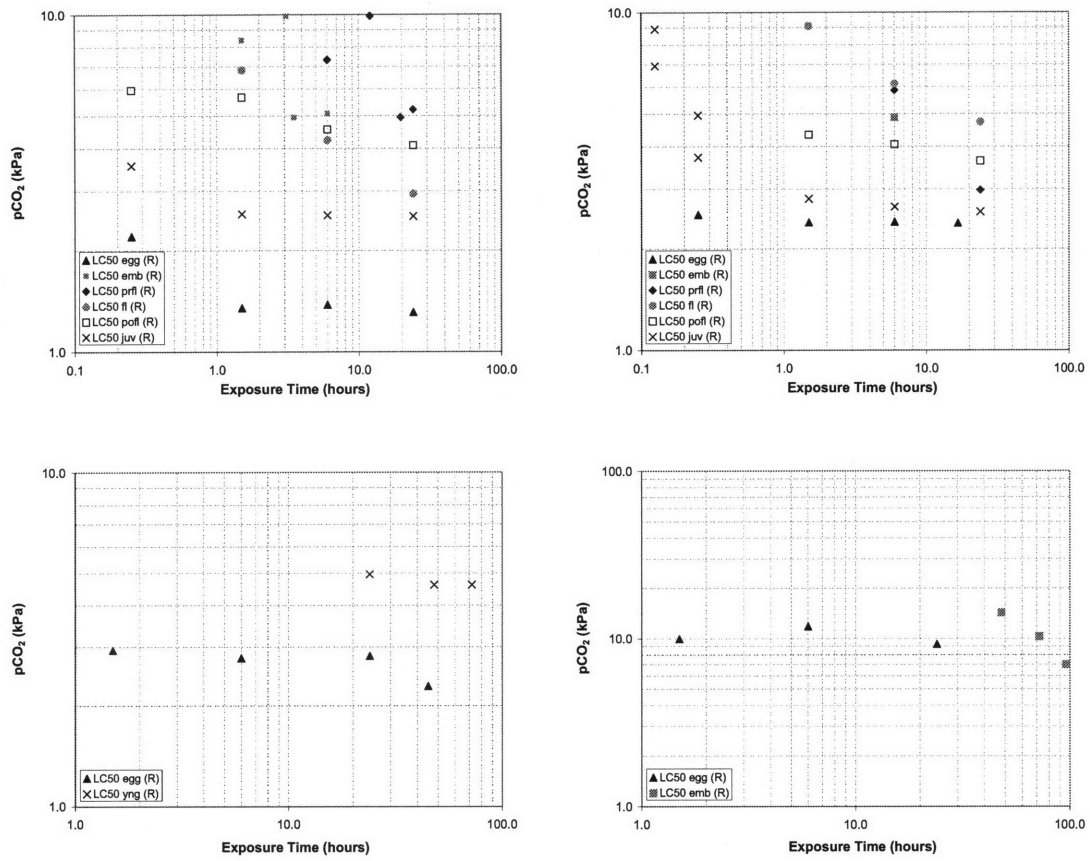
Figure 2-6: Combined CO_2 LC_{50} dataset for developmental fish for red sea bream (*Pagrus major*, top left); Japanese sillago (*Sillago japonica*, top right); Japanese flounder (*Paralichthys oliaceus*, bottom left); and eastern tuna cleavage-stage eggs (*Euthymnus affinis*, bottom right) with tomato clownfish embryos (*Amphipron frenatus*, bottom right). Note the different vertical scale used for the bottom right panel. Symbols refer to different stages: filled triangles = egg (cleavage); filled squares = egg (embryo); filled diamonds = preflexion larva; filled circle = flexion larva; open squares = postflexion larva; x = juvenile (juv) or young (yng). Includes reported and estimated data from [67], [68], [69], and [70].

2.2.3 Combined fish CO_2 toxicity dataset

Data for developmental as well as adult fish are available for two species, red sea bream and Japanese flounder. The combined LC_{50} dataset for these species is shown in Figure 2-7. The adult dataset only adds a small number of datapoints to each plot, and in each case exhibits more tolerance than most of the developmental dataset. With regard to constructing a revised isomortality curve of the type in [5] (see Chapter 3 for details), the following conclusions are drawn from the combined developmental and adult fish dataset:

- Fish are much more sensitive to hypercapnia than to an equivalent level of pH depression caused by another acid, as confirmed by [68] for developmental fish and by [51] for adult fish. Thus, acute impact estimates of CO_2 injection should be based on CO_2 mortality data rather than pH mortality data as in [5].

- Fish seem to be most sensitive to hypercapnia during the early and late developmental stages, as demonstrated for red sea bream and Japanese sillago by [69]. Thus, a conservative isomortality curve should be based on these life stages rather than the combined dataset.

- CO_2 tolerance is variable between different fish species. For example, adult starspotted dogfish were notably more tolerant than adult Japanese flounder and yellowtail [50] and eastern tuna eggs were more tolerant than red sea bream, Japanese sillago or Japanese flounder eggs [69]. Thus, a conservative isomortality curve should be based on the most sensitive species rather than the combined dataset.

- Hypercapnic mortality is strongly influenced by the time variability of the ambient CO_2 concentrations, as demonstrated by [70] and [67]. Mortality due to peak CO_2 concentrations may be reduced when the concentration is increased gradually, and a sudden return to normocapnic conditions can induce mortality. This casts doubt on the relevance of the integrated mortality concept, upon which the isomortality method of [5] is based, to fish.
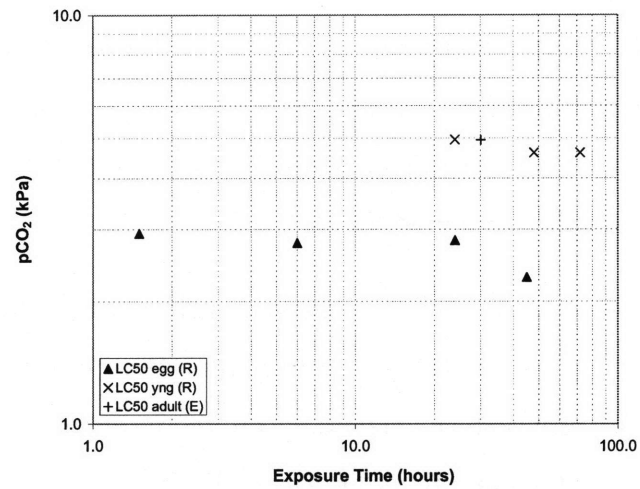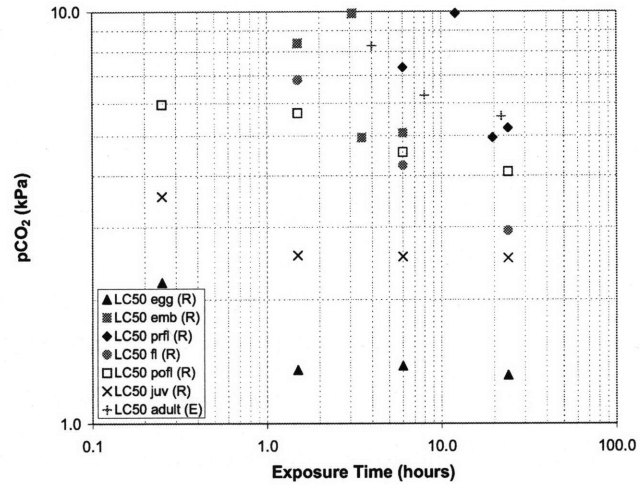
Figure 2-7: Combined CO_2 LC_{50} dataset for adult and developmental fish for red sea bream (*Pagrus major*, top) and Japanese flounder (*Paralichthys oliaceus*, bottom). Symbols refer to different stages: filled triangles = egg (cleavage); filled squares = egg (embryo); filled diamonds = preflexion larva; filled circle = flexion larva; open squares = postflexion larva; x = juvenile (juv) or young (yng); + = adult. Developmental stages include reported and estimated data from [68], [69], and [70]; adult data are estimated from [50], [51], and [123].

2.3 CO_2 toxicity studies of pelagic copepods

Three main studies have been identified which provide insight into the acute toxicity of pelagic copepods (a type of zooplankton): Kurihara *et al.* (2004(a), [73]), Watanabe [138] and Watanabe *et al.* [139]. The studies provide data on both developing and adult copepods, but are here treated as a group because the distinction is not as clear as in the fish studies.

Kurihara *et al.* (2004a)

Kurihara *et al.* [73] looked at the impacts of elevated CO_2 concentrations on the survival, egg production rates, and early development of *Acartia steueri* and *Acartia erythraea*, both shallow-water marine copepods. In the first part of the study, the survival rate of adult females and their egg production rate were measured during an 8-day exposure to seawater with pCO_2 values of 0.236, 0.536, and 1.036 kPa (control pCO_2 was 0.036 kPa). Although observed mortality increased with time in each case, this trend was also observed in the control samples, where mortality exceeded 60 and 40% for *A. steueri* and *A. erythraea*, respectively. For *A. steueri*, the differences in mortality between all elevated CO_2 cases and the control were not statistically significant. For *A. erythraea*, the 1.036 kPa exposure had slightly higher mortality rates but the difference from the control was only statistically significant in the early portion of the experiment. In contrast, the egg production rates were clearly impacted by elevated CO_2 exposure, decreasing with both time and CO_2 concentration. At the highest exposure tested (1.036 kPa), *A. steueri* and *A. erythraea* egg production rates were 40% and 5% of their control values, respectively, indicating a significant but different response by the two species.

The second part of the study looked at the hatch rate and survival of nauplii (larvae) of *A. erythraea* only. Eggs produced in each of the CO_2 conditions above were placed in vials of the same concentration, and the number of hatched and dead nauplii were counted after 24 hours. The hatch rate declined and the nauplii mortality increased when exposed to high CO_2, with differences from the control on the order

of 30 and 20%, respectively (hatch rate was significantly different from the control at 1.036 kPa; nauplii survival at 0.536 and 1.036 kPa).

In terms of mortality data of the type collected for adult and developmental fish, this study does not yield much data. An egg mortality rate could be inferred by combining the hatch rate and nauplii mortality observations (e.g., a 30% decline in hatch rate plus a 20% decline in nauplii survival, could be interpreted as a 44% mortality even though adult female mortality was statistically similar to the control). Such adjustments are not made here since it would be inconsistent with the previous interpretations of adult and developing fish mortality. This issue is, however, revisited in Section 3.3.2 and Chapter 5 since the observed reproduction impacts imply intergenerational consequences of CO_2 exposure.

Watanabe (2001)

The recuperation of several different species of copepods was studied after high pCO_2 exposure (200,000 μatm for 3-30 minutes) by Watanabe [138]. Each experiment used about 5 copepods of the same species, and their level of activity was observed and assigned a ranking based on a qualitative assessment. The scale went from 1 (not moving or reacting, appearing dead) to 7 (sensitive to touch stimulus). This activity or behavioral index was logged at regular intervals during and after the exposure. Because the metric is qualitative and the data are published only in Japanese with a short overview explanation provided by the author, certain assumptions regarding the interpretation of the data were necessary here. The most obvious result is that in most cases, the copepods generally returned to normal activity (7) within a relatively short time after being returned to normocapnic seawater (10-40 minutes) after reaching the lowest activity rank of 1 in the high pCO_2 environment. In some cases the longest exposed group activity only returned to about 4 after 40 minutes (when the experiment apparently ended). Taking the plotted behavioral index as a mean response, this suggests that mortality was minimal for short exposures to this pCO_2, and on the order of 0-50% for exposures up to 30 minutes over a fairly large range of copepod species. The study also looked at several reproductive factors but these are

not interpreted here due to the language barrier.

The data provided in this study are highly relevant to understanding the fate of a copepod encountering the plume, but do not lend themselves to inclusion in an isomortality analysis. A constant toxicity test would have identified an LT_{50} as being very short if the non-moving animals were assumed to be dead, but this would be incorrect. As described in Section 3.1.3, Chen *et al.* [23] used this activity data to construct a model of copepod response to elevated pCO_2 which allowed recovery of organisms but not mortality. The implications of the observed recovery for the validity of an isomortality approach is open to debate and should be the focus of more study. Still, the data are not used quantitatively in the present study for the reasons noted above.

Watanabe *et al.* (2006)

The largest source of copepod (zooplankton) mortality data comes from Watanabe *et al.* [139]. The purpose of the study was to remedy the lack of existing CO_2 toxicity data on deep-sea zooplankton species, i.e., for species that dwell in the depth ranges considered by some CO_2 injection schemes. Samples were collected from five stations in the Western North Pacific: three stations were in the subtropical region ({25° 26'N, 144° 50'E}; {24°N, 155°E}; {14°N, 155°E}), one was in the subarctic region (43°N, 155°E), and the remaining station was in the transitional region (36°N, 155°E). At each station, deep and shallow samples were collected using a vertical tow method (i.e., vertically integrating the sample over a depth range). Depth ranges for the shallow and deep samples were 0-150 and 0-1000 m for the subarctic station; 0-500 and 500-1500 m for the other four stations. CO_2 exposure experiments were conducted on the ship soon after collection. Sample specimens were placed in seawater of varying CO_2 concentrations and incubated in the dark at temperatures similar to their native environments (at atmospheric pressure). Animal behavior and mortality was assessed after 6 and 12 hours, and at 12-hour intervals thereafter. A total of 16 exposure experiments were conducted (2-5 experiments per station, with at least one shallow sample and one deep sample), where each experiment consisted

of a control ($530 \leq pCO_2 \leq 1,600$ μatm, $8.02 \geq pH \geq 7.64$) and multiple high CO_2 exposures ($1,100 \leq pCO_2 \leq 98,000$ μatm; $7.65 \geq pH \geq 6.02$). Zooplankton species were classified taxonomically and assigned to one of three groups: epipelagic (inhabiting shallow water), meso/bathypelagic (inhabiting deep water), and eurybathic (inhabiting a large depth range). The authors reported LT_{50} values for each exposure level for all experiments and provided complete mortality curves for experiments 1, 3, 15, and 16. The taxonomical breakdowns of each experiment are also included.

Watanabe et al. [139] make the following general conclusions from the dataset:

- Copepods do exhibit increased mortality when exposed to high CO_2 concentrations, and the mortality increases with increasing exposure time. The sensitivity to exposure time seems much greater for zooplankton than for fish, which are thought to adjust to external hypercapnic stress through the action of gill cells.

- Mortality to CO_2 exposure is significantly higher than mortality due to acification by another agent, based on a comparison of the pH mortality data of [5] and [144] with the data collected in this study.

- Deep-living copepods appear to be have better tolerance of high CO_2 concentrations than shallow-water copepods, which is contrary to the generally held belief that deep-sea organisms would be more sensitive. While observed differences can perhaps in part be attributed to the fact that some deep-living copepods go through a dormant stage or to the fact that toxicity of most chemicals is generally lower at lower temperatures such as the ones found in the deep ocean, the authors argue that these factors alone do not explain the observed difference in tolerance between deep- and shallow-water copepods. It is suggested that deep-sea organisms are adapted to better tolerate CO_2 because they are naturally exposed to higher CO_2 concentrations than surface organisms (pCO_2 peaks at about 1,000 m depth due to remineralization of sinking organic matter from primary production in the upper ocean). The higher tolerance of deep-sea organisms is most pronounced in the subarctic and transitional regions; in the subtropical region, there is a smaller but still significant difference between the
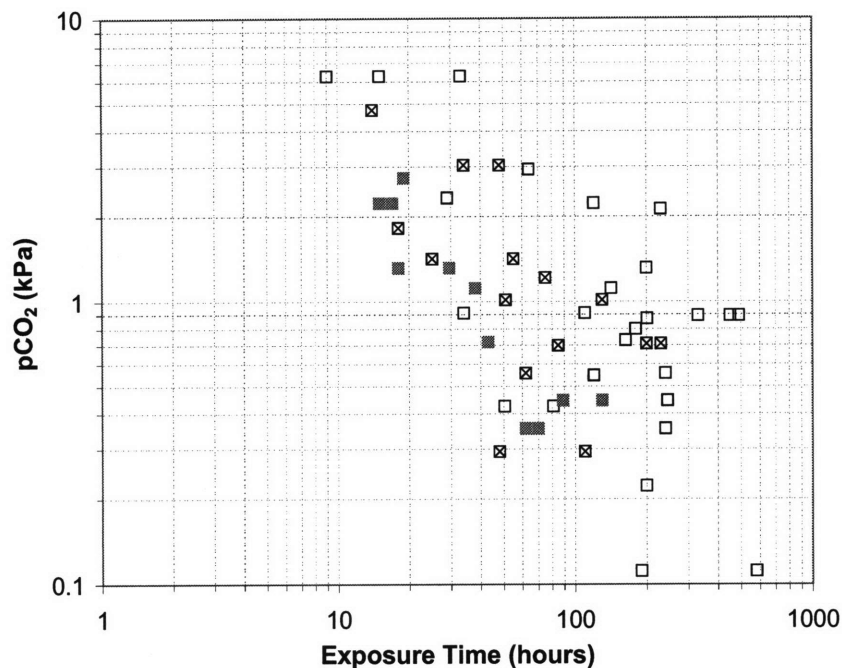
Figure 2-8: Reported LT_{50} values for copepods in the Western North Pacific from Watanabe *et al.* [139]. Filled squares: shallow-living copepods from the subarctic and transitional regions; hatched squares: shallow-living copepods from the subtropical region; open squares: deep-living copepods.

CO_2 tolerance of deep- and shallow-water copepods (see Figure 5 in [139]).

The combined Watanabe dataset is plotted in Figure 2-8, where the data for the various regions can be distinguished. The lead author of [139] has kindly provided the remaining raw mortality data not included in the original paper. The treatment of this additional data and their application to the development of a new isomortality function is described in Section 3.3.2.

2.4 CO_2 toxicity studies of benthic organisms

The isomortality curves developed by Auerbach *et al.* [5] were partially based on studies of benthic organisms. The response of such organisms to CO_2 exposure is relevant not only to sequestration schemes in which CO_2 is introduced on the sea

floor, but also to mid-depth releases since some benthic organisms are planktonic in their developmental stages. Only one of the benthic studies, Sato *et al.* (2005, [111]), yields data directly relevant to isomortality modeling. For the other studies reviewed below, there is little in the way of controlled toxicity data that would be useful in the evaluation of discharge scenarios in the next chapter. Nonetheless, the studies are reviewed below because they have general relevance to acute impact modeling across a range of species.

Sato *et al.* (2005)

The Sato *et al.* [111] study is highly relevant to the present discussion for two reasons. First, the authors report CO_2 mortality data on the harpacticoid (benthic) copepod *Metamphiascopsis hirsutus* for steady and time-variable exposures. Second, a more general form of the isomortality method of [5], the *extended probit mortality model* of Sato and Sato [110] and Sato *et al.* (2004, [108]) is tested using the experimental mortality data. The discussion below is restricted to the mortality data yielded by the study and its use in validating their model; theoretical considerations of how the probit model differs from the Auerbach *et al.* [5] isomortality calculations are discussed in Section 3.3.

The experimental portion of [111] consisted of 5 experiments of elevated pCO_2 and one control. In each case, 19-20 copepods were placed in individual vials containing seawater equilibrated with varying pressures of CO_2. Three of the experiments were one-step exposures to 2, 4, and 9% fCO_2 that lasted 96 hours. The other two experiments were two-step exposures; a fCO_2 of 4% was used for the first 48 hours of the experiments, followed by another 48 hours at 2 or 8% fCO_2. The raw mortality data are provided by the authors, from which mortality statistics have been estimated for the three one-step exposures.

The purpose of the two two-step exposure experiments was to test whether probit model mortality calculations based on one-step exposure data could accurately predict two-step exposure mortality. Sato *et al.* [111] found that the model performed "moderately well" in this respect and conclude that the time integration of CO_2

mortality data is valid for zooplankton (*Metamphiascopsis hirsutus* was chosen as a model organism for pelagic copepods based on unpublished observations, and pelagic copepods were taken to represent zooplankton in general). Although the two-step exposure data are not directly useful in constructing new isomortality curves, they provide an interesting comparison to the time variable exposure of juvenile Japanese sillago in [70]. While the fish showed greater tolerance to high CO_2 levels during step-wise exposures than one-step exposures, the mortality of *M. hirsutus* during a 4 to 8% two-step exposure seemed more additive, i.e., more consistent with the assumptions behind the time integration of the probit calculations in this study and of the calculations in [5]. This conclusion is qualitative at best since the corresponding one-step experiment accidentally used 9% fCO_2 instead of 8%, and there is only one datapoint. Nonetheless, the authors suggest that the ability of fish to compensate for gradual exposure to otherwise lethal pCO_2 (by accumulating bicarbonate ions in the blood) is not as well-developed in zooplankton, and thus the isomortality method (probit method in their parlance) may be valid for zooplankton but not fish.

Barry *et al.* (2004), Carman *et al.* (2004), and Thistle *et al.* (2005)

The *in situ* response of sediment-dwelling meiofaunal communities to small scale CO_2 releases has been studied by Barry *et al.* (2004, [9]), Carman *et al.* (2004, [17]), and Thistle *et al.* (2005, [127]). In each case, small corrals (48 cm in diameter) were filled with liquid CO_2 and meiofaunal abundance in sediment cores after roughly month-long exposures was compared to control samples (taken far away from the CO_2 sources). Barry *et al.* [9] observed a significant mortality of meiofaunal organisms in the CO_2 exposed cores, most notably for flagellates, amoebae, and nematodes (ciliates and allogromid foraminifera did not decrease in biovolume, but since these taxa have much lower abundances it was thought that the experimental design was inadequate to detect small changes in abundance/biovolume of these organisms). Carman *et al.* [17] did not detect significant declines in the abundances of the major groups (harpacticoid copepods, nematodes, nauplii, kinorhynchs, polychaetes) or total meiofauna, but this was attributed to slow decomposition of meiofaunal carcasses which

49

rendered the experimental procedure incapable of detecting mortality due to CO_2 exposure. Using the same samples, Thistle *et al.* [127] showed significant differences in mortality between control and CO_2 exposed harpacticoid copepods, using a new technique in which copepods were classified as alive or dead at the time of collection based on the appearance of striated muscles. Based on these results, Thistle *et al.* [127] and Carman *et al.* [17] concluded that meiofaunal communities were likely strongly impacted by CO_2 exposure, even though traditional abundance indicators failed to detect the signal due to slowly decaying carcasses. Thus, [9], [17], and [127] are consistent in their overall conclusion, namely that hypercapnia can induce high mortality on meiofaunal communities.

Takeuchi *et al.* (1997)

Takeuchi *et al.* [124] looked at the impact of high CO_2 concentrations on three species of nematodes and eleven species of marine bacteria. These were selected as representative of marine organisms because nematodes are the most abundant taxa and have the highest species diversity in the benthic ecosystem, and because bacteria are a major decomposer and an important genetic resource. For nematodes, 7-day exposure experiments were conducted under starvation conditions at varying concentrations of CO_2 and compared to a control. Mortality curves are provided by the authors, but as a function of pH and not CO_2. The CO_2 concentrations used to achieve the given pH levels are not reported, and insufficient supplemental information is given to estimate corresponding CO_2 concentrations after the fact. For the bacteria, 12-hour incubations under eutrophic conditions at various pH levels were performed and compared to control incubations, but again the CO_2 concentrations used were not reported. All eleven bacteria species were tested at atmospheric pressure, and two were also tested at 350 atm which is more typical of pressures in a deep ocean environment. The following results were obtained:

- No significant nematode mortality in excess of the control (pH 8.0) was observed during exposures of pH 7.0 and 6.2. At pH 5.4, all three species showed significantly higher mortality, and the effect was more pronounced in two of the

three species (*Mesacanthion* sp. and *Symplocostoma* sp. were more sensitive than *Metachromadora* sp.).

- Bacterial growth was strongly affected by CO_2 exposure, dropping to less than 50% of the control (pH 7.7) for pH < 6.0 for all bacteria, and for one species this decrease was achieved at pH $\leq$ 6.5. The authors suggest that the *in situ* sensitivity of bacteria may be higher because of the oligotrophic conditions (leading to higher stress) that prevail in the ocean.

- Bacterial sensitivity to CO_2 exposure was similar at high pressure, although growth rates were generally lower than at atmospheric pressure. The results did not support the generally held belief that deep-sea species are more sensitive than shallow-water species because they experience less environmental variability.

- Overall, the nematodes and bacteria showed acute effects when CO_2 concentrations were high enough to effect a pH of 6.0 or lower; above pH 6.0, acute effects were generally not observed.

The nematode mortality and bacteria growth rate decline data of Takeuchi *et al.* [124] are not used in developing new isomortality curves due to CO_2 exposure for two reasons. First, CO_2 concentrations were not reported and cannot be estimated without making assumptions regarding the seawater and incubation medium used in the experiments. Second, and more importantly, the CO_2 tolerance of the nematodes and bacteria in this study was apparently greater than that of pelagic copepods and fish, based on a comparison of observed mortalities and pH ranges. Thus, not using these data seems conservative from the standpoint of CO_2-induced mortality assessment.

Additional data on the microbial response to elevated CO_2 can be found in a series of mesocosm experiments reported in Sugimori *et al.* (2000, [120]), Takeuchi *et al.* (2002, [125]), and Sugimori *et al.* (2004, [119]); shifts in bacterial populations were noted for pCO_2 values in the range of approximately 1-10 kPa. For the reasons noted above, these data are not used further in the present analysis.

Ishida *et al.* (2005)

Ishida *et al.* (2005, [57]) used a benthic chamber to conduct one short (about 3 days) and two long (about two weeks) *in situ* CO_2 exposure experiments on benthic communities. In each experiment, the abundances of benthic meiofauna, nanofauna, and bacteria were observed for average CO_2 exposures of 5,000 ppm and 20,000 ppm and compared to the control. The results were mixed: meiofauna showed for the most part significantly decreased abundance at the highest CO_2 exposure when compared to the control; nanofauna showed decreased abundance only in one long-term experiment; and bacteria showed a significant increase in abundance in the two long-term experiments. Of the meiofauna, nematodes showed decreased abundance for the two long-term experiments with highest CO_2, and foraminifers showed decreased abundance in one long and the short experiment. The observed sensitivity of the meiofauna to high CO_2 exposure seems consistent with the conclusions of [9], [17], and [127], and the sensitivity of nematodes in particular seems consistent with the findings of [124]. The increase in bacterial growth in the presence of high CO_2 is not consistent with the findings of [124], and is thought to be caused the growth of bacteria adapted to the new environmental conditions, i.e., high CO_2 and reduced feeding pressure from nano and meiofauna. Taking the benthic community as a whole, Ishida *et al.* point out that the response to CO_2 perturbations was neither simple nor linear; the variable responses to CO_2 among the different trophic groups led to non-linear effects. Although the data do not lend themselves to isomortality modeling, they do suggest that biological impact calculations using mortality data collected on individual species may be inadequate as these will not capture impacts on the relative abundance of different trophic levels such as those noted herein.

Ishida *et al.* (2006)

Ishida *et al.* (2006, [56]) augment the above study with additional data from Storfjorden, a Norwegian fjord, using the same experimental setup. Somewhat different trends were observed. Meiobenthos abundance varied greatly, nanobenthos abun-

dance increased, and bacterial abundance was unchanged. As in [57], the response among the various trophic groups was neither simple nor linear.

Langenbuch and Pörtner (2004)

Langenbuch and Pörtner [76] studied the CO_2 sensitivity of the eurybathic sediment-dwelling marine worm *Sipunculus nudus*. They found that although the species can alter its metabolic rates to survive short-term exposure to hypercapnic conditions, long-term mortality is sensitive to sustained high CO_2 levels even when these levels are within the natural range experienced by the organism. Mortality curves are provided, but have not been incorporated into the isomortality analysis because the discharge scenarios studied herein are in the water column and because Pörtner *et al.* [100] identify *Sipunculus nudus* as showing exceptional tolerance to acutely elevated pCO_2, at least in the short term.

2.5 Combined mortality dataset for all species

The combined mortality dataset for all data (CO_2 and non-CO_2) is plotted in Figure 2-9 as a function of pH. The distinction between reported and estimated mortality statistics is not shown in this figure, although the reader is reminded that most of the adult fish data were estimated in the present study. The data in Figure 2-9 clearly indicate that marine organisms tend to be more sensitive to hypercapnia than the equivalent acidosis caused by another acidifying agent, as has been previously noted for a variety of species.

The dataset for CO_2-induced mortality is shown in Figure 2-10. Looking ahead to Section 3.3.2, it is noted that the adult fish data indicate a higher tolerance to CO_2 exposure than zooplankton (copepods). Also, if the adult fish data are excluded, then the remaining dataset is dominated by developmental stage fish for short exposures and by copepods for longer exposures; this has implications for the development of isomortality relationships in Section 3.3.2.

It should be noted that acute mortality data have apparently been collected for
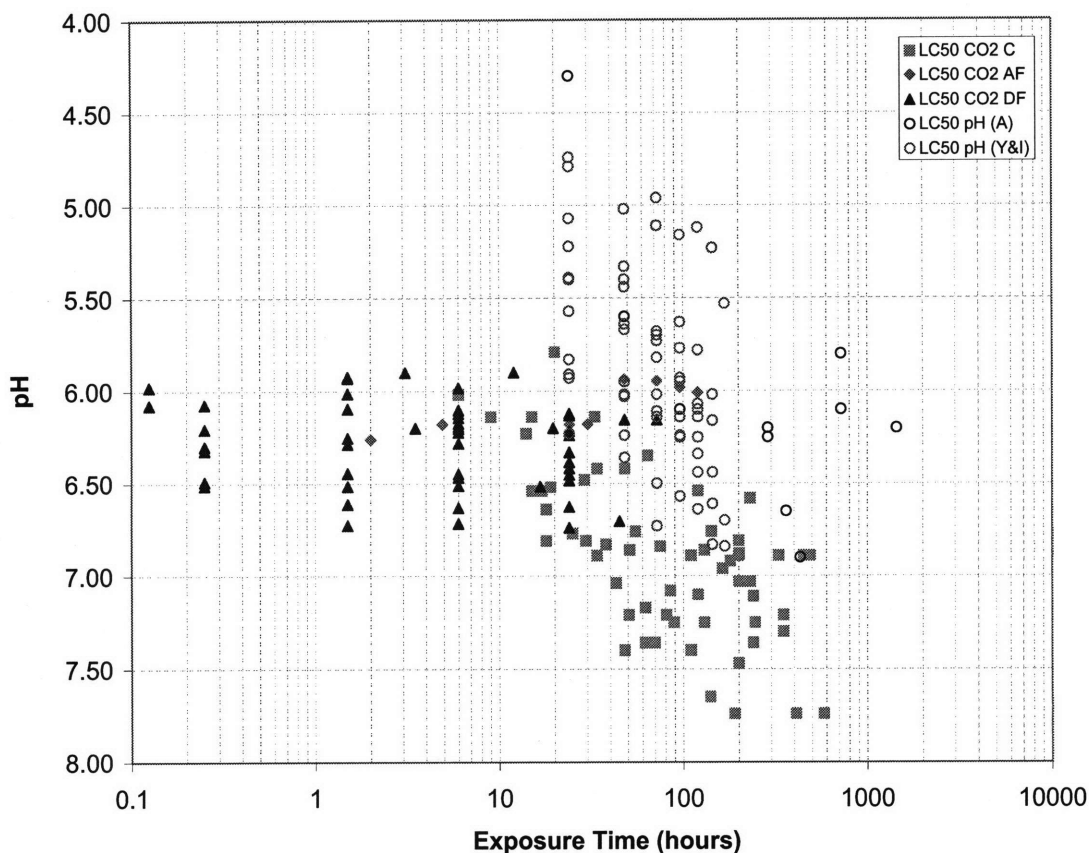
Figure 2-9: Combined LC_{50} dataset for mortality due to pH depression by CO_2 (filled symbols) and other acids (open symbols). The non-CO_2 dataset is mainly comprised of zooplankton [5, 144]; the CO_2 dataset consists of adult fish (AF, filled diamonds [47, 50, 51, 78, 123]), developmental fish (DF, filled triangles [67, 68, 69, 70]), and copepods (C, filled squares [111, 139]).

a number of other species as well, including cephalopods (*Sepia lycidas* [72], *Sepioteuthis lessoniana* [72], and the common octopus *Octopus vulgaris* [59]) and decapods (the prawn *Penaeus japonica* [72] and the western rock lobster *Panulirus cygnus* [59]). These species are not included in the present analysis as the data could not be found in the peer-reviewed literature, and the above sources only mention mortality statistics briefly. Moreover, with the exception of the common octopus, these species appear to be significantly more tolerant of CO_2 than copepods.
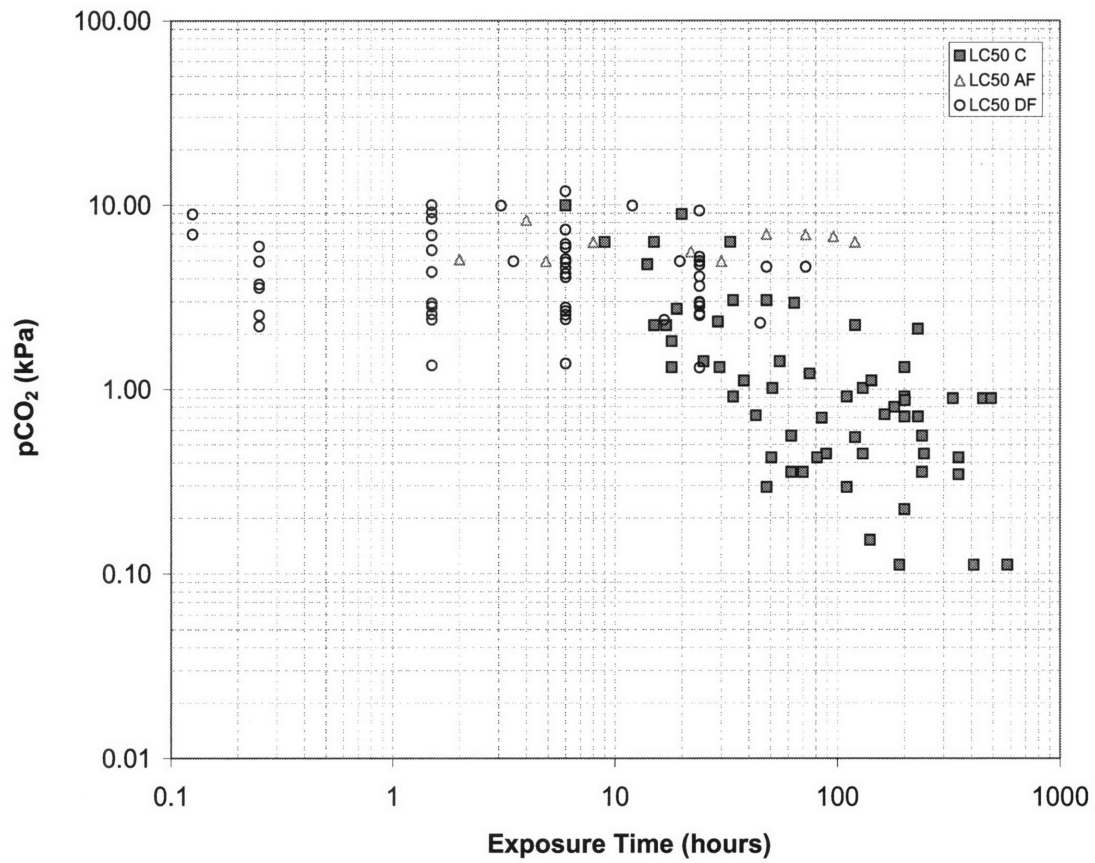
Figure 2-10: Combined LC_{50} dataset for mortality due to CO_2 exposure. The dataset consists of adult fish (AF, open triangles [47, 50, 51, 78, 123]), developmental fish (DF, open circles [67, 68, 69, 70]), and copepods (C, filled squares [111, 139]).

2.6 Sub-lethal impacts

The focus of the preceding literature review has been to identify sources of toxicity data that are well-suited for the specific objective of the study, namely to update the isomortality analysis provided by Auerbach [4] and Caulfield [18]. In addition, a sampling of closely related studies was reviewed in an attempt to provide a more complete picture of ongoing CO_2-related research and a better qualitative picture of the potential biological impacts of ocean sequestration. To that end, it would be remiss of us to not at least mention the substantial body of literature on sub-lethal effects of increased ocean CO_2 as well as the existence of a number of comprehensive review articles which attempt to integrate lethal and sub-lethal effects with physiological and ecosystem perspectives. In particular, the reader is referred to IPCC [55], Pörtner *et al.* [100, 101], Ishimatsu *et al.* [58, 60], Siebel and Walsh [113], and Kurihara *et al.* [74].

The potential importance of sub-lethal effects on both the organism and ecosystem level must be taken into consideration, and findings of some recent work in this area are discussed briefly below as an illustration. Kurihara and Shirayama [75] studied the effect of CO_2 on the early development of the sea urchins *Hemicentrotus pulcherrimus* and *Echinometra mathaei*, looking specifically at fertilization rate, cleavage rate, developmental speed, and pluteus morphology. Also, the effect of CO_2 and HCl were compared to differentiate between the effect of increased CO_2 and pH depression. CO_2 partial pressures of 10,000 μatm were used in the study, resulting in about a 1.2 unit drop in pH. All of the studied factors decreased with increased CO_2 concentration, but only fertilization rates showed a greater impact when CO_2 rather than HCl is used as the acifidying agent. From this the authors conclude that both reduced pH and increased CO_2 can significantly affect the development of these organisms and consequently alter the marine ecosystem. The study suggests, much like Kurihara *et al.* [73] did for pelagic copepods, that there can be deleterious, sub-lethal effects with intergenerational and ecosystem consequences. Such a conclusion is also supported by a longer term investigation of Shirayama and Thornton [112] on the effects of mildly

elevated pCO_2 (+200 μatm) on the growth rates of gastropods and sea urchins (both calcifying organisms). They demonstrate that adverse effects can be identified even at this low level. Growth rate impacts have also been observed for marine mussels for somewhat higher exposure levels [85]. Although such considerations are beyond the capacity of an isomortality-type analysis, results of the present study are interpreted in this context in the concluding chapter.

Chapter 3

Modeling Approach and Scenarios

The following section describes the approach taken to simulating the acute impact of three discharge scenarios, which are based on the scenarios put forth in Adams and Wannamaker [1], and which seek to maximize near-field dilution of the injected CO_2 in different ways. Previous investigations are first reviewed, in particular Auerbach [4], Caulfield [18], and Sato *et al.* [108], and then these methodologies are adapted to the present study. The specific discharge scenarios considered are also described in this section.

3.1   Previous studies

Since the goal of the present study is to update the original work of Auerbach [4, 5] and Caulfield [18, 19] with new biological data and enhanced discharge approaches, these studies are first reviewed in detail. Two additional acute impact modeling studies are also reviewed briefly, Sato *et al.* [108] and Chen *et al.* [21]. As discussed in Section 3.3, much of the biological impact modeling approach of Sato *et al.* [108] is ultimately adopted in favor of the Auerbach [4] approach, although many elements of the original framework of [4] and [18] are retained in the present study.

3.1.1 Auerbach *et al.* (1997) and Caulfield *et al.* (1997)

Together these studies simulated the acute biological impact to clusters of organisms due to a variety of discharges. Their approach consisted of three parts:

- Calculation of the CO_2 concentration and pH field due to the discharge.

- Simulation of the exposure history of each organism cluster, i.e., its trajectory through the plume.

- Calculation of cumulative impact to each organism cluster (% mortality).

The overall impact of a discharge scenario was calculated by considering the fate of a large number of organism clusters entering the discharge area at different locations. Each of these steps is described below. Note that the terms organism and organism cluster are used interchangeably even though the model technically simulates the latter (since a percent mortality does not make sense for a single organism).

Discharge scenarios (plume modeling)

Although Caulfield *et al.* [19] reports on only two discharge scenarios, the original work by Caulfield [18] considered four scenarios. A brief outline of each scenario is given below; details of the plume calculations can be found in [18] but will not elaborated on here as the present study considers different scenarios. For each scenario, CO_2 loadings of 130 and 1,300 kg/s were considered, which was taken as the CO_2 produced by 1 and 10 500-MW coal-fired power plants including an energy penalty for capture and storage. Summary statistics of the plumes modeled by [18] are shown in Table 3.1.

Dry ice release: Dry ice cubes would be released from a fixed location at the surface of the ocean. For the 3-meter cubes considered, this corresponds to one cube every 5.4 minutes for a single power plant release. Plume calculations assumed that the descending cubes form a two dimensional line source (extending to the sea-floor) spread by a combination of ambient and cube-induced (wake) turbulence.

Towed pipe release: Liquid CO_2 would be released from a pipe which is towed by a ship traveling at 5 m/s using a 1-m diameter pipe with diffusers which distribute the CO_2 over a depth range of 1000-1500 m. As in the dry ice scenario, plume calculations assumed a two dimensional line source spread by the combination of ambient and pipe-induced (wake) turbulence.

Unconfined droplet plume release: Liquid CO_2 would be released from a fixed multiport diffuser at 1000-1500 m, forming a buoyant plume which distributes the CO_2 vertically. CO_2 enters the surrounding water column through a series of discrete *peeling events* caused by the entrainment of seawater by the plume as the droplets rise. Here the entrainment dilutes the outer portion of the plume, causing it to detach from the more buoyant inner core of the plume and sink until it reaches neutral buoyancy, forming an *intrusion layer*. Although it is unclear what spacing between diffuser ports was used in the calculation, a flow of 13 kg/s was specified for each port and plumes from neighboring ports were assumed to interact only in the diffusive regime, i.e., after intrusion. All peeling events were combined into a single intrusion layer, forming a relatively thin but wide two-dimensional plane source. The maximum thickness of the intrusion layer was calculated as 23 m in each case, with widths of 880 m and 8800 m for the 1 and 10 plant releases (reflecting the fact that a longer diffuser was used in the 10 plant case).

Descending confined dense plume release: Here seawater would first be enriched with CO_2 in a confined vessel, and the resulting dense mixture would be released along the sea floor in a confined trench. The plume would eventually reach a level of neutral buoyancy and form an intrusion layer, which was modeled as a two-dimensional plane in a manner similar to the droplet plume. A single plant release created an intrusion layer 23 m thick (at its maximum) and 520 m wide at 1,000 m depth when released from 855 m; a ten plant release from 755 m reached the same depth and thickness but with a width of 3,000 m.

	Volume with pH < 7 (km^3)	Distance to pH 7 (km)	Min pH
Dry Ice, 1 plant	0.001	0.09	6.1
Dry Ice, 10 plants	1.1	2.2	5.8
Towed pipe, 1 plant	0.00004	0.2	6.5
Towed pipe, 10 plants	0.3	14	5.7
Droplet plume, 1 plant	1.8	23	5.5
Droplet plume, 10 plants	130	60	5.5
Dense plume, 1 plant	7.2	94	4.0
Dense plume, 10 plants	510	690	4.0

Table 3.1: Plume characteristics modeled by Caulfield [18]

The relative dilution achieved by each scenario modeled by Caulfield [18] is demonstrated by her plot of centerline dilution as a function of time (equivalent to distance assuming a current velocity of 0.05 m/s or a ship speed of 5 m/s), as shown in Figure 3-1. Caulfield attributes the advantage of the dry ice and towed pipe scenarios to their large plume thicknesses, but also points out the likely higher cost of these approaches. For the two fixed plume scenarios, she notes the advantage of the droplet plume in achieving greater dilution and allowing more design flexibility.

Organism exposure history

The exposure history of an organism cluster was obtained by simulating its trajectory through the plume. Caulfield [18] considered only planktonic organisms, i.e., floating organisms that move with ambient currents and exhibit little to no ability to influence their horizontal position. Although some planktonic organisms can migrate vertically hundreds of meters per day (diel migration), this effect was conservatively ignored as it was thought to lessen impact by allowing organisms to escape the plume. Thus, organisms were assumed to move only in the horizontal plane.

The fate of organisms drifting through the plume was modeled as a relative diffusion problem between the organism and the plume. Specifically, the separation distance y between the organism cluster and the plume centerline was modeled using
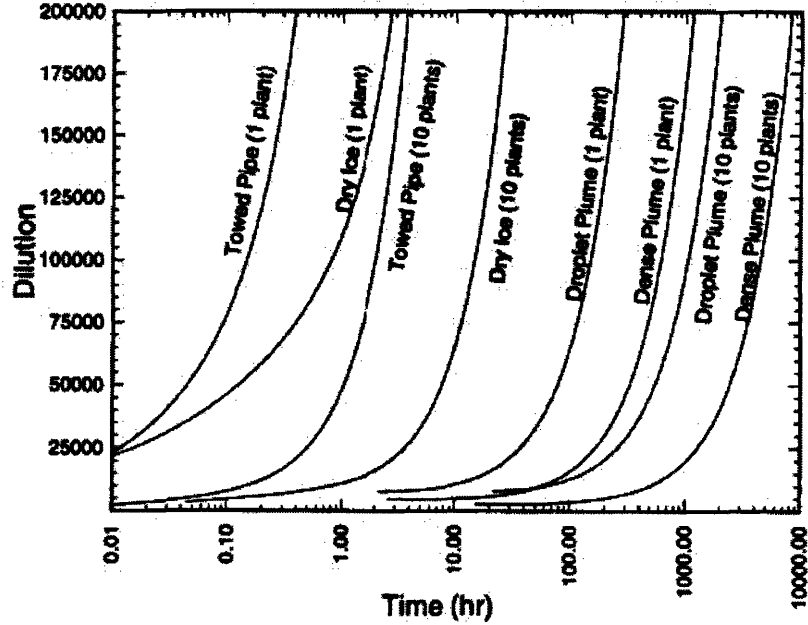
Figure 3-1: Centerline dilution over time for the base case scenarios considered by Caulfield [18].

a modified version of Richardsons's distance neighbor equation [103]:

$$\frac{\partial p(y)}{\partial t} = \frac{\partial}{\partial y}\left(F(y)\frac{\partial p(y)}{\partial y}\right) \tag{3.1}$$

where $p(y)$ is the probability that an organism is at y at time t given an initial separation of y_0, and $F(y)$ is a scale-dependent distance-neighbor diffusivity given by

$$F(y) = 0.0017y^{1.15} \tag{3.2}$$

where F and y have units of m^2/s and m, respectively. The diffusivity defined by (3.2) is based on the data from Okubo [92] on the radial spreading of dye releases in surface layers of coastal waters. Caulfield [18] describes simulating (3.1) with a Monte Carlo technique, although few details are given. Implementation of this modeling approach in the present study is given in Section 3.3.1.
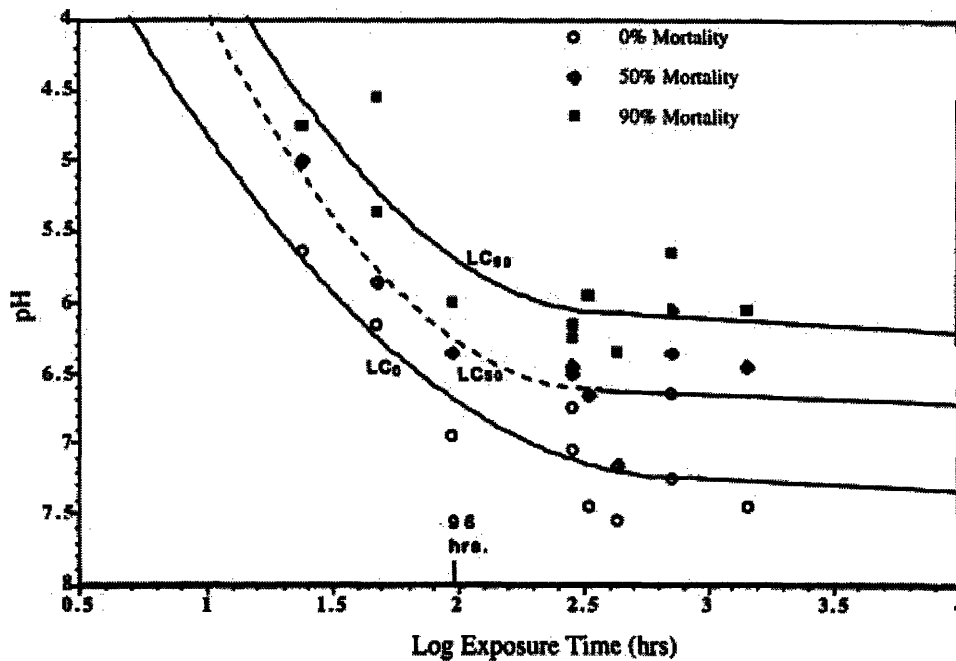
Figure 3-2: Compiled pH mortality dataset and derived isomortality curves from Auerbach [4].

Cumulative impact to the organism (isomortality modeling)

The response of the organism to the plume was modeled as consisting of two parts: (1) a % mortality based on observed relationships between mortality, exposure pH, and exposure time; and (2) a population recovery based on a growth rate which varies with exposure pH.

Isomortality calculations

Auerbach [4] developed the *isomortality* methodology for calculating the cumulative impact to an organism cluster based on its exposure history. He began by developing isomortality curves, which were equations expressing LC_0, LC_{50}, and LC_{90} as a function of exposure time, from a compilation of available pH mortality data (see Chapter 2). The dataset included zooplankton and benthos data, and in all cases the acidifying agent was not CO_2. The derived isomortality curves are shown in Figure 3-2.

Auerbach [4] gives few details of how the source data were merged and manipulated. However, it is noted that some data have been shifted to account for observed adverse reproductive effects, and that all datapoints were shifted "downward" by 0.25 pH units to be conservative.

The basic assumption behind this method is that there is an equivalence between low pH exposure for a short time and higher pH exposure for a longer time. Auerbach [4] discusses the justification of this approach. Although a number of variations of the isomortality calculation are described in [4], the basic method employed involves the following steps:

1. Divide the exposure history into N discrete time intervals (Δt_1, Δt_2, ..., Δt_N), and define an average exposure for each interval (pH_1, pH_2, ..., pH_N).

2. For interval Δt_1, calculate a fractional mortality (population deficit), D_1, by interpolating between the isomortality curves at $t = \Delta t_1$ to pH_1 (extrapolate if beyond LC_{90}).

3. Estimate the equivalent cumulative time, t_1^*, that corresponds to D_1 had the organism been exposed to pH_2 instead, i.e., move along the isomortality line that corresponds to D_1. Thus, t_1^* is defined by the equality

$$D(pH_2, t_1^*) = D_1. \qquad (3.3)$$

which must be solved iteratively since the curves are nonlinear and nonparallel.

4. Calculate the mortality after the second step, D_2, by interpolating/extrapolating between the isomortality lines at exposure time $t_1^* + \Delta t_2$ to pH_2.

5. Repeat steps (3) - (4) for all remaining time intervals.

Although not explicitly stated in [4] or [18], before reaching non-zero mortality the equivalent cumulative time is incremented by moving parallel to the LC_0 curve.

Population recovery

Caulfield [18] allowed for species recovery in regions of low stress to account for species reproduction. This was modeled using a logistic equation appropriate for a single species population:

$$\frac{d\frac{N}{K}}{dt} = r\frac{N}{K}\left(1 - \frac{N}{K}\right)$$ (3.4)

where N is the number of organisms, K is the "carrying capacity" (maximum number of organisms that can exist), and r is the growth rate with unlimited resources. Thus, $\frac{N}{K}$ is the fractional population, and $\left(1 - \frac{N}{K}\right)$ is the population deficit. The growth rate r was based on laboratory observations of surface copepods and specified as:

$$r = \begin{cases} 0 & pH \le 7.35 \\ 0.09\left(\frac{pH-7.35}{0.15}\right) \text{ day}^{-1} & 7.35 < pH < 7.5 \\ 0.09 \text{ day}^{-1} & pH \ge 7.5 \end{cases}$$ (3.5)

It should be noted that because a species recovery was included, a finite impact zone could be defined for each plume, i.e., at some distance from the source the plume becomes sufficiently dilute and species populations are allowed to recover to their original levels.

Acute impact estimates

The combined investigations of Caulfield [18] and Auerbach [4] yielded the acute impact estimates summarized in Table 3.2. Three measures of impact were used. First, *integrated total mortality* is the spatial integration of mortality over the impacted volume, which may be thought of as an equivalent volume of "dead water". Similarly, the *mortality flux* is the flow rate of "dead water" crossing a plane perpendicular to the plume centerline, which is expected to vary along the centerline. Third, the *maximum spatial defecit* is given by the grid cell with highest average deficit.

The results are qualitatively similar to the pH impact volumes in Table 3.1, i.e.,

	Integrated Total Mortality (km^3)	Max Mortality Flux (m^3/s)	Max Spatial Deficit (%)
Dry Ice, 1 plant	0	0	0
Dry Ice, 10 plants	0	0	0
Towed pipe, 1 plant	0	0	0
Towed pipe, 10 plants	0	0	0
Droplet plume, 1 plant	0.45	307	11
Droplet plume, 10 plants	162	27500	69
Dense plume, 1 plant	11	1980	50
Dense plume, 10 plants	800	46900	95

Table 3.2: Acute impact estimates from Caulfield [18]

the dry ice and towed pipe scenarios cause the lowest impact, the dense plume causes the most impact by far, and the droplet plume is in between.

3.1.2 Sato *et al.* (2004)

The use of the isomortality method has been extended and somewhat generalized by Sato *et al.* [108], based on initial work in Sato and Sato [110]. This *extended probit* model is based on the standard assumption used in the LC$_{50}$ concept, namely that the acute mortality of a species follows a sigmoid function of the log of the concentration of the toxic agent (see Finney [37]). The sigmoid function is made linear by the probit transformation

$$Z = \int_{-\infty}^{Y-5} \frac{1}{\sigma\sqrt{2\pi}} \exp\left(-\frac{(X-\mu)^2}{2\sigma^2}\right) dX \qquad (3.6)$$

where $X = \log(x)$ which has mean μ and standard deviation σ, x is the concentration of the toxic agent, Z is the probability (mortality), and Y is the probit of Z. Applied to $\log(x)$ vs $\log(t)$ plots of mortality (e.g., the data in Figure 2-8), (3.6) can yield a linear relationship between probit transformed mortality Y, $\log(x)$, and $\log(t)$:

$$Y = a\log(t) + b\log(x) + c \qquad (3.7)$$

67

where a, b, and c are regression constants. The cumulative mortality can then be expressed as

$$Y = a \log \left(\int_0^t [x]^{b/a} \, d\tau \right) + c \qquad (3.8)$$

which can be estimated numerically by dividing organism exposure into a series of discrete steps in a manner similar to Auerbach [4, 5]. Thus, the probit mortality model is a generalization of Auerbach's isomortality approach in that the assumption of a sigmoid function to describe acute toxicity yields a single probit function which describes all isomortality curves, as Auerbach called them. By contrast, Auerbach derived isomortality relationships for each of three different impact levels (LC_0, LC_{50}, and LC_{90}) by independently fitting curves to the data corresponding to these impact levels, and then interpolating linearly between them as needed. In the present study, the term isomortality curve or function is for convenience also used to describe the probit function (3.7) proposed by Sato $et\ al.$ [108], since this function defines lines of equal mortality for any mortality level.

Sato $et\ al.$ [108] fitted their probit function to copepod mortality data from the study later reported in Watanabe $et\ al.$ [139], focusing specifically on $Metridia\ pacifica$ (a species which exhibited relatively high CO_2 sensitivity). Two discharge scenarios were evaluated: (1) a fixed pipe discharging 1 kg/s CO_2 (spray droplets) from each of 100 nozzles spaced 10 m apart over 1,000 - 2,000 m depth, and (2) the same pipe towed by a ship moving at 4 knots (about 2 m/s). The resulting CO_2 plume was calculated using a CFD simulation forced by low-wavenumber ocean eddy velocity data (see [108] for details). Simulations predicted "nontrivial" mortality for the fixed pipe scenario and insignificant mortality for the towed pipe scenario. The latter finding was based on the fact that the target organism, a single copepod traveling with the plume, reached a ΔpCO_2 within 100 μatm of the ambient value $before$ reaching 0.125% mortality, which was taken as the threshold for adverse effects.

The work in Sato $et\ al.$ [108] was an improvement upon the earlier work by Sato and Sato [110] (where the probit approach was first introduced) and Sato [107]. Here the original isomortality curves by Auerbach were used to derive a probit equation,

i.e., the impact analysis was based on non-CO_2 induced mortality. The form of the resulting equation was quadratic in [110] and linear in [107], and it was applied to different discharge scenarios. The main scenario considered in each study was a 200 kg/s descending droplet plume released at 2,000 m depth over 10 hours (from a ship which changed location every 10 hours). Despite reaching pH values as low as 4.2, zero mortality was predicted in Sato and Sato [110] for three test organisms encountering the discharge nozzle, i.e., mortality did not surpass 0.125% (which was again taken as the threshold for impact). Similarly, the plume was predicted to reach pH as low as 4.7 in Sato [107], but with negligible biological impact. These findings were consistent with an earlier work, Sato and Hama [109], which considered the same injection scenario using Auerbach's method and data directly.

3.1.3   Chen *et al.* (2004)

Rather than constructing isomortality curves from observed mortality data, Chen *et al.* [21] used "biological activity" data to develop a relationship for activity as a function of pH and time of the form

$$A_k = \exp\left(\frac{-t^2}{\sigma}\right) \tag{3.9}$$

where A_k is an activity index which varies from 1 (normal activity) to 0 (no activity), t is the exposure time, and σ is a fitting parameter which varies with pH and organism type. Relationships were derived for pelagic zooplankton using the data from Watanabe [138] described in Section 2.3, and were implemented in an Eulerian-Eulerian scheme (see [21] for details). It is noted that the activity index method does not take mortality into account, meaning that organisms reaching $A_k = 0$ are allowed to recover. As such, the approach is an attempt to model sub-lethal effects due to pH perturbations, and the authors note that future improvements to the model will incorporate mortality effects.

A test case was studied in which 1 kg/s of CO_2 (droplets with lognormally distributed sizes and a mean diameter of 8 mm) was injected about 1,000 m depth into

a mean current speed of 2.35 cm/s. The resulting pH field for the buoyant plume was computed with the LES model described in [20], yielding a minimum pH of 5.6 near the nozzle (ambient pH was 7.57). Zooplankton were predicted to be most injured (lowest activity) about 20 m downstream from the nozzle and recovered to normal activity levels about 100 m further downstream (within 2 hours). Thus, the impact of this small injection on zooplankton was confined to a small region.

3.1.4   Other investigations

The studies in the prior sections were reviewed in detail because they develop original methods for assessing acute biological impacts. In addition, there are a large number of studies which provide quantitative estimates of water quality impacts of various discharge schemes to the open ocean. For example, near-field modeling studies of stationary sources (bubble, droplet or hydrate plumes) include Liro et al. [80], Golomb et al. [43], Haugan et al. [49], Thorkildsen and Alendal [129], Sundfjord et al. [121], Sato and Hama [109], Alendal and Drange [2], Drange et al. [35], Nihous et al. [89], Chen et al. (2003 [20] and 2005 [23]), Adams and Wannamaker [1], and Wannamaker and Adams [137]. Modeling studies of near-field CO_2 dilution from a towed pipe include Ozaki et al. [94], Chen et al. (2002 [22], 2005 [23], and 2006 [24]), Minamiura et al. [86], Hirai et al. [54], Adams and Wannamaker [1], Jeong et al. [66], and Tsushima et al. ([133], which also applies the Sato et al. [108] framework and concludes negligible biological impact for a 100 kg/s towed pipe discharge). In addition, the far-field water quality impacts of injection schemes have been considered by numerous studies, including Dewey and Stegen [31], Stegen et al. [116], Nakashiki and Ohsumi [88], Xu et al. [143], Dewey et al. (1997 [33] and 2000 [32]), Wickett et al. [142], Caldeira and Wickett [15], Masuda et al. [82], and Magi et al. [81].

3.2 CO_2 discharge scenarios & plume modeling

Three CO_2 discharge scenarios are considered in the present study: a sinking CO_2 hydrate plume released from a fixed platform, CO_2 hydrate particles released from a

moving ship, and rising CO_2 droplets released from a bottom manifold. The scenarios are based on those developed in Adams and Wannamaker [1], but have been adapted to incorporate enhanced understanding of discharge possibilities. For each discharge scenario, loadings of 10, 100, and 1000 kg/s are evaluated (for reference, a 500-MW coal-fired power plant generates about 95-126 kg/s CO_2 [53]).

3.2.1 CO_2 hydrates

Two of the scenarios discharge CO_2 as clathrate hydrate particles ($CO_2 \cdot 5.75H_2O$), which warrants some discussion. The benefit of hydrate particles is that they are negatively buoyant, meaning that a sinking plume can be generated at shallower depths than those that would otherwise be required using liquid CO_2 (which becomes negatively buoyant in the 2000 - 3000 m range, depending on ocean conditions). Although pure hydrate particles have a density of about 1,143 kg/m^3 (i.e., about 10% more dense than seawater), such particles have not yet been achieved in laboratory or field studies [78]. As discussed in West *et al.* [141], present approaches form hydrates in a reactor vessel by creating a slurry of the reactants in a coflow injector. Under a steady flow of CO_2 this setup yields an extruded cylindrical hydrate particle which breaks off at the nozzle due to shearing by the ambient current once it reaches some critical length. To date, particle diameters of up to 0.7 cm have been achieved in a laboratory setting. In field studies, CO_2 hydrate particles up to 2.2 cm in diameter with a typical length of 30 cm have been observed at about 1,500 m depth with conversions in the range 10-55% [104, 131, 132]. The result of a partial hydrate conversion is a composite particle that is partially pure hydrate and partially unreacted CO_2 and water "stuck" to the hydrates. For the present purpose, composites are referred to as hydrate particles even if conversion is less than 100%.

Both the size and conversion percentage of a particle are important in dictating the fate of the CO_2 that is locked within the particle. Conversion efficiency dictates the density and thus the settling speed of the discharged particle, while the particle diameter dictates the time required for it to dissolve. Observations of descending hydrate particles indicate a particle dissolution rate of about 6 μm/s, and that this

71
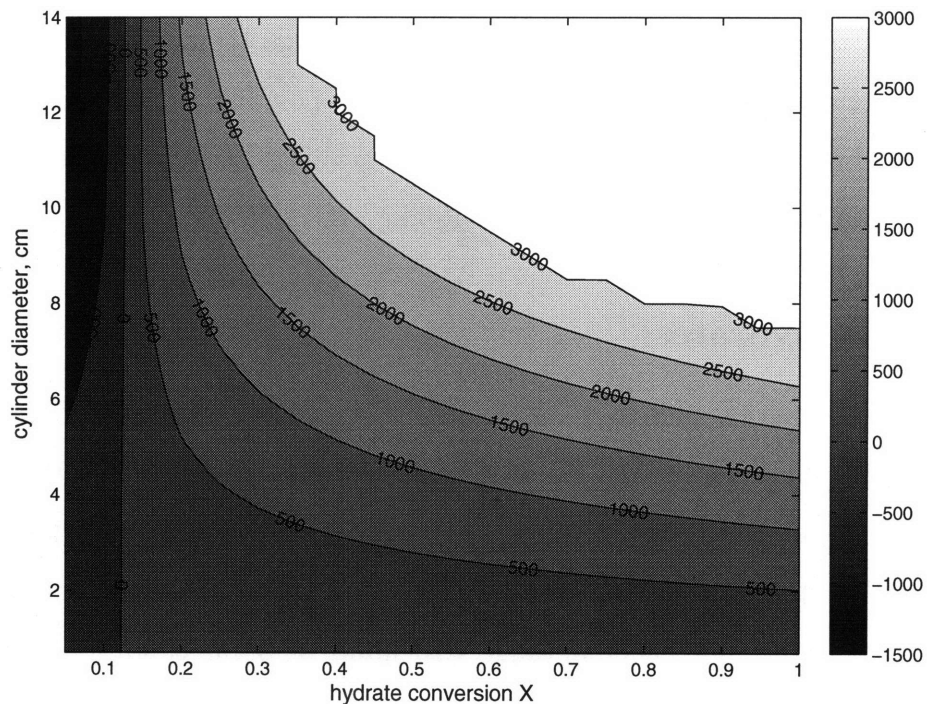
Figure 3-3: Descent depth as a function of particle diameter and conversion efficiency for 30 cm long cylindrical CO_2 hydrate particles released at 1,500 m depth into a typical ocean stratification (Aaron C. Chow, 2007, unpublished work conducted at MIT).

rate is not strongly dependent on the conversion percentage. Figure 3-3 shows the dependence of the settling depth on conversion percentage (X) and diameter for individual 30 cm long cylindrical hydrate particles discharged at 1,500 m depth into a typical stratified ocean of 4,500 m depth (i.e., a descent depth of 3,000 m indicates the particle reaches the sea-floor). Figure 3-3 is calculated using the approach of Riestenberg *et al.* [104], using a constant particle dissolution rate and a particle density that assumes that the unreacted CO_2 and water in the reactor vessel "stick" to the converted hydrates. If the particle loading is sufficiently large relative to the ambient crossflow, multiple particles will together form a descending plume which will sink further then the descent depths in Figure 3-3 due to the combination of a *group effect* and a *solute density* effect.

Before proceeding to the specific discharge configurations considered herein, it

should be noted that the main challenge ahead for improving hydrate formation techniques is to increase the conversion percentage. Ongoing research suggests that creating particles of larger diameter with conversion percentages similar to those created to date should not pose a major problem, although it may require different configurations for introducing the CO_2 into the reactor vessel (e.g., using multiple injection nozzles or a radial injection from around the perimeter). It is thus reasonable to assume that some flexibility will be available in the future to generate larger particles with higher and more controlled hydrate conversion percentages.

3.2.2 Stationary CO_2 hydrate plume

In this scenario an offshore stationary pipe extends from the ocean surface down to a depth of 1,500 m, discharging hydrate particles which are 30 cm long with a reaction efficiency of 25% (shown schematically in Figure 3-4, which was modified from [1]). The combination of the negatively buoyant particles and the increased density of the seawater surrounding the descending particles causes enhanced sinking. Particle diameter is calibrated to yield a plume which dissolves entirely over the remaining depth of the water column (3,000 m in this case) such that the CO_2 plume does not intercept the ocean floor. The discharge is somewhat idealized since with present day hydrate discharge technology the conversion efficiency is difficult to control, but nonetheless it is in theory possible to calibrate particle diameter for a given discharge configuration to generate a plume with the correct average descent depth even if a range of conversion efficiencies were created. For the present purpose this was achieved using a near-field integral plume model, specifically a version of the double plume model described in Adams and Wannamaker [1], which has been modified to handle cylindrical hydrate composite particles. The same model was applied in Riestenberg *et al.* [104]. Mass loadings of 10, 100, and 1000 kg/s resulted in plume descent depths near the ocean floor using initial particle diameters of 8.3, 5.8, and 3.1 cm, respectively, for a 25% hydrate conversion. As the plume descends, entrainment of the surrounding water column leads to reduced density in the outer core of the plume which causes detrainment of the outer core in a series of discrete *peeling events*.

Thus, the plume introduces CO_2 to the surrounding environment through a number of *intrusion layers* (one for each peeling event). As in [1], near field plume model results suggest that such a source can reasonably be approximated as a thin two-dimensional plane source extending from 1,500 m to the bottom of the ocean (at 4,500 m) with no particle deposition on the sea-floor. Following [1], the resulting plume is assumed to have an initial width w given by:

$$w = \frac{\dot{m}}{hDIC_0 u_a} \tag{3.10}$$

where $\dot{m}$ is the carbon mass loading rate, h is the plume height (3000 m), u_a is the ambient (mean) current speed, and DIC_0 is the average plume concentration of excess dissolved inorganic carbon (i.e., above background) within the intrusion layers as computed by the near-field model. Since the lateral shape of the source is likely closer to a Gaussian distribution than a rectangular plane source, the downstream lateral diffusion of this depth-averaged plume is modeled as:

$$DIC(t,y) = \frac{\dot{m}}{\sqrt{2\pi}hu_a\sigma_y} \exp\left[\frac{-y^2}{2\sigma_y^2}\right]. \tag{3.11}$$

where $\sigma_y = \sigma_y(t)$ is the standard deviation of the Gaussian concentration distribution and t is the time since discharge, which can be converted to longitudinal distance from the source (x) by substituting $t = \frac{x}{u_a}$. The initial concentration distribution is parameterized by $\sigma_{y,0} \equiv \sigma_y(t = 0)$, which is taken as

$$\sigma_{y,0} = \frac{w}{\sqrt{12}} \tag{3.12}$$

since this is the standard deviation of the "top hat" distribution corresponding to a uniform rectangular source of width w. In the interest of being conservative, vertical diffusion is ignored in (3.11). Lateral diffusion, i.e., the growth of $\sigma_y(t)$, is modeled using data from Okubo [92] on dye patch spreading in the surface layers of coastal waters:

$$\sigma_y(t) = a\left(t_0 + t\right)^n \tag{3.13}$$
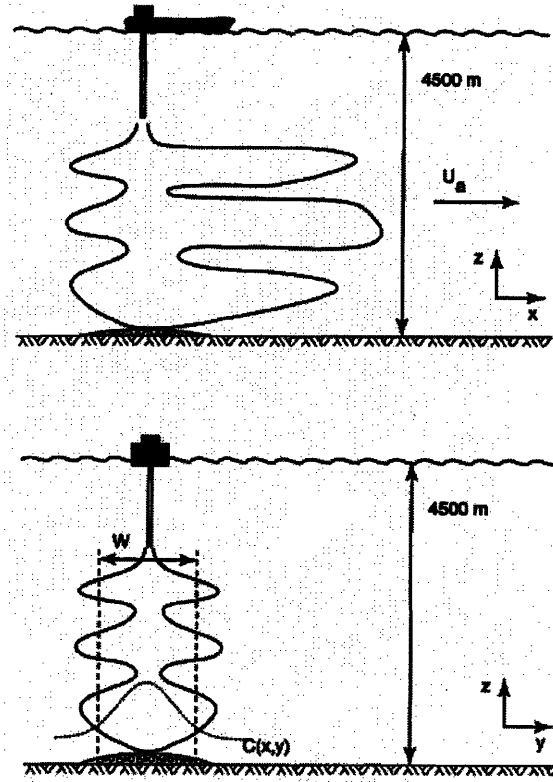
Figure 3-4: Schematic illustration of the stationary CO_2 hydrate plume discharge, adapted from Adams and Wannamaker [1].

where $a = \frac{0.00071}{\sqrt{10}}$ for t in s and $\sigma_y(t)$ in m; $n = 1.15$; and t_0 is a fictitious plume initial time, i.e., the time required for a point source ($\sigma_{y,0} = 0$) to reach the actual $\sigma_{y,0}$ of the plume being considered if it grows according to (3.13). In the interest of being conservative, the value of a used in the present study is reduced by a factor of $\sqrt{10}$ to reflect the reduced mixing expected for deeper waters (i.e., diffusivity is thereby reduced by a factor of 10). The nominal value of $u_a = 0.05$ m/s used by Adams and Wannamaker [1] is also applied here.

3.2.3 Moving CO_2 hydrate release ("towed pipe")

A ship traveling at speed u_s in a direction perpendicular to the ambient current u_a releases hydrate particles at 1,500 m depth from a towed pipe (Figure 3-5). The particles are 30 cm long and of a fixed diameter d with hydrate conversion percentages uniformly distributed over the range 10-55% (consistent with the range observed

75
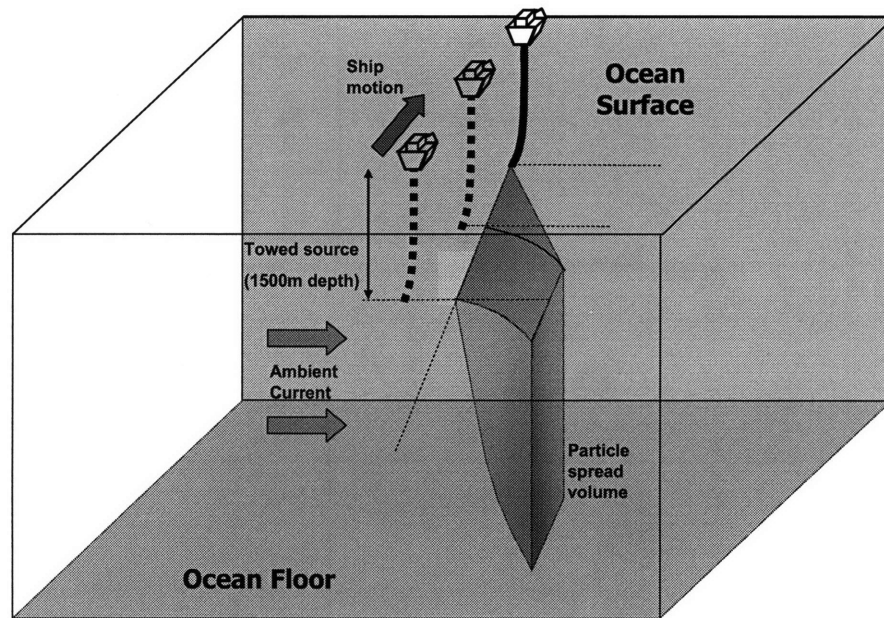
Figure 3-5: Schematic illustration of the towed pipe CO_2 hydrate plume discharge in a crossflow.

during a recent field study). The ship is moving sufficiently fast such that the descending particles do not form a negatively buoyant plume but rather settle as a collection of individual particles (i.e., the particles create a passive plume of CO_2, but not a buoyant plume which actively entrains the surrounding seawater). Thus, the descent depth of each particle depends on its diameter and conversion efficiency as was discussed previously (see Figure 3-3). Four different discharge configurations are considered using particle diameters of 2.5, 5, 10, and 15 cm. For each configuration, the discharged particles have the same diameter but varying hydrate fractions. Because a constant dissolution rate is assumed, all particles drift the same distance in the direction of the ambient current u_a but reach different depths before dissolving completely (e.g., the 10% hydrate particles are positively buoyant and will rise while the 55% hydrate particles will sink and reach the greatest depth). As illustrated in Figure 3-6, the result is a plume with a wedge-shaped cross sectional area.
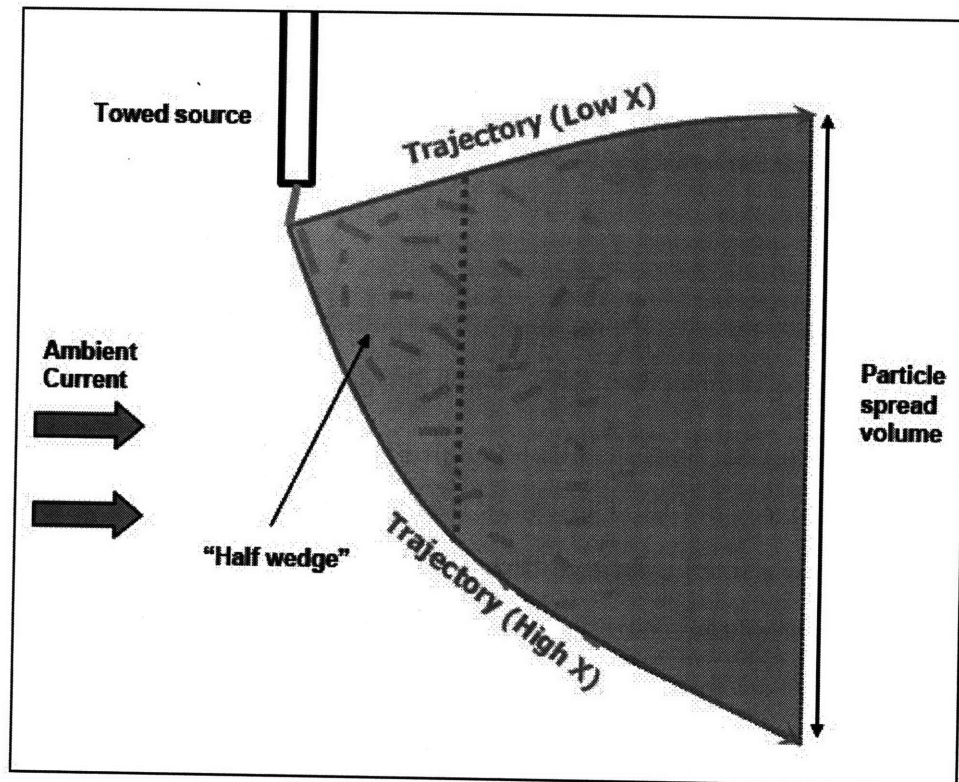
Figure 3-6: Schematic illustration of the source due to the towed pipe CO_2 hydrate plume discharge into a cross flow.
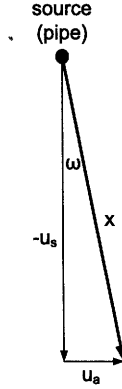
Figure 3-7: Illustration of towed pipe moving reference frame. The source travels (up) with velocity u_s and there is a prevailing ambient current u_a such that in a fixed reference frame the plume centerline (longitudinal coordinate x) would be at an angle $\omega = \tan^{-1}\left(\frac{u_a}{u_s}\right)$ to the $-u_s$ direction.

The plume created by this discharge can be modeled using (3.11) if u_s is sub-stituted for u_a, such that (3.11) describes the concentration distribution trailing the towed pipe in a moving reference frame, i.e., it is perfectly analogous to the situation where the source is fixed and the CO_2 mass is advected downstream by a current of speed u_s. In terms of a fixed reference frame, the longitudinal coordinate $x = u_s t$ is the distance along the plume centerline, which is at an angle $\omega = \tan^{-1}\left(\frac{u_a}{u_s}\right)$ to the negative u_s direction (see Figure 3-7), and the lateral coordinate y is perpendicular to x. For the present purpose, the moving reference frame is more relevant, since both CO_2 mass and organisms within the plume move at ambient current u_a, and since the relative diffusion as parameterized by Okubo's relation (3.13) is the same in either reference frame.

As in the fixed hydrate plume release scenario, the initial concentration distribu-tion is assumed to be Gaussian with an initial width $\sigma_{y,0}$. For analytical convenience, the wedge-shaped source shown in Figure 3-6 has been simplified in the following manner. First, the distance λ (in the direction of the ambient current) over which half of the CO_2 mass dissolves is calculated, which corresponds to about one third of the total distance traveled by the particle before dissolving. As shown in Figure 3-6, this defines a "half-wedge" with area A_{hw} and height h_{hw} (the vertical separation

between the lightest and heaviest particles after drifting λ with the ambient current). Second, the width of a rectangular source with area and height equal to that of the half-wedge is calculated:

$$w = \frac{A_{hw}}{h_{hw}} \tag{3.14}$$

Finally, the $\sigma_{y,0}$ is calculated by (3.12) in the same manner as for the stationary hydrate plume release scenario. These simplifications amount to placing all of the mass loading into the half-wedge area, i.e., the average excess DIC concentration through this region would equal $\frac{\dot{m}}{u_s A_{hw}}$.

The reasoning behind the simplification of the source shape is not limited to analytical convenience. The rate of mass loss from the descending particle is proportional to the surface area, which is proportional to $(1 - kt)^2$ (where k is the particle dissolution rate which is assumed to be constant). Thus, the wedge-shaped source will have the highest concentrations near the top left corner, with the lowest concentrations at the leading edge of the wedge. The area of the half-wedge (which in reality contains half of the mass) is only about 10% of the area of the total wedge. By placing all the mass in the half-wedge and by computing an equivalent width by (3.14), the source is made much shorter and thinner than it is in reality. This helps to offset the fact that we do not resolve the concentration gradients within the wedge, and from a biological impact perspective is an attempt to be more conservative.

The discharge scenario is implemented using $u_a = 0.03$ m/s and $u_s = 3$ m/s ($\approx$ 6 knots), which yields the plume characteristics summarized in Table 3.3. For this combination of u_a and u_s, the angle between the ship travel direction and the plume centerline is small ($\omega < 1°$). u_a has here been conservatively reduced from the value of 0.05 m/s used in the two other discharge scenarios because a ship trajectory will likely at times (1) traverse regions of the ocean with less favorable currents and (2) not maintain a right angle to the ambient current (if u_a is actually 0.05 m/s, an effective u_a of 0.03 m/s corresponds to a 36° angle between the current and ship).

Hydrate diameters of 2.5, 5, 10, and 15 cm are considered, since as noted previously the formation of large diameter particles is not foreseen to be a major hurdle given

d (cm)	λ (m)	h_{hw} (m)	A_{hw} (m^2)	w (m)	$\sigma_{y,0}$ (m)
2.5	36.6	220	4.13 x 10^3	18.8	5.40
5	73.2	588	2.22 x 10^4	37.7	10.9
10*	146	1550	1.18 x 10^5	76.2	22.0
15**	220	2690	3.11 x 10^5	116	33.4

*about 0.4% of mass is predicted to reach the ocean floor
**about 14% of the mass is predicted to reach the ocean floor

Table 3.3: Plume characteristics for each towed pipe discharge scenario.

current technology. For the largest hydrate diameters, a small fraction of the particle mass is predicted to accumulate on the ocean floor. This effect is ignored in the plume calculation (where all the mass is placed in the "half-wedge") since the mass fraction is small (14% or less) and since the discharge configuration would be refined to avoid this if implemented. For the range of mass loadings and particle diameters considered, the ship speed is sufficiently large to prevent the formation of a buoyant plume, i.e., treatment of the discharge as a collection of individual particles is appropriate. This is concluded from the fact that the predicted plume separation depth due to the "crossflow" (ship motion) is much smaller than the depth at which a plume peeling event would be predicted to occur, as per the methodology of Socolofsky and Adams [115].

This version of a "towed pipe" scenario is thought to be more realistic than the one in Adams and Wannamaker [1], where a single stream of pure hydrate particles was assumed to create a thin plume with $\sigma_{y,0} = 0.1$ m. The scenario described here is based on field observations where a range of conversion percentages was achieved. Combined with an ambient crossflow u_a, this causes a fractionation of the particle trajectories, which offers a beneficial increase in the lateral spreading of the dissolved CO_2 plume. As hydrate formation technology improves, it is conceivable that it will eventually be possible to custom design a discharge configuration which maximizes lateral dilution by optimizing the distribution of discharged particle sizes and/or conversion percentages.
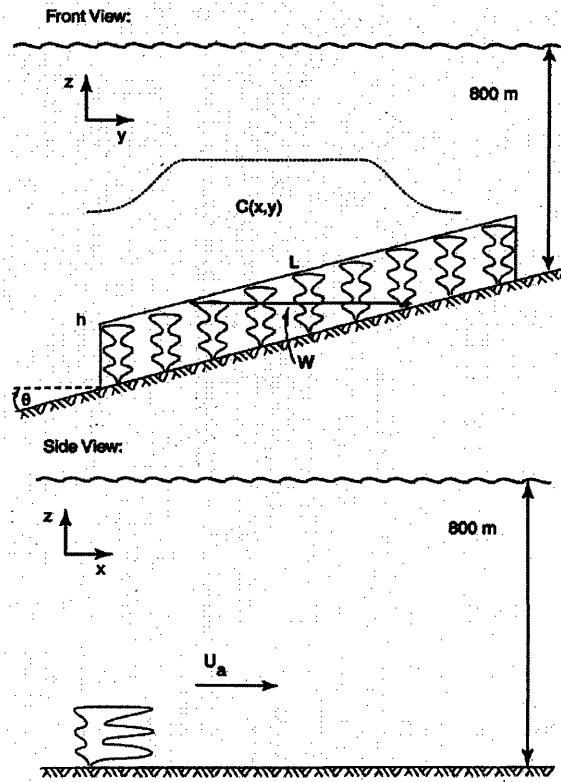
Figure 3-8: Schematic illustration of the bottom manifold CO_2 discharge from Adams and Wannamaker [1].

3.2.4 Rising CO_2 droplets from a bottom manifold

A bottom manifold extends along the sea-floor and liquid CO_2 is injected through equally spaced multiport diffusers starting at 800 m depth to form a series of positively buoyant (rising) plumes which are oriented perpendicular to the ambient current (u_a). Assuming a slope (θ) of 5°, the pipeline would be 13.5 km long in total (L_0), of which approximately the last 4.5 km (L) would be below 800 m (Figure 3-8). Port nozzles with an appropriate diameter would be spaced along L such that a plume height h of 250 m would be achieved (a taller plume would be undesirable for sequestration purposes since the CO_2 would form gas bubbles in the depth range 400-500 m). For example, for $\dot{m} = 100$ kg/s, 100 ports of diameter 0.7 cm each discharging 1 kg/s each would achieve such a plume height, where rising droplets would become covered with a thin hydrate film at this depth.

As in [1], the discharge is simplified into a rectangular source of width $w =$

81

min $\left(\frac{h}{\tan\theta}, L\right)$ and height $h^* = L\sin\theta$ (which is used in favor of the plume trap height h in order to preserve the cross-sectional area of the source). For consistency with the other two discharge scenarios, downstream diffusion of the source is here computed using the Gaussian solution (3.11) in favor of the rectangular source equation used by [1]. As in the other scenarios, (3.12) is used to compute $\sigma_{y,0}$, and the nominal value of $u_a = 0.05$ m/s is used.

In contrast to the other two scenarios in which the CO_2 mass is discharged at 1,500 m depth, this scenario discharges over the depth interval 1,200 - 800 m with a constant plume trap height of 250 m. Thus, from the standpoint of sequestration efficiency (i.e., the length of time the CO_2 is sequestered from the atmosphere), the scenario is less attractive. This can of course be addressed by changing the manifold configuration to reach deeper depths. Likewise, the manifold configuration can be changed to achieve higher dilution by "painting" a larger cross-sectional area with the CO_2. Indeed, it should be possible in theory to select a mass loading and a manifold design that avoids significant acute biological impact altogether (e.g., the total mass loading can be restricted, the diffuser can be extended to deeper depths and the diameter of the diffuser nozzles can increase with depth to achieve greater plume rise). However, cost/benefit considerations will of course dicatate what is feasible in reality. For the present study we have chosen to simply adopt the configuration proposed by Wannamaker and Adams [1] as an illustrative example, recognizing that in the absence of cost constraints the bottom manifold design has a number of degrees of freedom that could be exploited.

3.2.5   Plume representation in the discharge scenarios

The CO_2 discharges are modeled in a manner similar to Auerbach and Caulfield in that an analytical solution is used. By contrast, some previous studies [23, 108, 110] have conducted detailed hydrodynamic modeling near the injection point to resolve small-scale plume gradients. Simplifying the geometry of the source and using an analytical solution amounts to simulating an ensemble plume, i.e., the average plume conditions that might occur over many realizations (see discussion in [62]). This

naturally ignores the small-scale gradients that would be present within the plume during any one realization of the discharge, i.e., the CO_2 concentrations near the source are "smeared" relative to the concentrations that would be observed in a real plume. This approach has two counteracting effects from a biological standpoint. On the one hand, the inherent patchiness and high concentrations that would occur in the immediate vicinity of the source are not represented, likely underpredicting the peak concentration that an organism might experience during a realization. On the other hand, the ensemble plume introduces elevated concentrations to a larger area, which in turn means that a larger number of organisms are exposed to elevated concentrations. The shape of each source has been simplified, but in a manner which attempts to err on the side of keeping concentrations on the high side. For the towed pipe case, all the mass is placed within the "half-wedge" closest to the source (see preceding discussion). For the stationary hydrate plume case, the average concentrations within the intrusion layers is applied over the entire depth of the plume even though the CO_2 really only leaves the plume at these layers, thus yielding a narrower plume (because DIC_0 in (3.10) is higher). In addition, by representing all sources as being Gaussian in shape, peak concentrations are specified near the source so as to reduce the "smearing" effect of the inherent averaging of the plume representation approach.

The approach used here is somewhat analogous to defining a mixing zone as is usually done when setting water quality compliance guidelines for ocean wastewater diffusers. In these cases, water quality standards are typically only enforced at the edge of the mixing zone, i.e., the environmental impact of the discharge is evaluated in terms of its impact on a larger scale rather than on the details of what occurs within the small dynamic mixing zone. Likewise the analysis here focuses on larger scale average impacts as opposed to near-source, small-scale impacts. Although future work might attempt to resolve these effects in the analysis, the reader should note that small-scale patchiness and high concentrations could to some extent be minimized by refining the design of the discharge configurations to homogenize the near-field region.

3.2.6 Treatment of carbonate system chemistry

When CO_2 is introduced to seawater a series of reactions take place which are collectively referred to as the carbonate system [34, 87]:

$$CO_2(g) \rightleftharpoons CO_2(aq) \tag{3.15a}$$

$$CO_2(aq) + H_2O(l) \rightleftharpoons H_2CO_3(aq) \tag{3.15b}$$

$$H_2CO_3(aq) \rightleftharpoons H^+(aq) + HCO_3^-(aq) \tag{3.15c}$$

$$HCO_3^-(aq) \rightleftharpoons H^+(aq) + CO_3^{2-}(aq) \tag{3.15d}$$
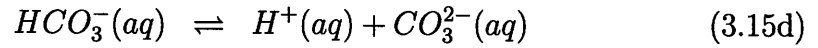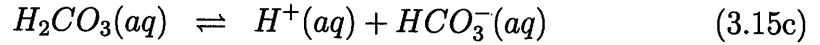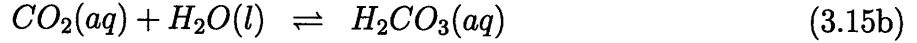
which is here shown for a water sample at equilibrium with the gaseous phase (e.g., at the air-water interface). However, because H_2CO_3(aq) and CO_2(aq) are difficult to distinguish analytically, it is common to combine these terms and designate their sum as $H_2CO_3^*$(aq). Thus, the carbonate system may be expressed as

$$CO_2(g) \rightleftharpoons H_2CO_3^*(aq) \tag{3.16a}$$

$$H_2CO_3^*(aq) \rightleftharpoons H^+(aq) + HCO_3^-(aq) \tag{3.16b}$$

$$HCO_3^-(aq) \rightleftharpoons H^+(aq) + CO_3^{2-}(aq) \tag{3.16c}$$
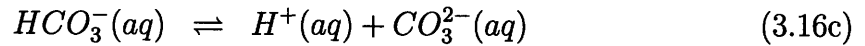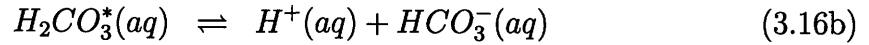
For the present study, the approach summarized by Wannamaker [136] is applied to solve for the equilibrium concentration of the carbonate system components. This approach combines the methodology outlined in Morel and Hering [87] with the equilibrium constants defined by Dickson and Goyet [34]. Briefly, the concentrations of the individual species in (3.16) are calculated by solving the following nonlinear equation for the hydrogen ion concentration [H$^+$]:

$$C - Alk = -[H^+] + 10^{-pKw}[H^+]^{-1} + \alpha_1 DIC + 2\alpha_2 DIC \tag{3.17}$$

where $C - Alk$ is the carbonate alkalinity

$$C - Alk \equiv -[H^+] + [OH^-] + [HCO_3^-] + 2[CO_3^{2-}], \tag{3.18}$$

DIC is the total dissolved inorganic carbon

$$DIC \equiv [H_2CO_3^*] + [HCO_3^-] + [CO_3^{2-}], \qquad (3.19)$$

and α_1 and α_2 are ionization fractions for the bicarbonate (HCO_3^-) and carbonate (CO_3^{2-}) ions

$$\alpha_1 \equiv \left(1 + 10^{pK_1}[H^+] + 10^{-pK_2}[H^+]^{-1}\right)^{-1} \qquad (3.20a)$$

$$\alpha_2 \equiv \left(1 + 10^{pK_2}[H^+] + 10^{(pK_1+pK_2)}[H^+]^2\right)^{-1}. \qquad (3.20b)$$

Here the notation $pK \equiv -\log(K)$ is applied for brevity to K_1, K_2, and K_w, which are the dissociation constants of $H_2CO_3^*$, HCO_3^-, and water, respectively:

$$K_1 \equiv \frac{[H^+][HCO_3^-]}{[H_2CO_3^*]} \qquad (3.21a)$$

$$K_2 \equiv \frac{[H^+][CO_3^{2-}]}{[HCO_3^-]} \qquad (3.21b)$$

$$K_w \equiv [H^+][OH^-]. \qquad (3.21c)$$

The equilibrium concentrations of the carbonate system species are given by

$$[H_2CO_3^*] = \alpha_0 DIC \qquad (3.22a)$$

$$[HCO_3^-] = \alpha_1 DIC \qquad (3.22b)$$

$$[CO_3^{2-}] = \alpha_2 DIC \qquad (3.22c)$$

where the ionization fraction for $H_2CO_3^*$ is given by

$$\alpha_0 \equiv \left(1 + 10^{-pK_1}[H^+]^{-1} + 10^{-(pK_1+pK_2)}[H^+]^{-2}\right)^{-1}. \qquad (3.23)$$

The values for the dissociation constants as a function of temperature and salinity are taken from Dickson and Goyet [34]. Pressure effects on the constants are not included as the present study considers a range of depths and the pressure adjustments are

expected to be minor based on a cursory analysis with the CO2SYS program [79].

Equation (3.17) is solved for [H$^+$] with given values of DIC and $C - Alk$, where DIC is computed during the plume calculations (see Section 3.2) and $C - Alk$ is a constant specific to the seawater being studied. Note that addition of CO$_2$ does not change the value of $C - Alk$. Once [H$^+$] is determined, all species concentrations can be calculated easily. All pH values are reported on the total hydrogren ion scale (as opposed to the free hydrogren ion scale, see [34]).

In the present application, the source of DIC is not in equilibrium with a gaseous phase as indicated by the first equation in (3.15) and (3.16). Instead, CO$_2$(aq) is introduced directly (by dissolving hydrates or droplets). Had the seawater instead been in equilibrium with a gaseous phase, [H$_2$CO$_3^*$] would be constrained to be (e.g., [40])

$$[H_2CO_3^*] = pCO_2 \ K_0(T, S) \tag{3.24}$$

where pCO$_2$ is the partial pressure of the gaseous CO$_2$ and $K_0(T, S)$ is the solubility of CO$_2$, which is an empirical function outlined in Weiss [140] (the difference between fugacity and partial pressure has here been ignored as it is $< 1\%$ for CO$_2$ in seawater at 1 atm). In the present study, (3.24) is used to convert computed H$_2$CO$_3^*$ concentrations to an equivalent pCO$_2$ at atmospheric pressure. This is motivated by the biological mortality data reviewed in Chapter 2, which were for the most part reported in terms of pCO$_2$. pCO$_2$ is a convenient measure because it is easily compared to prevailing atmospheric concentrations. It is usually reported in units of μatm or kPa. In the present study, the latter unit is used, but readers more comfortable with μatm can easily do an approximate conversion by multiplying the pCO$_2$ values by 10^4 (1 kPa $\approx 9.87 \times 10^3 \mu$atm).

In the above calculations, the kinetics of the reactions (3.16) are ignored, i.e., equilibrium is assumed to be established instantaneously. Zeebe *et al.* [147] estimates the timescale to reach equilibrium in seawater to be on the order of 16 s. While this timescale is comparable to that of some near-field plume processes, the present study considers the average conditions caused by simplified representations of the

CO_2 sources and thus disequilibrium kinetics are appropriately ignored, consistent with common practice.

3.2.7 Ambient ocean conditions

The plume and hydrate particle descent calculations above use an ambient density profile taken from a 1999 survey cruise near Keahole Point, Hawaii, as in previous studies (e.g., see [1, 136]). For ocean chemistry calculations, global average values for depths > 2000 m were selected from Volk and Hoffert [135]: salinity = 35 ppt, DIC = 2306 μmol/kg, and C-Alk = 2367 μmol/kg[1]. The temperature used was 3°C for the stationary and towed hydrate releases and 5°C for the bottom manifold, based on the observed temperatures at Keahole Point at release depths of 1,500 and 800 m. For comparison, Volk and Hoffert [135] used a temperature range of 1.5 - 3°C as representative of the deep ocean. The ambient pH computed for these conditions is about 7.94 and 7.90 for temperatures of 3 and 5°C, respectively.

3.3 Biological impact analysis approach

The following section details the methodologies employed in simulating the biological impact. Following Auerbach [4] and Caulfield [18], this consists of two parts: (1) simulating the exposure history of planktonic marine organsism and (2) simulating the biological impact of the exposure. The approach implemented herein is a combination of the approaches of Auerbach [4], Caulfield [18], and Sato et al. [108].

3.3.1 Organism exposure modeling

The present study simulates organisms in a manner that is highly similar to that of Caulfield [18], i.e., planktonic organisms are advected with the CO_2 plume and sample different concentrations as they undergo a random walk in the lateral direction using a diffusivity that increases with distance from the plume centerline. The following

---

[1]Computed using CO2SYS [79] from a reported total alkalinity of 2414 μmol/kg with a phospate concentrations of 2.21 μmol/kg.
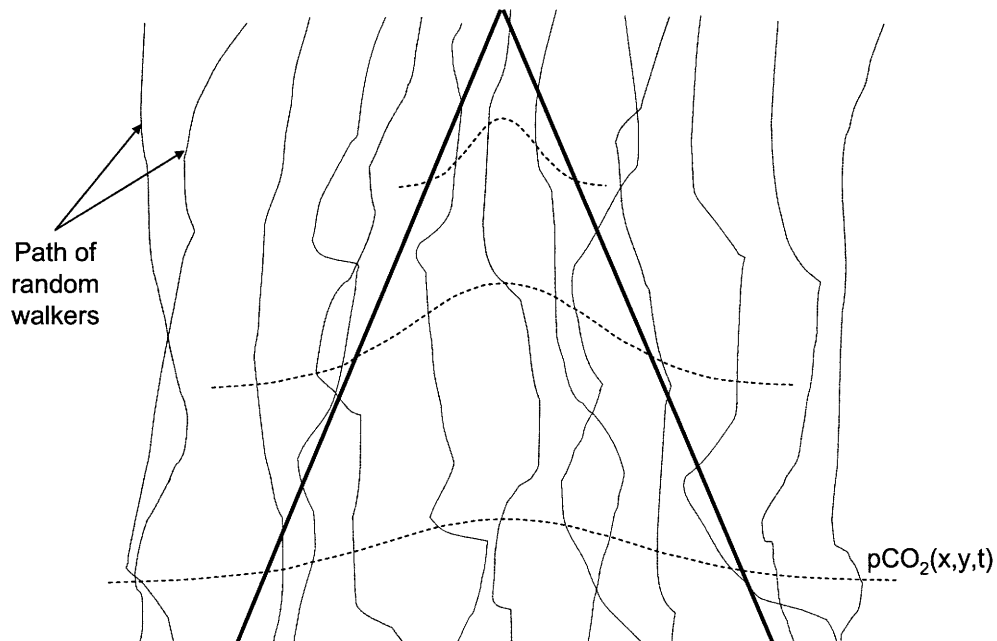
Figure 3-9: Schematic diagram of the simulation of drifting organisms through a CO_2 plume. Organisms undergo a random walk relative to the plume centerline.

section describes the implementation of this approach, expanding on the work of Caulfield [18] and modifying the methodology as needed.

Stochastic simulation of organism trajectory

Caulfield [18] discusses various ways in which (3.1) can be employed to estimate the trajectory of an organism through a plume, including stochastic simulation by a Monte Carlo approach and a number of other approaches aimed at reducing computation time. The subsequent paper Caulfield *et al.* [19], however, only mentions the stochastic approach, and such an approach is employed here. A schematic diagram of this approach is shown in Figure 3-9, where the paths of drifting organisms are tracked through a CO_2 discharge plume.

Although details are not provided, presumably the stochastic simulation was con-

ducted by finding the random walk equivalent of (3.1). Rearranging (3.1) yields

$$\frac{\partial p(y)}{\partial t} + \frac{\partial}{\partial y}\left(p(y)\frac{\partial F(y)}{\partial y}\right) = \frac{\partial^2}{\partial y^2}\left(p(y)F(y)\right). \tag{3.25}$$

Equation (3.25) is similar in form to the one-dimensional Fokker-Planck equation

$$\frac{\partial f}{\partial t} + \frac{\partial Af}{\partial x} = \frac{\partial^2}{\partial x^2}\left(\frac{1}{2}B^2 f\right) \tag{3.26}$$

where $p = p(x)$ is the probability density function of the stochastic variable f, and A and B are coefficients to be determined. Since (3.25) and (3.26) are equivalent if $A = \frac{\partial F(y)}{\partial y}$ and $B = \sqrt{2F(y)}$, (3.25) can be simulated by the random walk equation

$$\Delta y = \frac{\partial F(y)}{\partial y} + \xi\sqrt{2F(y)\Delta t} \tag{3.27}$$

where ξ is a random number drawn from a Gaussian distribution with zero mean and unit standard deviation [42, 128], Δt is the timestep, and Δy is the lateral displacement over Δt.

Equation (3.27) is used to simulate the lateral position of particles (organism clusters) relative to the plume, where both the plume and the organisms move longitudinally with the ambient current u_a. Although Caulfield [18] adapts the method to be more computationally efficient by calculating transition probabilities between cells on a spatial grid rather than for individual organisms, initial simulations with the "brute force" approach described above show that computation time is not a major constraint with present computing technology. Thus, the computational domain is initialized with a sufficiently large number of particles which are all placed at $x = 0$ (where x is the longitudinal coordinate) but spaced out evenly across the domain in y. The domain is bounded in the lateral direction by a reflecting wall placed sufficiently far away from the centerline so as to make it highly unlikely that a particle will reach the plume centerline and the domain boundary multiple times during a simulation. Because of the symmetry of the plumes being modeled, only half of the domain needs to be simulated with particles, and thus another reflecting wall is placed

along the plume centerline. At each timestep, the average pCO_2 experienced by a particle is used to update that organism cluster's % mortality (population deficit) via the isomortality calculation detailed later in this section. A spatial grid is used to bin particles and calculate gridded variables as needed.

Scale-dependent diffusivity

The motion of the organisms relative to the plume centerline is inherently scale-dependent. As organisms move further away from the plume centerline, the scale of eddies that can differentially advect them increases. Since this unresolved motion is parameterized as a diffusivity, this diffusivity must be dependent on the separation distance of the organisms and the plume centerline. This is directly analogous to using a scale-dependent diffusivity to compute the spreading of the discharged CO_2 plume; as the plume becomes larger, it is subject to shearing by eddies of larger scales.

The field data from Okubo [92] on observed diffusion in coastal waters have been reinterpreted to yield a new scale-dependent diffusivity relationship which is applied to simulating the lateral diffusion of organisms relative to the plume centerline. The relationship differs from (3.2), which was used by Caulfield [18]. The derivation of the new equation is outlined below.

Okubo [92] examined the growth of dye patches in coastal waters in two ways. First, he defined the apparent diffusivity K_a implied by the growth of the length scale of dye patches:

$$K_a \approx 0.0103^{1.15} \tag{3.28}$$

where $l \equiv 3\sigma_r = 3\sqrt{2}\sigma_y$ is his length scale, σ_y is the one-dimensional standard deviation of the concentration distribution, and $\sigma_r = \sqrt{2}\sigma_x$ is the equivalent radial standard deviation of the distribution. Second, he developed an equation describing the time rate of growth of the radial variance of the dye patches

$$\sigma_r^2 \approx 0.0108t^{2.34} \tag{3.29}$$

where σ_r is in cm and t is in s. From (3.29) the effective diffusivity E_r and the

apparent diffusivity K_a can be calculated:

$$E_r \equiv \frac{1}{4}\frac{d\sigma_r^2}{dt} \approx 0.00631t^{1.34} \tag{3.30}$$

$$K_a \equiv \frac{\sigma_r^2}{4t} \approx 0.0027t^{1.34} \tag{3.31}$$

where E_r and K_a are in cm^2/s. Thus, (3.29) implies that the effective diffusivity is 2.34 times larger than the apparent diffusivity. The difference is that $K_a(t)$ is the constant diffusivity that would achieve $\sigma_r(t)$ in t, whereas $E_r(t)$ is the actual scale-dependent diffusivity at time t. Thus, multiplying (3.28) by a factor of 2.34 yields the effective diffusivity in terms of the length scale l:

$$E_r \approx 0.0241l^{1.15}. \tag{3.32}$$

Inserting $l \equiv 3\sigma_r$ and (3.29) into (3.32) confirms that (3.32) and (3.30) are equivalent. Because the length scale used by Okubo [92] is arbitrary, for the present purpose E_r is expressed in terms of σ_r or σ_y:

$$E_r \approx 0.0853\sigma_r^{1.15} = 0.127\sigma_y^{1.15}. \tag{3.33}$$

The result in (3.33) is then adapted to the distance-neighbor diffusivity $F(y)$ needed by (3.1) to simulate organism diffusion relative to the plume centerline. Consider a group of particles spread out according to an arbitrary spatial distribution. Richardson [103] showed that for any distribution, the variance of the separation distance between the particles is twice the variance of the distribution. Thus, if the variance of the particle distribution grows at a certain rate, then the variance of the separation distances must increase twice as fast, i.e., its diffusivity must be twice as large. When applying this logic to (3.33) to simulate the separation between a plume centerline at $y = 0$ and an organism located at y, it is not obvious which of σ_y and σ_r is most analogous to the separation distance y. To be conservative, σ_r is selected because it results in a smaller diffusivity. Multiplying (3.33) by a factor of 2

to convert it into a distance-neighbor diffusivity yields

$$F(y) \approx 0.171 y^{1.15} \qquad (3.34)$$

where y is in cm and $F(y)$ is in cm^2/s. Finally, to be consistent with the assumption of reduced horizontal mixing in the deep ocean used in the CO$_2$ plume diffusion calculation, the diffusivity $F(y)$ is reduced by a factor of 10, yielding

$$F(y) \approx 0.00034 y^{1.15} \qquad (3.35)$$

where the units of $F(y)$ and y have been converted to m^2/s and m, respectively. Overall the diffusivities used to separate organisms from the plume centerline in the present study are about one fifth of the values used by Caulfield [18].

3.3.2 Organism impact modeling

As in Auerbach [4] and Caulfield [18], the general approach of adding exposures via an isomortality model of biological impact is used in the present study. However, the specific approach used is adapted from Sato *et al.* [108]. The following section outlines the biological impact calculations and also derives the isomortality relationships employed in the present study from a subset of the CO$_2$ mortality data reviewed in Chapter 2.

Implementation of isomortality model

The implementation of the *isomortality model* in the present study differs in three main ways from that of the original investigation by Auerbach [4] and Caulfield [18]. First, based on the data reviewed in Chapter 2, pCO$_2$ is used as the stressor rather than pH. Second, the *extended probit model* developed by Sato and Sato [110] and Sato *et al.* [108] is used in favor of the original approach in [4]. Third, the species recovery included in previous modeling efforts is not included in the present study.

As discussed in Section 3.1.2, the main difference between Auerbach's isomor-

tality approach and Sato's extended probit model approach lies in the form of the isomortality functions. Both methods add up exposures by translating an organism cluster's accumulated percent mortality from one stress level (pH or pCO_2) to another by defining an equivalent cumulative exposure time. However, while Auerbach [4] developed regression curves based on independent fits of the LC_0, LC_{50}, and LC_{90} data, Sato [108] used a single function fitted to all the mortality data to derive regression equations. The mathematical elegance of the latter approach makes it more convenient in that a single probit equation is used to describe the biological impact, allowing the process of adding exposures to be done without iteration if the function is linear. More importantly, the form of the equation is based on the probit method commonly used to estimate LC values and is therefore more consistent with the underlying toxicity data. Specifically, the inherent assumption in the probit method for calculating an LC_{50} (for example) is that the cumulative mortality of organisms follows a sigmoid function of the log of the stressor, and thus a sigmoid curve is fitted to the observed toxicity data so that any LC can be calculated directly. This imposes a specific form to the LC values (e.g., in log space, $LC_{50} - LC_{10} = LC_{90} - LC_{50}$; $LC_{50} - LC_{40} \neq LC_{40} - LC_{30}$). The extended probit method respects these relationships since it is based on the probit method. In contrast, the Auerbach method does not in that it independently regresses relationships for each mortality level and linearly interpolates between them. Furthermore, to avoid having isomortality lines converge, the form of the curves must be adjusted manually. On the basis of these considerations, the Sato approach to isomortality modeling was selected because it permits less subjectivity on the part of the modeler. As noted previously, for simplicity the probit function of Sato *et al.* is here referred to as an isomortality function since it accomplishes the same goal as the original curves of Auerbach [4].

Thus, the isomortality function used in the present study is of the form:

$$Y = a \log(t) + b \log(\Delta pCO_2) + c \qquad (3.36)$$

where Y is the probit of mortality (defined by (3.6)), t is the exposure time, ΔpCO_2

93

is the excess pCO_2 over the ambient pCO_2, and a, b, and c are regression coefficients. Excess pCO_2 is used instead of the absolute value so that data with different background values can be used together. The specific regression coefficients used in the present study are developed in the next section. It should be noted that the isomortality function does not necessarily have to be linear; the fit could be performed using, for example, a quadratic, such as $Y = a_1 (\log(t))^2 + a_2 \log(t) + b \log(\Delta pCO_2) + c$ (this was the form of the function used in Sato and Sato [110]). For the present purpose, however, a linear function provides a reasonable fit to the data and is convenient for its simplicity and consistency with Sato *et al.* [108, 111].

The algorithm to step through time is similar to the approach by Auerbach [4] (see Section 3.1.1), with a few modifications. First, calculations are performed in terms of Y instead of D, i.e., using the probit unit instead of fractional mortality. Second, Y is calculated directly from t and ΔpCO_2 using (3.36) without interpolation between specific LC curves, and no special treatment is required for low mortality since a zero mortality does not exist in probit space ($D \to 0$ as $Y \to -\infty$). Consequently, (3.3) becomes $Y(\Delta pCO_2, t^*) = Y_1$ from which t^* can be solved without iteration. Lastly, the probit value must be converted back into fractional mortality for output (and for insertion into a species recovery function, if applicable):

$$D = \frac{1}{2} \left[1 + \mathrm{erf} \left(\frac{Y - 5}{\sqrt{2}} \right) \right] \tag{3.37}$$

which was derived by integrating the Gaussian distribution in (3.6) with zero mean and unit standard deviation.

The extended probit method is here modified to include a minimum stress level, $[pCO_2]_{min}$, below which mortality is not incurred. This is introduced to avoid an inherent problem, namely that (in the absence of species recovery) an infinitesimal mass of CO_2 would be predicted to eventually kill all organisms. Sato *et al.* [108] also recognized this effect, and as a result they discounted mortality effects when pCO_2 dropped to within 100 μatm (≈ 0.01 kPa) of the ambient value.

The fact that the present study does not include a species recovery as in Caulfield

[18] warrants some discussion. Solving equation (3.4) yields the discrete form of the species recovery which was likely implemented in [18]:

$$D(t + \Delta t) = 1 - \frac{1 - D_{im}(t + \Delta t)}{1 + D_{im}(t + \Delta t)\left(e^{-r\Delta t} - 1\right)}. \tag{3.38}$$

where D_{im} is the population deficit (fractional mortality) predicted by the isomortality method and r is the growth rate. Thus the deficit of each particle decreases for each timestep that it encounters a low stress environment. In Caulfield's case, this corresponded to pH > 7.35. The benefit of including such a recovery formulation is twofold: (1) it seems realistic to expect a population to recover when stress is reduced, and (2) it allows the calculation of a finite footprint for each CO_2 discharge, i.e., the entire population will recover to its carrying capacity at some distance from the source. However, recovery is not included in the present study because the recovery rate is unknown and poorly constrained. Instead, calculations are made as transparent as possible and the issue of species recovery is deferred until later in the analysis.

Isomortality functions

Listed below are some conclusions from the literature review in Chapter 2 that are relevant to the development of isomortality functions. Since they are based on limited data for a small number of species, they can hardly be taken as generalizations of all marine organisms; rather, they will be used to select the most appropriate data from the existing CO_2 mortality dataset.

- Marine organisms are much more sensitive to pH depressions caused by CO_2 than by other acidifying agents [69, 51, 139].

- Fish are among the more CO_2 tolerant marine species due to their internal compensation mechanisms [100, 111], and there is considerable variability among different species [68, 60]. Tolerance varies over the life cycle, with the lowest tolerance exhibited during the early developmental (egg cleavage) and juvenile stages [68]. The tolerance is highly dependent on the nature of the CO_2

exposure; a gradual increase in concentration gives a higher tolerance in developmental and adult fish than a sudden increase, and mortality can be induced by a sudden return to normocapnic conditions from an elevated but sub-lethal CO_2 concentration [70, 67]; this implies that they do not fit into the isomortality cumulative approach [111]. As for whether juvenile and adult fish will be able to sense and avoid high CO_2 plumes, the data are mixed [126, 134].

- Copepods generally exhibit less CO_2 tolerance than fish, apparently lacking similar compensation mechanisms [100, 111]. There is variability between the CO_2 tolerance of different species, and between different geographical regions [139]. While some data suggest that deep-sea copepods may be more tolerant of CO_2 than their shallow-water counterparts [139], the generality of this conclusion is controversial [55] as it may be limited to the "oxygen minimum zone" that exists at about 1,000 m depth. As for gradual versus sudden changes in CO_2 concentration, the response of copepods appears to be more linear, i.e., unlike fish [111].

- CO_2 exposure effects are not limited to acute mortality; a wide range of sub-lethal effects have been noted. In particular, a significant effect on reproduction has been noted in copepods and gastropods [73, 75, 74], and in fish [60, 68].

Based on these considerations, the main isomortality function used in the present study is based on the pelagic copepod dataset of Watanabe *et al.* [139]. Despite the comparatively large dataset, the fish data are not incorporated into the main isomortality function for the reasons noted above, although some of the data are used in a sensitivity analysis. The dataset compiled by Auerbach *et al.* [5] and the pelagic copepod data from Yamada and Ikeda [144] are not used because they consider mortality due to non-CO_2 acidification. The benthic species datasets are not used because (a) there is little in the way of controlled dose-response data, (b) the limited data available suggest higher tolerance than pelagic species at least in the short term, and (c) the discharge scenarios considered herein are dilution strategies most likely to impact pelagic species (since they seek to distribute CO_2 over large

volumes rather than concentrate it on or beneath the sea-floor). Thus, the present study uses copepods as the main target organisms, which are assumed representative of zooplankton in general. The conservative nature of this choice is supported by the conclusion of Kita and Watanabe [72], who identified copepods as being among the more sensitive species to high-CO_2 conditions.

In generating the isomortality functions from the Watanabe *et al.* [139] copepod dataset, the most sensitive species are selected. Watanabe *et al.* [139] identified these as being the "surface-living groups", which they further divided into two groups: (1) subarctic and transitional regions and (2) subtropical region (see Figure 3-10). In each of these groups, the shallow-living copepods exhibited greater sensitivity than their deep-living counterparts. The first group consisted of three single-species experiments (*Calanus pacificus*, *Metridia pacifica*, and *Euchaeta marina*) while the second group consisted of 4 experiments each comprising a mix of epipelagic species (see [139] for a taxonomic breakdown). A comparison of the LT_{50} values in Figure 3-10 suggests that in general the first group (subarctic and transitional regions) displays greater sensitivity. Two datapoints are excluded from the figure because the authors could not calculate an LT_{50}. From the subarctic/transitional group, an $LT_{50} > 140$ hours was observed for a pCO_2 of about 0.15 kPa ($\Delta pCO_2 \approx 0.04$ kPa), and from the subtropical group, an $LT_{50} < 6$ hours was observed for a pCO_2 of about 9.9 kPa ($\Delta pCO_2 \approx 9.8$ kPa).

From the raw data plots for these stations (provided by the lead author of [139]), LT_{10}, LT_{50}, and LT_{90} values were estimated using the probit method of sigmoid curve fitting as in [139] (see Finney [37] for an overview). Good agreement was achieved between the estimated and reported LT_{50} values after certain assumptions were made during the analysis: (1) the first observed instances of 0% and 100% mortality were assigned values of 1% and 99% during the regressions, and (2) death in the control samples was ignored[2]. This latter assumption has little impact on the first (subarctic and transitional) group as these exhibited little control sample mortality. However,

---

[2]These assumptions were needed to achieve good agreement with reported LT_{50} values; we have been unsuccessful in contacting the lead author of [139] to confirm since receiving the raw data plots.
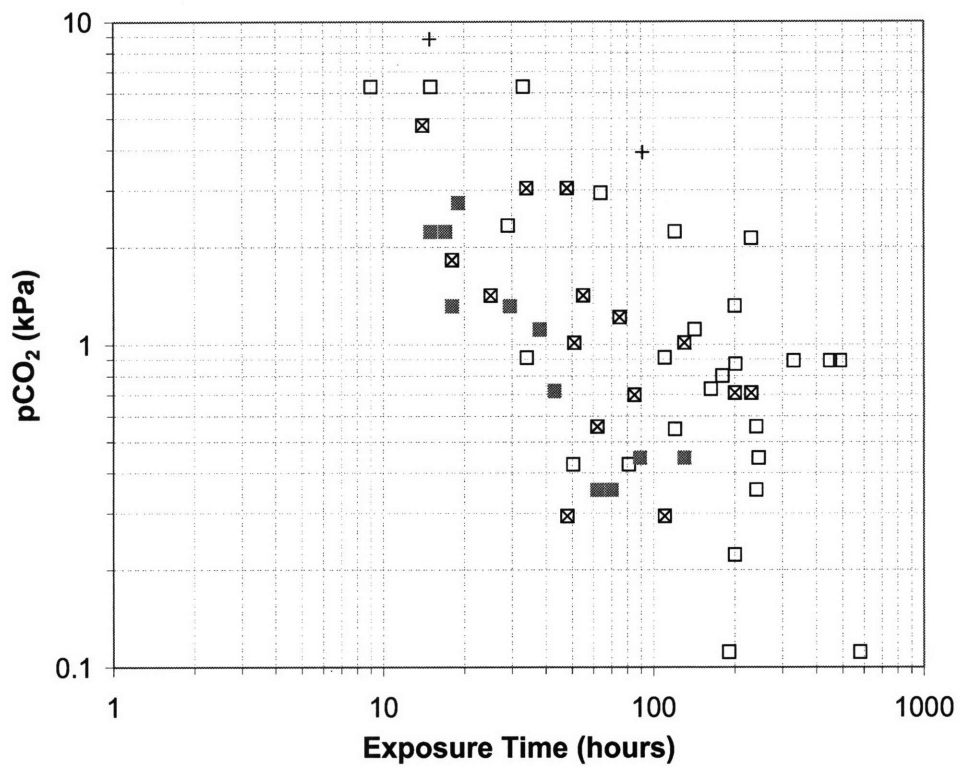
Figure 3-10: Reported LT_{50} values for Western North Pacific copepods from Watanabe *et al.* [139]. Filled squares: shallow-living copepods from the subarctic and transitional regions; hatched squares: shallow-living copepods from the subtropical region; open squares: deep-living copepods. For comparison, the harpacticoid copepod data from Sato *et al.* [111] are shown (plus signs).

	a	b	c	R^2
subarctic/transitional copepods	2.32	1.69	1.36	0.64
subtropical copepods	1.56	0.741	2.27	0.68
developmental fish	0.357	3.64	3.40	0.49

Table 3.4: Regression coefficients for various isomortality functions of form (3.36) for time in hours and ΔpCO_2 in kPa.

substantial control mortality was observed in all four experiments in the second group, and as a result these values must be considered rather conservative.

Multilinear regression was applied to both shallow-living copepod groups to determine the coefficients in a probit-type isomortality function (3.36). The regressions were performed on the estimated LT_{10}, LT_{50}, and LT_{90} values rather than the raw data because of the required assumptions mentioned above. Prior to regression, the pCO_2 values were converted to ΔpCO_2, i.e., the control sample pCO_2 was subtracted out. The resulting regression lines are plotted together with the underlying datasets in Figures 3-11 and 3-12, and summarized in Table 3.4. Because the reported LT_{50} values are less scattered for the first group (see [139]), and because of the significant control mortality not accounted for in the second group statistics, the isomortality function for the subarctic and transitional region (Figure 3-11) is selected as more realistic. The reader should note that basing the isomortality function on the shallow-living copepods is conservative, since the discharge scenarios considered herein are at or below the Watanabe et $al.$ deep-living sample depths.

There are two obvious gaps in the copepod mortality dataset which require some discussion, and which future investigations may want to address. The first is the lack of mortality data for low ΔpCO_2 exposure levels/long times. This could be due to experimental design or to the fact that the acute toxicity signal is too subtle to measure, i.e., if the LT_{50} approaches the natural lifespan of the organism. The data suggest that the latter is the case. Watanabe et $al.$ [139] noted significant control mortality in the 4-7 day range, and for several lower exposure experiments in the ΔpCO_2 range 0.03 - 0.4 kPa there was less then 50% mortality during experiments of duration 6 - 10 days. Similarly, Kurihara et $al.$ [73] noted control mortality in
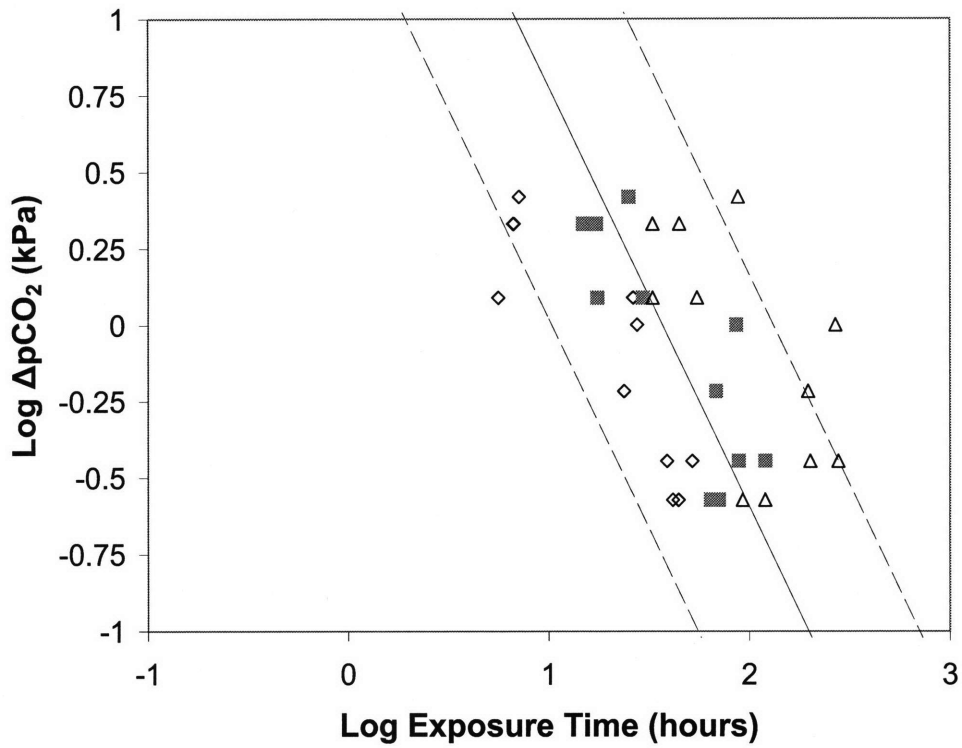
Figure 3-11: Isomortality function derived from shallow copepod samples from the subarctic and transitional regions of the Western North Pacific of Watanabe *et al.* [139]. Open diamonds: LT_{10}; filled squares: LT_{50}; open triangles: LT_{90}. Solid line: LT_{50} function; dashed lines: LT_{10} (left) and LT_{90} (right) functions.
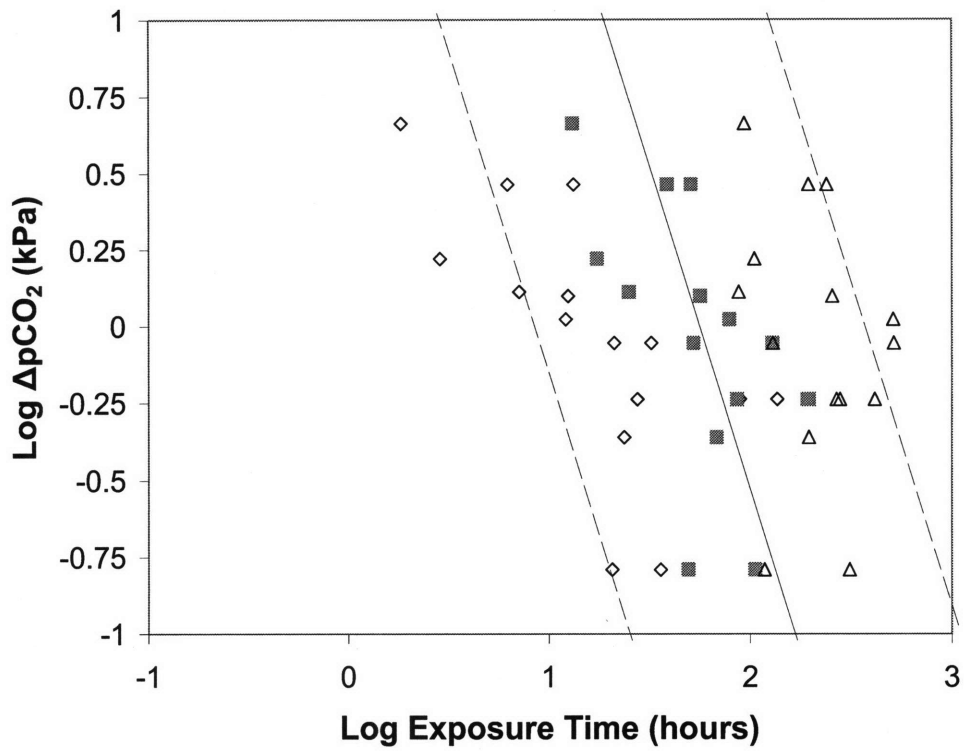
Figure 3-12: Isomortality function derived from shallow copepod samples from the subtropical region of the Western North Pacific of Watanabe *et al.* [139]. Open diamonds: LT_{10}; filled squares: LT_{50}; open triangles: LT_{90}. Solid line: LT_{50} function; dashed lines: LT_{10} (left) and LT_{90} (right) functions.

excess of 40-60% after 8 days for adult females of two surface-dwelling copepods with no significant added mortality for ΔpCO_2 exposures in the range 0.1 - 1 kPa. In addition, the same study indicated that strong impacts on egg production rate, hatching rate, and nauplius survival rate were only observed for $\Delta pCO_2 \geq 0.5$ kPa [73], i.e., sub-lethal effects were not observed for lower pCO_2.

In the absence of quantitative mortality data for low exposures, the isomortality function is extrapolated to a $[\Delta pCO_2]_{min}$ of 0.015 kPa, i.e., mortality is accrued above this level. Such an extreme low value implies extrapolating well beyond the data range, since the smallest value of ΔpCO_2 used in group 1 regression is 0.26 kPa. Anecdotally it is noted that the reported datapoint of $LT_{50} > 140$ hours for a ΔpCO_2 of 0.04 kPa is not inconsistent with the extrapolation of the LT_{50} line to 0.015 kPa. The 0.015 kPa criteria is similar to the 100 μatm (≈ 0.01 kPa) used by Sato [108], and has been chosen because, with the selected ocean chemistry parameters at 3°C, $\Delta pCO_2 = 0.015$ kPa corresponds to $\Delta pH \approx -0.1$. As discussed in Section 4.2, natural pH variability in the ocean suggests that marine organisms should be capable of tolerating a pH drop of 0.1 without any *sub-lethal* impacts [8], which is supported by the observations of Kurihara *et al.* [73]. Furthermore, this value is well below the Predicted No Effect Concentration (PNEC) for CO_2 of +500 μatm estimated for copepods by Kita and Watanabe [72], based on acute and chronic toxicity data. Thus, to allow acute impacts (mortality) to accrue until this level is very conservative within the bounds of the present study.

The other gap in the copepod dataset is the lack of mortality data for short times/high pCO_2. For the data used in the regression, the highest ΔpCO_2 is 4.6 kPa. The data provided by Watanabe [138] (see Chapter 2) in which copepods were exposed to 20 kPa for short durations are not true toxicity data in the sense that organisms were allowed to recover after appearing dead, and indeed the fact that most of them survived indicates little mortality for exposures of 20 kPa for 30 minutes (and are therefore not inconsistent with the extrapolated curves). Conversely, the datapoint from the subtropical group of $LT_{50} < 6$ hours for $\Delta pCO_2 \approx 9.8$ kPa suggests that extrapolating the isomortality function into short times and high ΔpCO_2 is not

conservative.

The latter gap in the data is addressed by a sensitivity analysis in which a second isomortality function is developed from a subset of the developmental fish dataset. The dataset is attractive because mortality was observed for short times (minutes) at concentrations well below those predicted by extrapolating the copepod isomortality curve. It could be argued that they are appropriately considered since a CO_2 discharge design should seek to avoid harming any species. However, as noted previously, the response of these organisms is not well-suited to the isomortality approach and thus they are of questionable applicability. Nonetheless, in the interest of being as conservative as possible in the absence of a better dataset, a subset of these data is used. Specifically, the embryo and juvenile Japanese sillago and red sea bream data from Kikkawa *et al.* [68] are selected because they exhibited the highest sensitivity (Figure 3-13). An isomortality function has been developed in the same manner as for the copepod dataset (Table 3.4), as shown in Figure 3-14 along with the main (copepod) function.

The sensitivity analysis using the developmental fish dataset is conducted in a special manner in the interest of being conservative. At each timestep, the organism's mortality is evaluated with both the base copepod function and the developmental fish function, and the larger of the two impacts is selected. At the end of the timestep, the cumulative equivalent exposure time using each curve is calculated for the final mortality and exposure pH in preparation for the next step. Thus, the organism's actual equivalent time is discontinuous as it may vary from timestep to timestep depending on which curve is used. Overall, this approach maximizes impact by allowing a single simulated organism to experience the sensitivity of multiple species[3].

---

[3]This approach was selected in favor of a single regression line using a combined copepod/developmental fish dataset because a linear fit was too poor to be of value, and experimentation with nonlinear fits did not yield well-behaved functions.
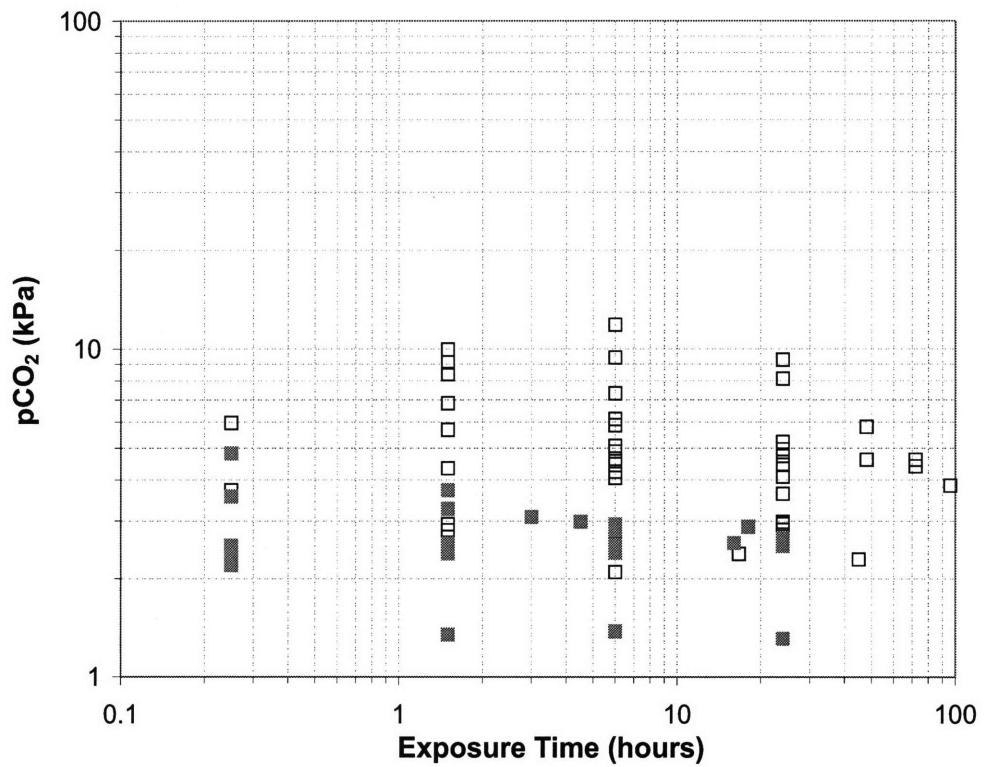
Figure 3-13: LC_{50} values for developmental fish from Kikkawa *et al.* [68]. All reported data are plotted. The cleavage stage embryos and juvenile japanese sillago and red sea bream were selected for the sensitivity analysis isomortality function and are shown as filled symbols.
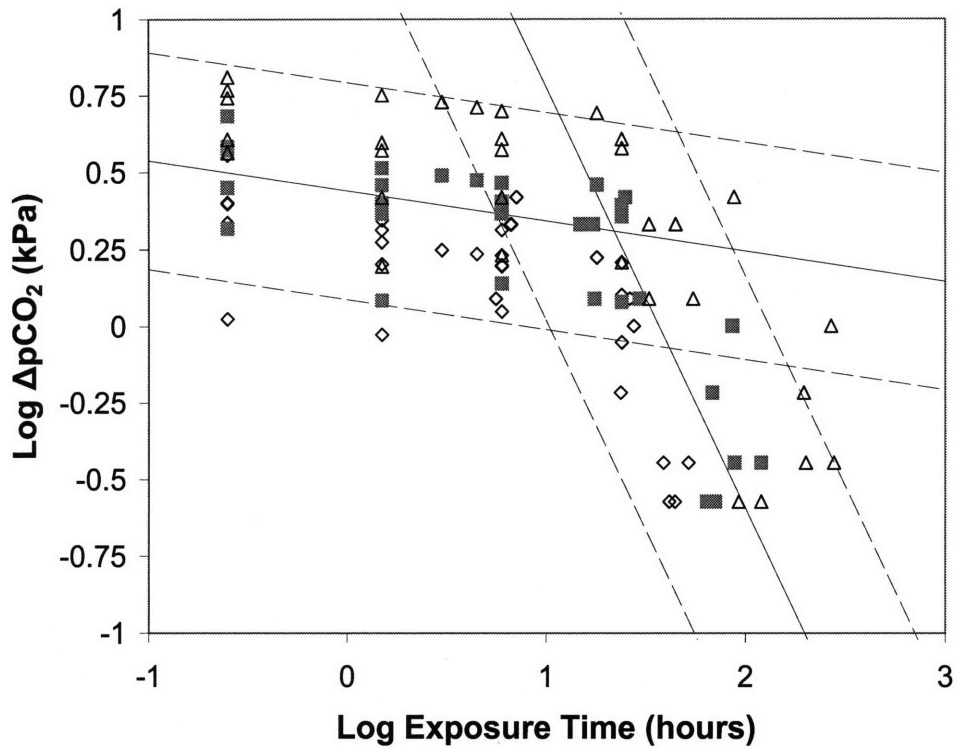
Figure 3-14: Isomortality function derived from selected subset of developmental fish data from [68], plotted together with the main copepod isomortality function and the selected subset of copepod data. Open diamonds: LT_{10}; filled squares: LT_{50}; open triangles: LT_{90}. Solid line: LT_{50} function; dashed lines: LT_{10} and LT_{90} functions. Note that LC values were reported by the author, but in the isomortality framework the LT and LC concepts are interchangeable.

Chapter 4

Results

Overall, 6 different discharge configurations are studied: a stationary hydrate plume released at 1,500 m and just reaching the ocean bottom at 4,500 m; a bottom manifold releasing CO_2 droplets over a 4.5 km distance from the depth range 800-1200 m with a plume rise of 250 m; and four towed pipe scenarios in which single diameter hydrate composite particles (2.5, 5, 10, and 15 cm) are released at 1,500 m with a range of hydrate conversion percentages $(0.1 < X_{hyd} < 0.55)$ into an ambient current that is not parallel to the path of the towing ship. For each discharge configuration, CO_2 mass loadings of 10, 100, and 1,000 kg/s are evaluated, corresponding roughly to the output of 0.1, 1, and 10 500-MW coal-fired power plants [53].

Calculation results are presented below in the following order: water quality impacts, biological response, and sensitivity analysis. Result interpretation is deferred until the final section of this chapter.

4.1 Water quality impacts of discharges

Figure 4-1 shows the pH and pCO_2 impact volumes (i.e., the volume with pH below or pCO_2 above a given level) for CO_2 mass loadings of 100 kg/s and 1,000 kg/s. Only those combinations which cause a ΔpCO_2 impact greater than 0.015 kPA ($\Delta pH \lesssim$ -0.1) are shown. The 10 kg/s mass loading is not shown as only the stationary hydrate plume exceeds the ΔpCO_2 criterion.
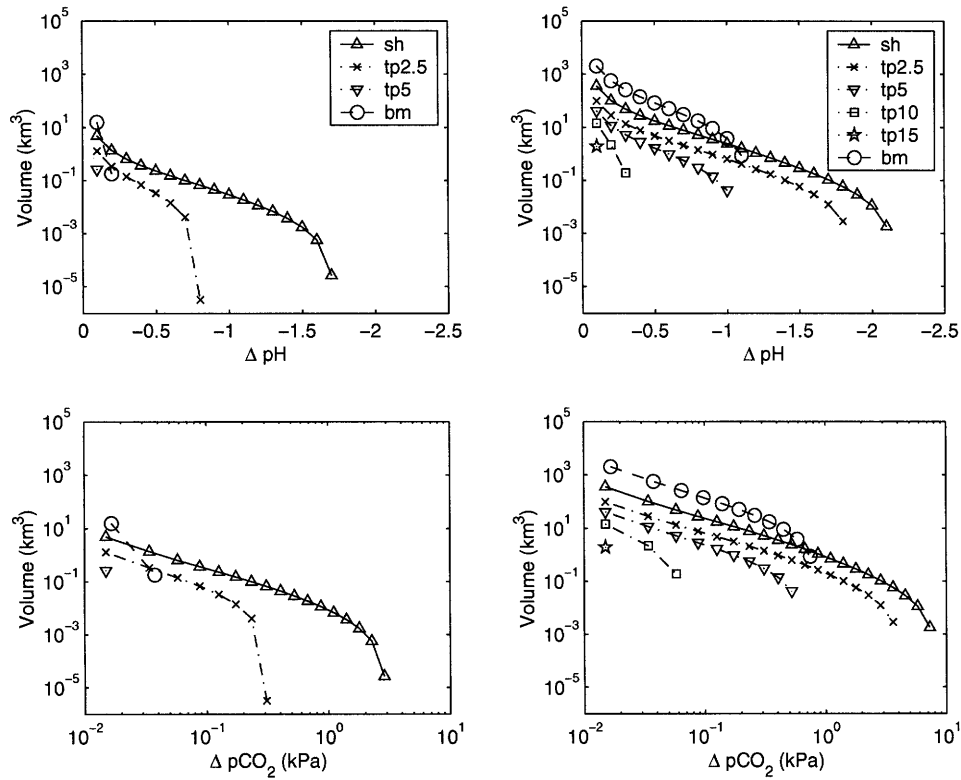
Figure 4-1: Impact volumes for discharge scenarios in terms of pH (top panels) and pCO_2 (bottom panels) for mass loadings of 100 kg/s (left panels) and 1,000 kg/s (right panels). Only those scenarios which achieve an impact of $\Delta pCO_2 \geq 0.015$ kPa are shown: sh = stationary hydrate plume; tpX = towed pipe with X cm particle diameter; and bm = bottom manifold

For a low impact level of $\Delta pH = -0.1$ ($\Delta pCO_2 \approx 0.015$ kPa), the bottom manifold has the greatest impact volume, but with maximum impact levels of -0.2 and -1.1 pH units (about 0.038 and 0.75 kPa) for the 100 and 1,000 kg/s loadings, respectively. In contrast, the stationary hydrate plume scenario has a lower impact volume than the bottom manifold for the lowest impact level, but eventually yields the highest volumes as the impact level increases, with non-zero impact volumes for a ΔpH of -1.7 and -2.2 (ΔpCO_2 of about 2.9 and 9.2 kPa) for the 100 and 1,000 kg/s loadings, respectively. The relative performance of the bottom manifold to the stationary pipe decreases as the loading is increased from 100 to 1,000 kg/s. The towed pipe scenarios demonstrate lower volumes than the stationary hydrate plume at any impact level for any combination of loading and particle diameter. The same is true when comparing to the bottom manifold if the towed pipe particle diameter is 5 cm or more. The impact of the towed pipe method decreases with increasing particle diameter, with little impact observed for $d = 15$ cm, the largest diameter tested, for a 1,000 kg/s loading.

The same trends are demonstrated in Figure 4-2, which shows the pH and pCO_2 variation along the centerline of the plumes for the same mass loadings. Since the plumes are modeled analytically, the highest concentration is always located at the centerline. It is, however, worth noting that the spatial extent of the plumes differs between scenarios. The horizontal axis of Figure 4-2 is time, i.e., for any point on the centerline the horizontal axis shows the time since that point was colocated with the injection source. The axis can be converted to a distance from the source, $x = ut$, where u is the ship speed for the towed pipe scenarios and the ambient current for the other scenarios, as shown in Figure 4-3 and Table 4.1. While the towed pipe scenarios are the shortest in terms of time to reach a ΔpH of -0.1, they are longer in distance than the stationary hydrate plume and generally longer than the bottom manifold because of the high speed of the ship relative to the ambient current. As a result, the lateral extent of the towed pipe plumes is also much smaller than the other two discharge methods (see Table 4.1).
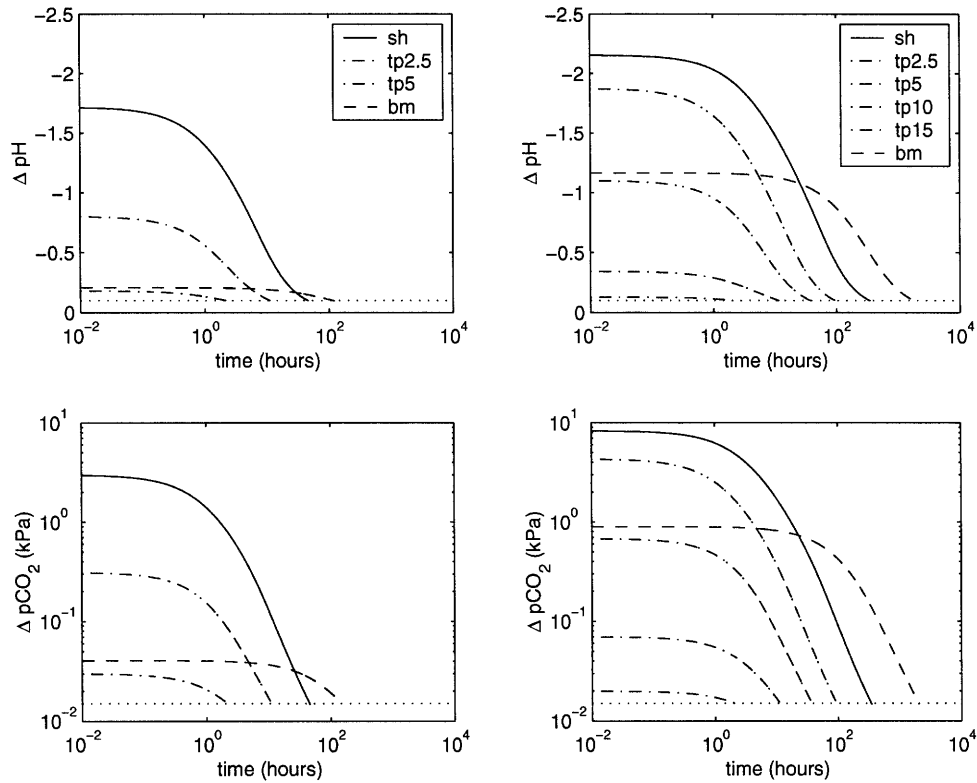
Figure 4-2: Centerline variation in pH (top panels) and pCO_2 (bottom panels) as a function of time from the source for discharge scenarios with mass loadings of 100 kg/s (left panels) and 1,000 kg/s (right panels). Only those scenarios which achieve an impact of $\Delta pCO_2 \geq 0.015$ kPa are shown: sh = stationary hydrate plume (solid line); tpX = towed pipe with X cm particle diameter (dashdot lines; the larger the particle diameter, the smaller the impact); and bm = bottom manifold (dashed line). $[pCO_2]_{min}$ is shown as a dotted line ($\Delta pH \approx -0.1$) to indicate the endpoint of the biological impact simulations.
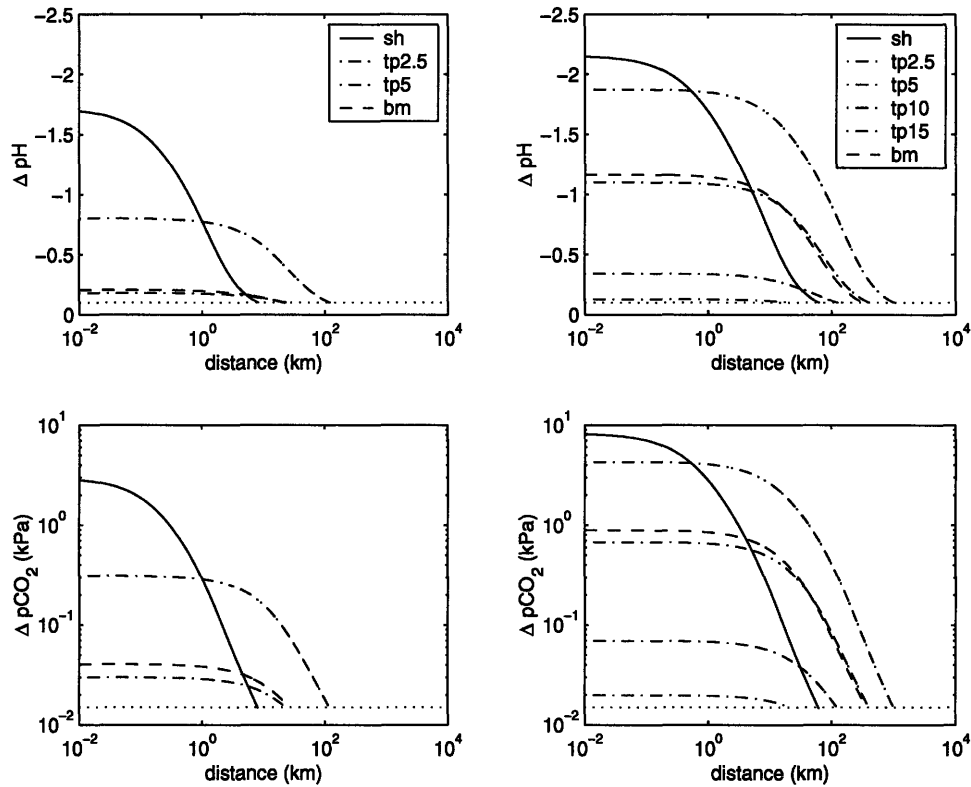
Figure 4-3: Centerline variation in pH (top panels) and pCO_2 (bottom panels) as a function of distance from the source for discharge scenarios with mass loadings of 100 kg/s (left panels) and 1,000 kg/s (right panels). Only those scenarios which achieve an impact of $\Delta pCO_2 \geq 0.015$ kPa are shown: sh = stationary hydrate plume (solid line); tpX = towed pipe with X cm particle diameter (dashdot lines; the larger the particle diameter, the smaller the impact); and bm = bottom manifold (dashed line). $[pCO_2]_{min}$ is shown as a dotted line ($\Delta pH \approx -0.1$) to indicate the endpoint of the biological impact simulations.

Scenario	CO_2 loading (kg/s)	Distance to $\Delta pCO_2 = 0.015$ kPa (km)	Final $2\sigma_y$ (km)	Plume Height (km)	Area (km^2)
Stationary hydrate	10	1.06	0.0461	3	0.138
Stationary hydrate	100	8.14	0.458	3	1.37
Stationary hydrate	1,000	61.3	4.57	3	13.7
Towed pipe, 2.5 cm	100	119	0.104	0.220	0.0228
Towed pipe, 2.5 cm	1,000	1,006	1.04	0.220	0.228
Towed pipe, 5 cm	100	23.2	0.0388	0.588	0.0228
Towed pipe, 5 cm	1,000	400	0.388	0.588	0.228
Towed pipe, 10 cm	1,000	122	0.147	1.55	0.228
Towed pipe, 15 cm	1,000	22	0.085	2.69	0.228
Bottom manifold	100	26.8	3.76	0.392	1.48
Bottom manifold	1,000	362	37.6	0.392	14.7

Table 4.1: Plume characteristics of the modeled discharge scenarios. Only those scenarios which achieve a $\Delta pCO_2 \geq 0.015$ kPa ($\Delta pH \lesssim$ -0.1) are shown.

4.2   Biological impacts of discharges

A central result of the biological data and modeling analysis is that a subset of the discharge configurations proposed herein yield a prediction of no adverse impact for the region modeled, i.e., outside of the dynamic mixing zone. This conclusion rests on the fact that sufficient dilution is achieved within the dynamic mixing zone to prevent concentrations from exceeding $[\Delta pCO_2]_{min}$, which was set to 0.015 kPa (corresponding approximately to a 0.1 decrease in pH) in an effort to be highly conservative. Since it has been suggested that such a low impact level would likely avoid acute and chronic (sub-lethal) effects alike, the present analysis must conclude "zero" impact. Discussion of the validity and implications of this result is deferred to Section 4.4 and Chapter 5; the remainder of this section summarizes the calculated impacts of each discharge configuration.

Before quantifying the biological impact predicted by the isomortality analysis described in Chapter 3, the nature of these calculations is first illustrated graphically. Figure 4-4 shows the trajectory of an organism cluster traveling along the centerline of the stationary hydrate plume and also the *cumulative trajectory* which reflects the cumulative exposure predicted by the isomortality method. In the latter case, the

horizontal axis is the log of cumulative equivalent exposure time (t^* in (3.3)), i.e., the exposure time that embodies cumulative lethal effects had the organism been exposed to a constant pH throughout. As the organism moves along a trajectory that maintains a ΔpCO_2 higher than the $[\Delta pCO_2]_{min}$, it incurs mortality due to the exposure (the probit function extends to $-\infty$ meaning that even exposures infinitesimally larger than $[pCO_2]_{min}$ will cause some added mortality). Since the centerline particle is always exposed to the highest plume pH throughout its trajectory, it always experiences the highest mortality of any organism in the plume. Its mortality is entirely due to the predicted plume spreading and the isomortality curve since it experiences no diffusion relative to the plume. Organisms with initial positions not on the centerline experience non-zero relative diffusivity and therefore sample concentrations lower than the centerline as they undergo lateral diffusion.

The predicted mortality of the centerline organism cluster is shown in Figure 4-5 for all discharge configurations and loadings. The reader is reminded that if no mortality is predicted for the centerline organism, then no other organisms experience mortality either. For a 10 kg/s CO_2 loading, only the stationary hydrate plume causes any mortality ($< 10^{-3}$). For 100 kg/s CO_2, the bottom manifold and towed pipe with particle diameter $\leq$ 5 cm also cause some mortality. For 1000 kg/s, all discharge configurations yield impact. For loadings of 100 kg/s or higher, the bottom manifold shows the greatest impact with near complete mortality being achieved for 1,000 kg/s. In each case, the towed pipe scenarios offer the lowest impact, with decreasing impact for increasing hydrate particle diameter. If the $[\Delta pCO_2]_{min}$ is increased from 0.015 kPa to 0.05 kPa to be consistent with the PNEC estimate of Kita and Watanabe ([72], see Section 3.3.2), then a finding of no impact would also apply to the 100 kg/s bottom manifold and 5 cm diameter towed pipe scenario, and the 1,000 kg/s 15 cm towed pipe scenario.

Further insight into the differences in the dilution strategies of the three scenarios can be gained by considering the trajectory of the centerline organism in each case. Figures 4-6 and 4-7 show the trajectories for the bottom manifold and towed pipe (2.5 cm) cases for a 100 kg/s CO_2 loading, respectively. The bottom manifold has

Figure 4-4: Simulated trajectory of an organism cluster traveling along the centerline of the stationary hydrate plume for a 100 kg/s discharge. The *centerline trajectory* is a time series of ΔpCO_2 values experienced by the particle. The *cumulative trajectory* is the centerline trajectory translated to equivalent exposure time via the isomortality method, and thus reflects cumulative exposure. The mortality trajectory shows the mortality incurred by the organism. In this case, the organism cluster incurs about 8.4% mortality before reaching the $[\Delta pCO_2]_{min}$ of 0.015 kPa, after which point no further mortality is incurred.

114
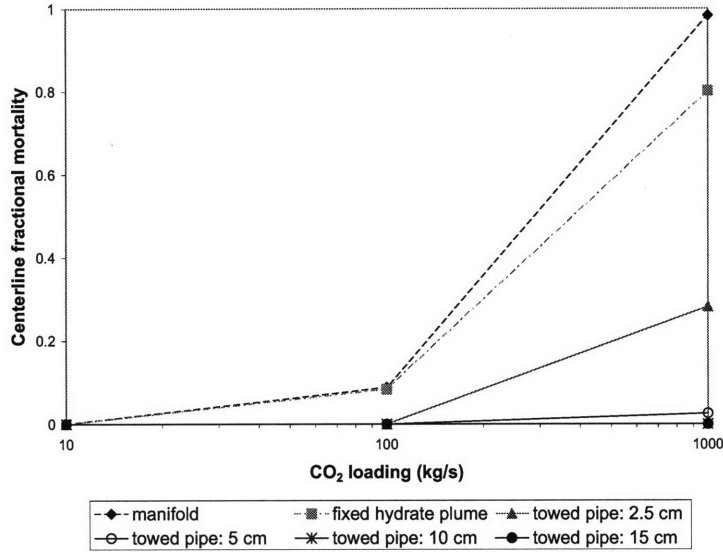
Figure 4-5: Fractional mortality incurred by an organism traveling down the plume centerline for all scenarios and loadings considered.

the lowest initial pCO_2, but it persists the longest, reaching a mortality of about 9%. The towed pipe has an order of magnitude higher initial pCO_2, but it persists for a much shorter time, reaching mortality 0.035%. The initial pCO_2 for the stationary hydrate plume is yet another order of magnitude higher with a persistence in between that of the other two scenarios, reaching a mortality of 8.4%.

Centerline mortality is a useful indicator of the highest possible impact of a discharge, but it does not provide a measure of predicted impact for the plume as a whole. One such measure is the integrated mortality flux (Q_M) as a function of distance downstream (x) from the discharge [4, 18]:

$$Q_M(x) = uh \int_{-\infty}^{\infty} D(x,y)dy \tag{4.1}$$

where $D(x,y)$ is the fractional mortality, and y is the lateral coordinate (the centerline is at $y = 0$). Since $D(y)$ is dimensionless, Q_M has units $\left[\frac{L^3}{T}\right]$ and can therefore be thought of as a flowrate of "dead" water. In the absence of species recovery, this quantity reaches a steady state value at the point where the centerline concentration drops below $[\Delta pCO_2]_{min}$.

115
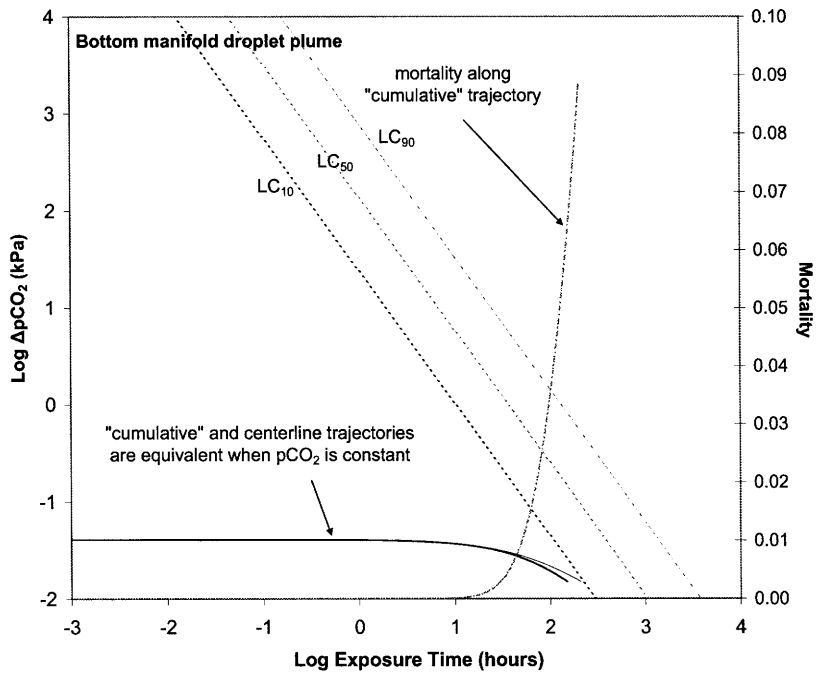
Figure 4-6: Simulated trajectory of an organism cluster traveling along the centerline of the bottom manifold plume for a 100 kg/s discharge.
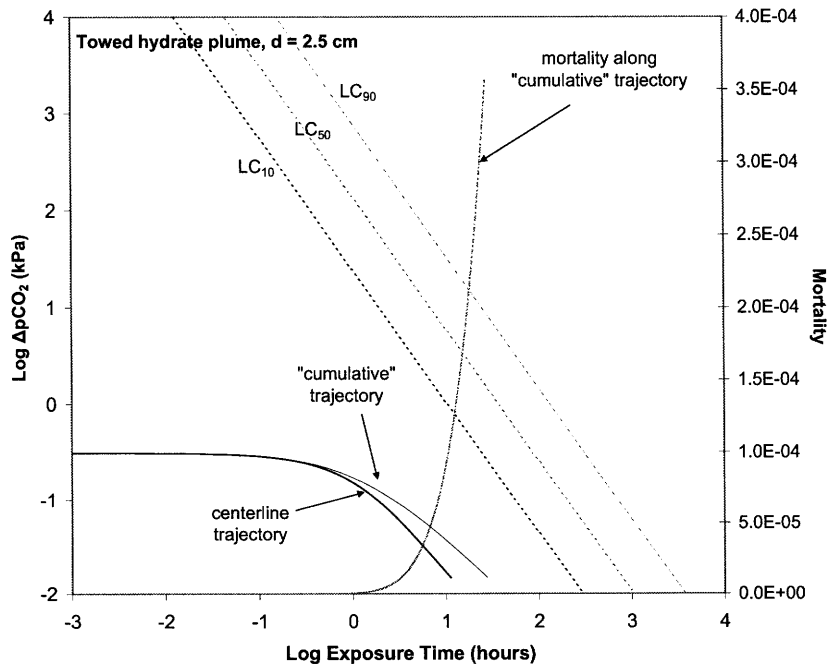
Figure 4-7: Simulated trajectory of an organism cluster traveling along the centerline of the towed pipe (2.5 cm diameter) plume for a 100 kg/s discharge.
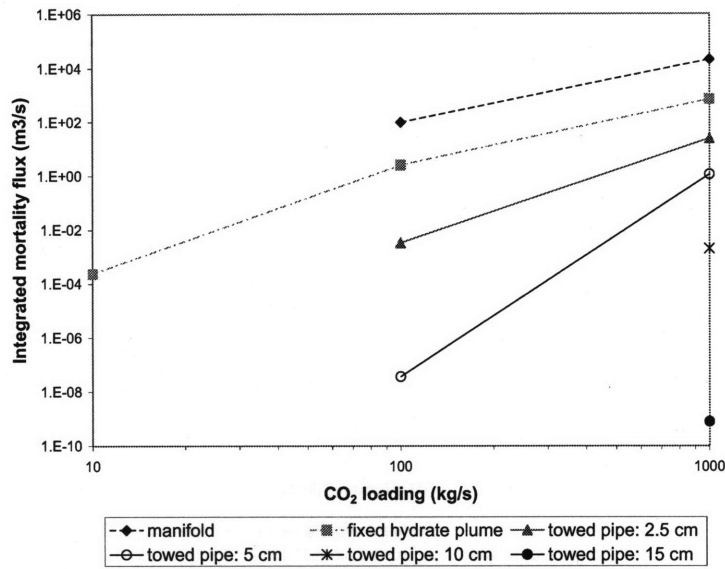
Figure 4-8: Integrated mortality of organisms encountering each discharge plume. Only scenarios which cause $\Delta pCO_2 \geq 0.015$ kPa are shown.

Figure 4-8 shows the integrated mortality flux for each scenario that causes $\Delta pCO_2 \geq 0.015$ kPa. The same relative trends are noted here, but the separation between the scenarios is multiple orders of magnitude. For example, the mortality flux of the bottom manifold is about 1,000 times greater than the least effective towed pipe scenario ($d = 2.5$ cm) for a 1,000 kg/s CO_2 loading.

An average fractional mortality for the plume can be calculated by normalizing the integrated mortality flux by the cross sectional area of the plume. The resulting average mortalities are shown in Figure 4-9, where the cross-sectional area is based on a lateral width of $2\sigma_y$ of the CO_2 plume at the downstream location where the mortality flux reaches its steady state (see Table 4.1). The same relative trends are again noted, with a maximum average mortality of about 5% being achieved for a 1,000 kg/s loading for the bottom manifold. For a 100 kg/s loading, the maximum average mortality (again for the bottom manifold) is about 0.3%. The average mortalities are orders of magnitude lower for the other scenarios.

117
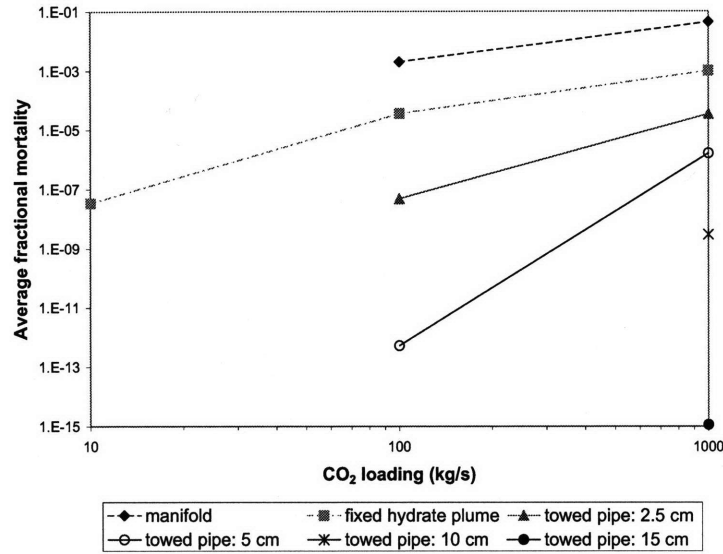
Figure 4-9: Average mortality of organisms encountering each discharge plume. Only scenarios which cause $\Delta pCO_2 \geq 0.015$ kPa are shown.

4.3 Sensitivity analysis on isomortality function

During the development of the plume calculations detailed in Section 3.2, choices were consistently made to be conservative. For example, the observed diffusivity relationship of Okubo [92] was reduced by a factor of ten to reflect deep ocean mixing, vertical diffusion has been ignored, and source representations were crafted to restrict initial plume width to give narrower plumes with higher initial concentrations at the edge of the dynamic mixing zone. While we recognize that more sophisticated simulation of the near field plume formation regime would result in small scale patchiness with higher concentrations near the injection point (e.g., of the type noted by Chen *et al.* [23]), such impacts would be limited to a small zone. While future work may seek to apply isomortality simulation to high-resolution modeling of the mixing zone, this is beyond the scope of the present study. Rather, the mixing zone analogy is maintained and attention is focused on impacts outside of this zone. Because the plume calculations already make a number of conservative assumptions, and because discharge scenarios such as the towed pipe and bottom manifold can be adjusted to further reduce the predicted environmental impact, no additional sensitivity analysis

on the plume calculations is offered at this point. The interested reader may, however, refer to Adams and Wannamaker [1] for a discussion of plume sensitivity to current speed, lateral diffusion, and mass loading as their analysis is highly applicable to the plumes considered in the present study.

The sensitivity analysis is instead focused on the isomortality function. As described in Section 3.3.2, an alternative isomortality function has been developed using the most sensitive subset of the developmental fish dataset (see Figure 3-14) to compensate for a lack of copepod toxicity data for short exposures at high pCO_2. The discharge scenarios were simulated again using this additional function in the manner described previously, in which the organism chooses the isomortality function which yields the highest impact at each timestep. To demonstrate the impact of using dual isomortality functions in this manner, the centerline trajectory of an organism in the stationary hydrate plume is shown in Figure 4-10, which can be compared to the previous result in Figure 4-4. In the dual function case, the organism switches from the first (developmental fish) isomortality function to the second (copepod) function at about 0.36 hours into the simulation, where the equivalent cumulative time t^* jumps from 2.5 hours to 16.7 hours. The second function is then used for the rest of the simulation. Here the impact of the more severe isomortality function for short times is substantial; the mortality of the centerline organism goes from 8.4% to 51%.

The centerline mortality and average plume mortality for each discharge scenario are shown in Figures 4-11 and 4-12, where again only those scenarios with $\Delta pCO_2 \geq$ 0.015 kPa are shown in the latter figure (the other scenarios, as modeled here, have no sensitivity to the isomortality function). The comparison with the base case is summarized in Table 4.2. The stationary hydrate plume shows the greatest absolute increase in the impact parameters because, as noted previously, it causes the highest pCO_2 values initially. The bottom manifold shows the least sensitivity because of its low initial pCO_2. Most of the stationary hydrate plume and towed pipe discharges show sensitivity, although the towed pipe impact remains low relative to the stationary hydrate plume. Overall, the bottom manifold impact remains the largest and the towed pipe the smallest.
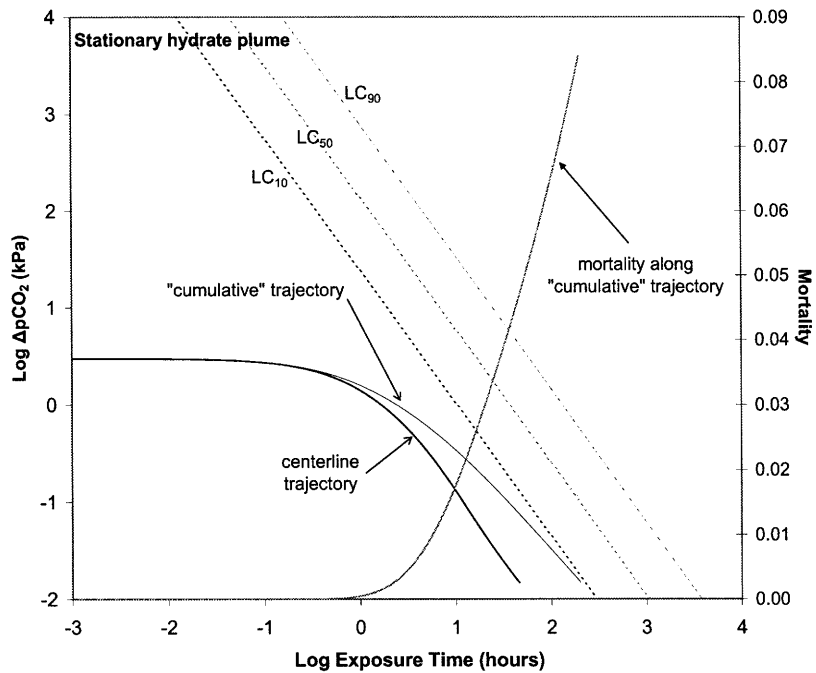
119
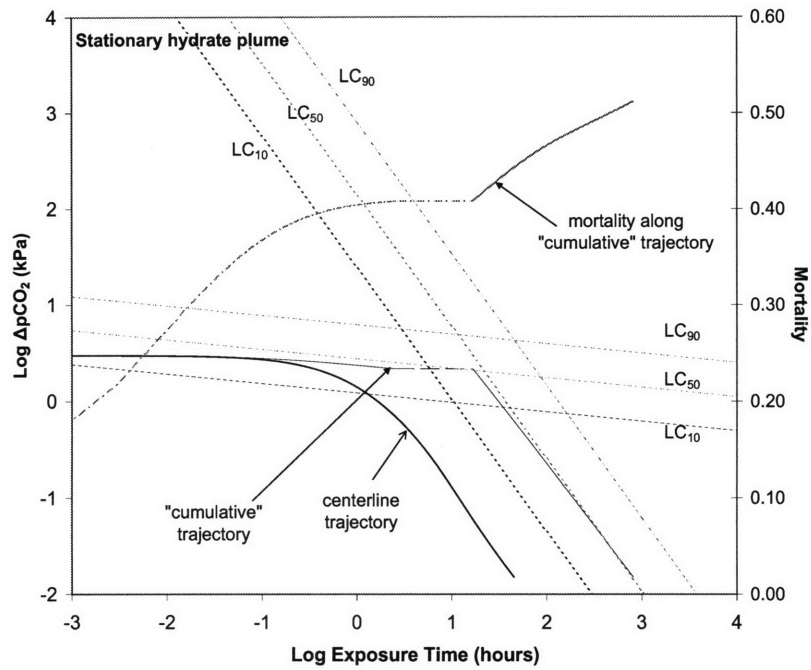
Figure 4-10: Simulated trajectory of an organism cluster traveling along the centerline of the stationary hydrate plume for a 100 kg/s discharge, when the dual isomortality functions in Figure 3-14 are used.
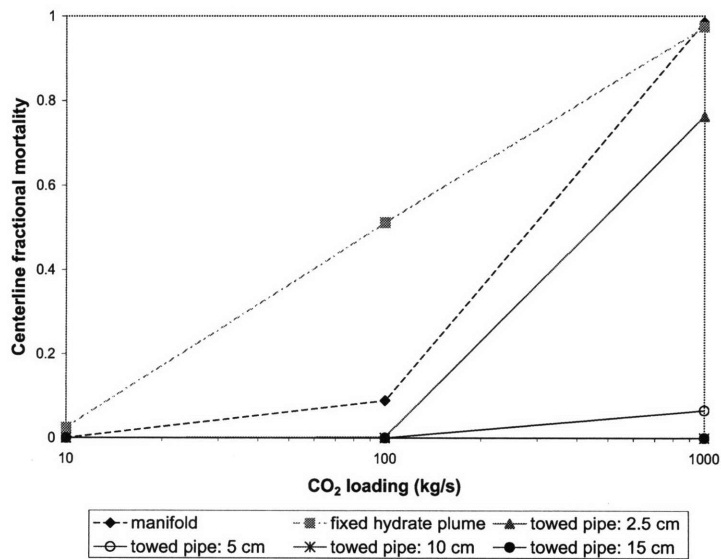
Figure 4-11: Fractional mortality incurred by an organism traveling down the plume centerline, when the dual isomortality functions in Figure 3-14 are used.
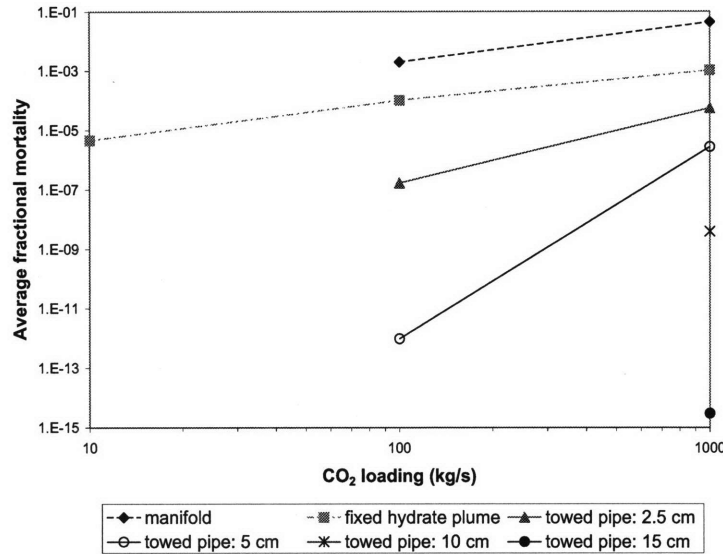
Figure 4-12: Average mortality of organisms encountering each discharge plume, when the dual isomortality functions in Figure 3-14 are used. Only scenarios which cause $\Delta pCO_2 \geq 0.015$ kPa are shown.

Scenario	CO_2 loading (kg/s)	Change in centerline mortality	Change in average mortality
Stationary hydrate	10	$1.1 \times 10^{-4} \to 2.5 \times 10^{-2}$	$3.4 \times 10^{-8} \to 4.6 \times 10^{-6}$
Stationary hydrate	100	$8.4 \times 10^{-2} \to 5.1 \times 10^{-1}$	$3.6 \times 10^{-5} \to 1.0 \times 10^{-4}$
Stationary hydrate	1,000	$8.0 \times 10^{-1} \to 9.7 \times 10^{-1}$	$1.0 \times 10^{-3} \to 1.0 \times 10^{-3}$
Towed pipe, 2.5 cm	100	$3.6 \times 10^{-4} \to 1.8 \times 10^{-3}$	$4.9 \times 10^{-8} \to 1.7 \times 10^{-7}$
Towed pipe, 2.5 cm	1,000	$2.8 \times 10^{-1} \to 7.6 \times 10^{-1}$	$3.5 \times 10^{-5} \to 5.5 \times 10^{-5}$
Towed pipe, 5 cm	100	$5.4 \times 10^{-9} \to 1.1 \times 10^{-8}$	$5.3 \times 10^{-13} \to 9.6 \times 10^{-13}$
Towed pipe, 5 cm	1,000	$2.6 \times 10^{-2} \to 6.6 \times 10^{-2}$	$1.6 \times 10^{-6} \to 2.7 \times 10^{-6}$
Towed pipe, 10 cm	1,000	$7.7 \times 10^{-5} \to 1.0 \times 10^{-4}$	$3.0 \times 10^{-9} \to 3.9 \times 10^{-9}$
Towed pipe, 15 cm	1,000	$1.7 \times 10^{-9} \to 2.6 \times 10^{-9}$	$1.2 \times 10^{-15} \to 3.0 \times 10^{-15}$
Bottom manifold	100	$8.9 \times 10^{-2} \to 8.9 \times 10^{-2}$	$2.0 \times 10^{-3} \to 2.0 \times 10^{-3}$
Bottom manifold	1,000	$9.8 \times 10^{-1} \to 9.8 \times 10^{-1}$	$4.5 \times 10^{-2} \to 4.5 \times 10^{-2}$

Table 4.2: Change in predicted centerline and average mortalities when dual isomortality functions are applied.

4.4 Discussion of results

The results of the preceding analysis can be interpreted in two main ways. First, as a means of comparing the various discharge strategies to each other and to those proposed in other studies. Second, as a means to say something about the expected absolute impact of these sequestration schemes. The following section considers each of these, and closes with a brief discussion of the limitations of the present analysis.

4.4.1 Relative performance of discharge scenarios

Relative to each other, the preceding results suggest that the towed pipe scenario offers the best performance. As the particle diameter is increased, the predicted impact drops to "zero" for a 100 kg/s loading and approaches "zero" for a 1,000 kg/s loading. The second best performer is the stationary hydrate plume on the basis of biological impact, even though it generates volumes with higher levels of pH/pCO$_2$ perturbation than the other two methods. The bottom manifold exhibits the worst performance as configured here; although it generates lower peak perturbations, it covers a larger area and therefore causes more overall impact.

Conclusions based on these results alone are, however, incomplete. The bottom manifold configuration, which was selected from [1], has more degrees of freedom from a design standpoint than the stationary hydrate plume. The dilution strategy of the manifold is to "paint" as large a region as possible with low concentrations by extending far in the lateral direction and creating a buoyant plume which spreads the CO$_2$ vertically. In contrast, the stationary hydrate plume covers only a small horizontal length scale but takes advantage of the negative buoyancy of the hydrate composite particles to spread the CO$_2$ over the full height of the water column and to dilute it through turbulent entrainment of the surrounding seawater. While the bottom manifold design could be altered to achieve greater dilution by "painting" a larger cross-sectional area (e.g., a longer manifold reaching greater depths with higher plume rise), the stationary hydrate plume does not offer the same flexibility. Although some additional lateral dispersion could be achieved by having a distributed

source, (e.g., a platform with many nozzles), it is limited in comparison to the bottom manifold for practical reasons and also because the flow through each nozzle must be large enough to achieve the buoyant plume effect. Caulfield [18] also noted this design flexibility of a bottom manifold approach when considering her droplet plume, in particular looking at the impact of distributing diffuser nozzles in the horizontal as well as the vertical. Thus, in the absence of cost constraints, the length, depth, and spatial loading distribution of the bottom manifold could be configured to reduce environmental impact much the same way the towed pipe particle diameters, reaction efficiencies, and ship speed could be adjusted to reduce impact. Therefore, the lack of design flexibility in the stationary hydrate plume effectively makes it the least attractive option of the three.

4.4.2   Comparison to past studies

The discharge scenarios proposed herein seem capable of offering equal or better near-field dilution than comparable strategies in previous studies, some examples of which are reviewed below (only studies which used roughly similar loadings as the present study are considered). Chen et al. [23] studied a 10 x 10 m horizontal platform located 20 m above the seafloor at 878 m with a uniform array of 100 1-kg/s nozzles injecting liquid CO_2 droplets with a mean diameter of 0.8 mm. The plume achieved a maximum rise of 190 m but significant interaction between nozzles apparently caused a descending plume with significant accumulation of CO_2 enriched seawater at the seafloor and pH depressions up to 2.6 units. Chen et al. also simulated a towed pipe releasing 100 kg/s of liquid CO_2 droplets from an array of nozzles at 1500 m depth moving at 3 m/s. The resulting buoyant droplet plume was reported to dissolve (after 70 minutes) into a passive plume 450 m tall and over 150 m wide, with a maximum pH decrease of 1.7 units. Impact volumes (given in [55]) for the platform release were much larger than those considered in the present study for $\Delta pH < -1$ and slightly higher than the 100 kg/s stationary hydrate plume for $-0.3 < \Delta pH < -1$. For the Chen et al. towed pipe scenario, impact volumes are two orders of magnitude larger than the 2.5 cm hydrate particle towed discharge in the present

study, which is surprising given the reported extent of the plume. The pH impact volumes predicted by Adams and Wannamaker [1] for their bottom manifold and stationary hydrate plumes are generally smaller than those predicted herein, largely due to the ten-fold decrease in ambient diffusivity employed in the present study as a conservative measure. Employing the same diffusivities, the bottom manifold scenarios are the same, the stationary hydrate plumes are similar ([1] used a shallower release depth which yields slightly greater dilution), and the towed pipe scenarios offer more favorable dilution in the present study due to the increased lateral source width. The impact volumes reported by Caulfiled [18] (volume with pH < 7 are reported, see Table 3.1) for the droplet plumes are 0.5-2 orders of magnitude higher than the stationary hydrate and bottom manifold plumes in the present study (Caulfield's droplet plume scenario is most similar to the bottom manifold scenario considered here). Impact volumes for her towed pipe scenario are comparable to the present 2.5 cm particle towed pipe scenario. This comparison is complicated by the fact that 30% higher loadings were used in [18] (130 kg/s for one plant, 1,300 kg/s for ten plants) along with an order of magnitude higher ambient diffusivity; it is however expected that the present scenarios offer better dilution than the ones considered by Caulfield, save for her dry ice scenario which was dismissed due to cost concerns. The impact volumes for the 25 kg/s stationary droplet release modeled by Drange et $al.$ [35] (5 ports discharging 100 m above the sea-floor in a 0.05 m/s current) are smaller than those of the 100 kg/s stationary hydrate plume considered here. Compared to the 100 kg/s towed pipe 2.5 cm hydrate particle release considered here, the Drange et $al.$ volumes are similar for $\Delta pH \geq -0.5$ and larger for $\Delta pH \leq -0.5$. Comparisons to the plumes simulated by Sato and Hama [109], Sato and Sato [110] and Sato [107] (a 10-hour 200 kg/s liquid CO_2 injection at 2,000 m) and Sato et $al.$ [108] (a 100 kg/s liquid CO_2 injection over depth interval 1000-2000 m moving at speeds of zero and 4 m/s) are difficult in that no impact volumes are reported. Nonetheless, the organism ΔpCO_2 experience reported by Sato et $al.$ for the stationary release appears to be greater than the centerline ΔpCO_2 for the stationary hydrate plume in the present study, and the ΔpCO_2 of the towed pipe scenario of Sato et $al.$ is comparable to the

centerline ΔpCO_2 of the 2.5 cm diameter towed pipe scenario in the present study (higher for $t < 4$ hours, somewhat lower for $t > 4$ hours). The towed pipe scenario of Minamiura *et al.* [86] (100 kg/s liquid CO_2 discharged through dual horizontal 10-m long diffusers with 50 ports each, towed at 3 m/s) yields a maximum ΔpCO_2 of about 600 μatm after 3 hours, which is very close to the towed pipe scenario of Sato *et al.* [108] and the centerline ΔpCO_2 of the 2.5 cm towed pipe scenario in the present study. The towed pipe scheme proposed by Hirai *et al.* [54] and Tsushima *et al.* [133] (see Section 3.1.4) appears to offer the greatest dilution of past studies, with only about 5×10^{-6} km^3 exceeding a ΔpCO_2 of 0.015 kPa for a 100 kg/s loading [133] after about 1 hour; this is far less than the centerline dilution of the 100 kg/s 5 cm towed pipe scenario considered here. Furthermore, the fact that the ΔpCO_2 perturbation predicted by Tsushima *et al.* [133] becomes negligible after 2 hours suggests that their scheme yields dilution on par with the present towed pipe scenario with 10 or 15 cm diameter hydrate particles.

The predicted biological impact for the towed pipe scenarios and the stationary hydrate plume can be compared to the findings of several of the previous studies listed in Section 3.1. In Caulfield [18], a finding of zero impact was reported for her towed pipe scenarios even at loadings of 1,300 kg/s. The present study only predicts zero impact for loadings of 100 kg/s or less (for diameters above 2.5 cm). This difference can be attributed to Caulfield's higher ship speed, more favorable isomortality curve, a source dispersed vertically over 500 m, and more favorable lateral diffusivities. For the droplet plume considered by Caulfield, mortalities reached as high as 11 and 69% for the 130 and 1,300 kg/s cases, respectively, with maximum mortality fluxes of 307 and 27,500 m^3/s. The centerline mortalities in the present case are 8.4% (8.9%) and 80% (98%), for 100 and 1,000 kg/s, repectively, with mortality fluxes of 2.5 (96) and 690 (21,000) m^3/s for the stationary hydrate plume (bottom manifold). Thus, the biological impact of the scenarios considered herein is less than or similar to that computed by Caulfield despite her more favorable diffusivities and isomortality curve and despite that fact that her diffuser length increases with loading. This is presumably due to the larger vertical extent of the plumes in the present study.

Still, the basic conclusion is similar to the one herein, namely that the towed pipe offers negligible impacts while a fixed plume results in some impact (although some of the impact could perhaps be reduced by optimizing design variables). This is essentially the same conclusion as in Sato *et al.* [108], which found non-zero but negligible mortality for a ship speed of 2 m/s and a droplet injection distributed vertically over 1,000 m, but "non-trivial" impact when the ship speed was 0. Although Sato and Hama [109], Sato and Sato [110] and Sato [107] found negligible impacts for a 200 kg/s fixed pipe scenario, this conclusion was based on Auerbach's non-CO_2 isomortality function and their mortality simulations appear to have been truncated before ambient pH was recovered. As discussed in Section 3.1.3, Chen *et al.* [21] found minor biological impact for a stationary discharge using a biological activity approach, but this was for a small loading (1 kg/s). Negligible biological impact was also found using CO_2-induced mortality data (with Sato's approach) for the 100 kg/s towed pipe scheme of Tsushima *et al.* [133], which as noted above seems to offer the best dilution of past studies. Lastly, Masuda *et al.* [82], using an OGCM to predict far-field CO_2 concentrations but ignoring near-field peaks, estimates that a towed pipe discharge of 420, 500, and 270 kg/s in a region of the North Pacific within the approximate depth intervals 1,000 - 1,500, 1,500 - 2,000, and 2,000 - 2,500 could avoid exceeding Kita and Watanabe's [72] PNEC (Predicted No Effect Concentration) of ΔpCO_2 of 500 μatm.

Thus, overall the present study is consistent with past studies in identifying a towed pipe of some sort as generally being able to avoid significant biological impacts if configured appropriately, and to a greater degree than a fixed descending or ascending plume (e.g., Caulfield *et al.* [19], Sato *et al.* [108], Jeong *et al.* [66]). To the previous assessments we add: (1) the conclusion holds up even considering the most recent CO_2-induced mortality data across a range of species; (2) CO_2 hydrates provide an effective way to achieve greater vertical and lateral dilution with relatively shallow injection depths, and (3) a bottom manifold can likely also be configured to largely avoid biological impacts (also suggested by [18]), although the design may be constrained by cost.

4.4.3 Consideration of absolute impact

While the present analysis is a useful way to compare the efficacy of various discharge strategies and to confirm the general findings of previous investigations, the ultimate goal of the investigation is to say something about the absolute impacts of ocean sequestration discharges. Water quality impacts are less controversial in this respect. While the extent of mixing in both the dynamic zone and the passive zone is open to some debate due to the complex fluid mechanics of multi-phase flows and inherent turbulence of the ocean, the chemistry of the carbonate system is well understood and thus bounds can be placed on the expected water quality impacts of a discharge. The challenge of translating the water quality impact into a biological impact is, however, much greater even on an individual species basis, let alone for an entire ocean ecosystem.

The tool employed in the present study is an isomortality-type analysis which is an attempt to integrate acute toxicity data in a mathematically tenable manner such that water quality impacts can be "translated" into a biological impact. Recent research suggests that this may be a reasonably accurate approach for modeling the acute response of zooplankton but not for fish [111] (see discussion in Chapters 2 and 3). Thus, two fundamental approaches can be taken in interpreting the results presented above. First, accepting the isomortality modeling approach as valid and as a decent surrogate for ocean species in general, and second, by attempting to interpret the water quality results directly without the aid of the isomortality analysis. Interpreting the findings of no acute impact for some of the discharge scenarios falls into the second category since it does not rely on adding exposures to come up with a cumulative mortality statistic. Rather we first attempt to interpret the non-zero mortality results in terms of an absolute impact.

The approach of Sato and Sato [110] and Sato *et al.* [108] is to consider the mortality of a single test organism and call it significant if it exceeds 0.125% (i.e., a probit value of 2, corresponding to three standard deviations of a tolerance distribution which is assumed to be Gaussian with the log of the stressor, see Finney [37]).

Applying this to the centerline results in Section 4.2 implies that there are no impacts for any 10 kg/s discharge, only for the stationary hydrate plume and bottom manifold for a 100 kg/s loading, and for all but the towed pipe with diameter of 10 cm or above for a 1,000 kg/s loading. Using the dual isomortality function sensitivity results, the stationary hydrate plume also yields impact at 10 kg/s, as does the towed pipe 2.5 cm diameter for 100 kg/s. Although this criterion could in theory be imposed as a design constraint, its binary nature (impact vs no impact) yields little in the way of overall impact of a plume.

As one step further, Caulfield [18] and Auerbach [4] estimated mortality fluxes and mortality volumes, the latter being the spatial integration in the downstream direction of the mortality flux given by (4.1) to yield a volume of "dead" water. Such a measure is convenient in that it can be normalized by the volume of the ocean, or of some ocean subregion of interest. However, it can only be defined if a species recovery is implemented, e.g., as done by Caulfield and Auerbach via (3.4), because otherwise the volume increases with time indefinitely. As noted earlier, a recovery process is not included in the current calculations because it requires specifying a growth rate which is not well-known and which makes assumptions regarding the response of organisms beyond the considerable ones already made by the isomortality modeling approach. Instead, a different interpretation of the predicted mortality fluxes is offered below.

Simplistically, Q_M can be used to characterize the timescale to kill all the organisms in the ocean, by ignoring all ecosystem effects and regenerative ability of the organisms, i.e., $T = \frac{V_O}{Q_M}$, where V_O is the volume of the ocean. But such a timescale is hardly useful. A more informative interpretation of Q_M can be gained by considering a simple equation governing the balance of a single species of organisms in the ocean:

$$\frac{dN}{dt} = k_g N - k_d N - S_{CO_2} \tag{4.2}$$

where N is the species population, k_g is the rate of generation or growth, k_d is the rate of death under natural conditions, and S_{CO_2} is the sink of organisms caused by the CO_2 discharge. Taking the ambient concentration of organisms to be C, then

$S_{CO_2} = Q_M C$, i.e., S_{CO_2} has units $\left[\frac{\text{Num organisms}}{T}\right]$. Perhaps more intuitively, (4.2) can be written in terms of the concentration of organisms:

$$\frac{dC}{dt} = k_g C - k_d C - S_{CO_2} \tag{4.3}$$

where S_{CO_2} now has units $\left[\frac{\text{Num organisms}}{L^3 T}\right]$. In this case, $S_{CO_2} = \frac{Q_M C}{V}$ where V is a characteristic volume. Assuming that the concentration of organisms is naturally in a quasi steady state such that $\frac{dC}{dt} \approx 0$ and $k_g \approx k_d$, the impact of the CO_2 discharge can be characterized by comparing it to the magnitude of k_d, i.e., how much extra mortality can be attributed to the discharge. Thus, the following balance can be considered:

$$k_d = \frac{Q_M}{V}. \tag{4.4}$$

Taking $k_d \approx \frac{1}{\tau}$ (where τ is the average lifespan of the organism) as a roughly known constant, the magnitude of V required for the sink due to the CO_2 discharge to be some fraction of natural death can be calculated. For example, for the CO_2 discharge to cause a 1% increase in mortality above the natural sink, a critical Q_M can be defined:

$$Q_{M,crit} = 0.01 k_d V_O \tag{4.5}$$

where the V in (4.4) has been taken as V_O. Since each discharge contributes Q_M, $Q_{M,crit}$ can be translated into a critical number of discharges, $N_{d,crit} = \frac{Q_{M,crit}}{Q_M}$. Based on this analysis alone, one would conclude that introducing less than $N_{d,crit}$ of these discharges into the ocean would increase the natural global sink of organisms by less than 1%. Alternately, for a given number of discharges, one could determine the critical volume V_{crit} of ocean required to keep the CO_2 induced sink less then 1% of the natural sink. This latter approach has been used to interpret the previous findings, as shown in Figure 4-13 for the base case isomortality function and in Figure 4-14 for the dual function sensitivity analysis. For context, it has been assumed that there would be about 4,000 100-kg/s discharges, which is based on the Pacala and Socolow [95] estimate of about 175 GtC in avoided emissions over the next 50 years required to

129
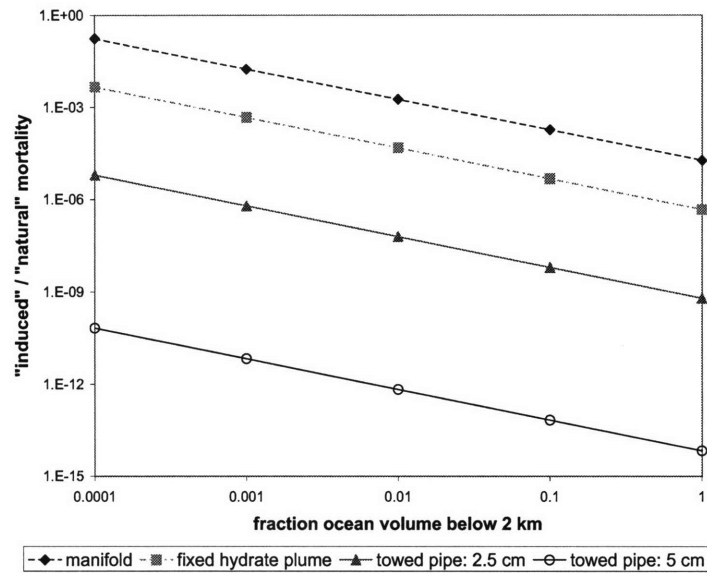
Figure 4-13: Induced vs natural mortality over various percentages of the ocean volume using the base case isomortality analysis.

stabilize atmospheric concentrations at 500 ppm. Since the base isomortality function is derived from copepod data, τ was conservatively taken as 1 year as an upper bound estimate on a deep ocean copepod ([3] and references therein). This analysis suggests, for example, that the towed pipe 2.5 cm scenario would only cause a 0.001% increase in copepod mortality in about 0.01% of the ocean below 2 km, whereas the bottom manifold would cause a 1.7% increase in the same volume. Overall, the analysis suggests that significant disruption of the ocean's copepod population would occur only in a small percentage of the ocean. Of course, the impact may have importance on a regional scale if, for example, a large number of discharges were concentrated in a smaller volume. Furthermore, it suggests that the impact of the discharge is linearly dependent on the average lifespan of the target organism, so if for example the isomortality curves and approach could also be considered realistic for a fish species with a lifespan of 10 years, then its large scale population would be ten times more sensitive to the perturbation caused by the discharges.

The estimates provided by the above analysis are admittedly crude and full of simplifications. For example, they ignore the interaction of multiple sources on each

130
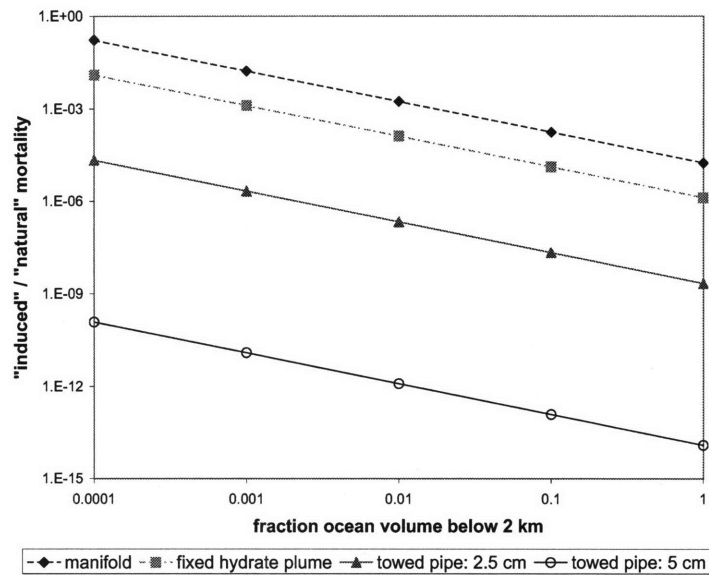
Figure 4-14: Induced vs natural mortality over various percentages of the ocean volume using the dual isomortality function sensitivity analysis.

other and the background CO_2 concentration, chronic effects to individual organisms, the relative tolerance of different species, and ecosystem level impacts of the discharge. Nonetheless, the approach gives a crude measure of impact for a given isomortality result.

Referring back to the discussion at the beginning of this section, the other way to interpret the results of the present analysis is to forego the isomortality analysis and interpret the water quality impacts directly. This is attractive because it does not rely on the functional form of an isomortality function and does not require extrapolating toxicity data across species. Such an approach was taken by Barry *et al.* [8] to determine, in the absence of species specific data, a possible "safe" threshold for avoiding chronic (and acute) biological impacts. Specifically, the pH variability across various zoogeographic regions and bathymetric ranges relevant to ocean sequestration was analyzed. Average pH variability of 0.05 to 0.24 units was observed, from which it was concluded that a pH decrease of 0.1 units may be a reasonably conservative threshold for ecosystem impacts. Unwilling to call any level safe, Pörtner *et al.* [100] concludes that present data indicate that a moderate increase of 200 μatm (≈ 0.02

kPa) may have significant long term effects, i.e., concerning chronic/ecosystem effects rather than acute toxicity. Thus, the value of $[\Delta pCO_2]_{min} = 0.015$ kPa used in the isomortality analysis seems if anything highly conservative from an acute impact analysis. Since some of the discharge scenarios can meet this strict threshold, overall the present study must conclude that, in the absence of complicating factors such as cost, ocean sequestration schemes can be engineered to largely avoid deleterious environmental impact beyond that which is already occurring under the "business as usual" scenario.

One major caveat to the present analysis of which the reader is reminded is that organism exposure within the dynamic mixing zones of the plumes has not been included in the analysis. Although they did not model hydrate particle plumes or a pure rising droplet plume from a bottom manifold, the detailed fluid mechanics investigations of, for example, Chen *et al.* [23] and Sato *et al.* [108] indicate that resolving the dynamic mixing zone will yield small-scale perturbations well in excess of the above threshold. Future work should therefore focus on a combined modeling approach in which near-field active plume mixing and far-field dilution are simulated together by, for instance, coupling a CFD code with a finely resolved ocean general circulation model (e.g., as in Drange *et al.* [35]), together with an isomortality calculation of the type applied herein. However, it is also noted that because of the design flexibility in the towed pipe hydrate plumes (and the bottom manifold), it seems likely that the proposed discharge scenarios could be further refined as needed to reduce peak concentrations to some extent. For example, hydrate injection nozzles could be distributed laterally at the end of the towed pipe to further increase the initial width of the plume and thereby lessen peak concentrations (analogous to the diffuser used in [133], for example).

132

Chapter 5

Summary, Conclusions, and Policy Implications

The specific objective of the present study is to provide an updated assessment of the expected acute biological impacts of direct ocean injection. This has been achieved by adapting the methods developed in previous studies (Auerbach *et al.* [5] and Caulfield *et al.* [19]) and applying them to new biological data and improved discharge scenarios. An extensive literature review of CO_2-induced mortality data has been performed, and it clearly demonstrates the need for an update to the initial work of [5] and [19] because (a) a substantial amount of CO_2 toxicity data has since been collected and (b) the sensitivity of marine organisms to CO_2 is greater than the sensitivity to equivalent pH depression by other acids (i.e., the type of data upon which [5] was based). Likewise, advances in, for example, CO_2 hydrate formation techniques have led to the development of new discharge approaches which offer enhanced dilution with less effort. The modeling approaches of the previous studies were updated as deemed appropriate, e.g., the extended probit model of Sato *et al.* [108] was adopted in favor of the original isomortality approach in [5]. A revised isomortality function has been developed based on pelagic copepod data from the Western North Pacific [139], thus using a similar target organism for quantifying environmental impact as previous studies. The functions were applied to discharge scenarios developed from those proposed in Adams and Wannamaker [1], including a stationary sinking hydrate

plume, a towed pipe releasing CO_2 hydrate composite particles, and a rising droplet plume from a bottom manifold. These discharge methods are believed to offer greater or equal dilution than those considered in [18] and subsequent studies. Although the updates to the previous analyses are considerable, the overall conclusion is the same, namely, that ocean discharge scenarios can likely be designed to largely avoid acute impacts. This conclusion is based on two sets of results. First, for some discharge scenarios the peak impact at the edge of the dynamic mixing zone is predicted to be less than a 0.1 unit drop in pH ($\approx$ 0.015 kPa increase in pCO_2), which is a highly conservative criterion for judging acute impacts since this level has been suggested as a possible "safe" threshold for avoiding chronic/ecosystem effects on the basis of natural pH variability in the deep ocean [8] (and is less then a third of a recent estimate of the Predicted No Effect Level [72]). Second, even when acute impacts are predicted to occur, discharge scenarios such as the towed pipe result in small impacts relative to the other scenarios and also in an absolute sense by comparison to the expected natural sink of copepods in the ocean. This latter conclusion is, however, crude in the approach used and in the applicability of a copepod as a surrogate for all deep-sea species.

On a practical note, the considerations above coupled with the analysis in the preceding sections suggest that a towed pipe hydrate particle discharge scenario holds the most promise. Although a bottom manifold could in theory be configured to achieve a similar level of dilution, its major drawback is that it is fixed to one location with large up-front capital costs. Site selection would be critical and design alterations are difficult once constructed. In contrast, towed pipe scenarios would likely have lower up-front costs and are inherently more flexible due to their mobility, allowing the sequestration region to be shifted as necessary to minimize regional hotspots in background pCO_2. Although operating costs are expected to be higher [55] than a fixed pipe or platform release, the approach has not been ruled out due to economic infeasibility by past investigators.

The analysis of acute impacts could be strengthened by additional research from the biological community. Additional copepod toxicity data on short-term, high-pCO_2

and long-term, low-pCO_2 exposure would be helpful to constrain the isomortality function (although as noted in Section 3.3.2, the latter category may not be accessible through additional data collection). In addition, data on toxicity due to realistic time variable exposures would be useful in refining and/or confirming the applicability of the isomortality approach to simulate copepod mortality. Equally important would be the collection of toxicity data on a variety of other species in the target depths being considered. Pörtner et al. [100] suggests that the lack of accessibility of such organisms for in vivo laboratory analysis could perhaps be remedied by the use of an appropriate model organism such as benthic Antarctic eelpout (Pachycara brachycephalum). Such data would need to be reconciled with the data reviewed herein to delineate the applicability of an isomortality-type approach (since fish data do not seem to fit well into this model [111]). New functional models of acute harm could perhaps be developed, e.g., some combination of the isomortality approach and the activity model proposed by Chen et al. [21], or perhaps incorporating elements of ongoing work on modeling stress and recovery of fish in thermal plumes [11]. In addition to acute impacts, research to better understand chronic and ecosystem impact thresholds would be highly useful in this assessment, as discussed later in this section.

Beyond the biological data, additional research into the behavior of the proposed droplet and hydrate particle plumes would be useful to augment the analysis with a consideration of the dynamic mixing zone, both in terms of the resulting shape of the plumes as well as the distribution of excess DIC within the zone. This could partially be addressed by more resolved modeling of the mixing zone but would ultimately require field verification. Also, a thorough characterization of cost constraints to the design options would be necessary to arrive at economically viable discharge configurations.

Although the focus herein is on acute impacts, we recognize that chronic (sub-lethal) and ecosystem impacts are at least equally important for assessing the viability of ocean sequestration. Chronic impacts to individual organisms (e.g., reduced lifespan or reproduction rate) are important because they can result in intergenerational effects, i.e., population decline of a species over longer timescales. Reduced repro-

duction rate due to CO_2 exposure has been studied for a variety of species, and has been quantified by metrics such as reduced egg production rates, reduced hatching rates, and reduced survival of larvae/nauplii (e.g., [73, 74, 75]). Such data have not been incorporated directly into the analysis because they do not fit well into the iso-mortality approach used herein. On the one hand, they could be interpreted as acute mortality data in an effort to make the isomortality analysis reflect some intergenerational effects; this approach was taken in the original work by Auerbach [4, 5] where mortality data for adults was shifted in rough accordance with observed declines in reproduction. On the other hand, such a treatment is incomplete because it is not an accurate prediction of the expected population level over many generations, since the equilibrium population is dictated by the balance of many factors of which reproductive rate is only one. Although developmental fish data were used in a sensitivity analysis on the isomortality function for short, high-pCO_2 exposure, this treatment was motivated by data gaps in the copepod dataset and was not intended as a compensation for chronic or intergenerational effects. Given the complexity of predicting intergenerational dynamics, the LC_0 or LC_1 is sometimes adopted as a conservative threshold at which chronic impacts can be expected. The approach taken here has some similarity to this notion in that a $[\Delta pCO_2]_{min}$ for the isomortality analysis was set to a very low level (0.015 kPa, based on a ΔpH = -0.1, or the possibly "safe" threshold identified by [8] to avoid chronic effects). The fact that acute impacts are accrued well below the observed toxicity data and down to a supposed chronic impact threshold does not make the isomortality approach an adequate treatment of chronic impact. However, the fact that at least some of the discharge configurations resulted in impact levels below this threshold suggests that they could be expected to largely avoid chronic impacts to individual species.

Accurate estimation of ecosystem impacts is an even greater challenge. The acute and chronic impacts on population levels are species specific [100, 57], meaning that CO_2 injection could cause a shift in the ecological balance of the ocean. Such effects could perhaps be measured in mesocosm experiments, but few such investigations have been done to date and they are complicated by the huge range of species and

ecosystems that would need be considered for large scale deployment of direct injection. Long-term observations of population levels due to natural CO_2 perturbations could lend some information, but these would not be controlled experiments. Thus, in the absence of adequate data, the "safe" level of a 0.1 pH decrease previously discussed provides an attractive surrogate. Again, the fact that at least some of the discharge scenarios satisfy this constraint at the edge of the dynamic mixing zone suggests that ecosystem effects could be minimized by optimization of these methods.

Given the present state of knowledge, however, the conclusion that ocean discharges can be configured in a way that largely avoids acute and chronic impacts is controversial and subject to a number of substantial caveats. First, the present analysis does not resolve the dynamic mixing zone, where it is very likely that over small distances the 0.1 pH drop threshold would be violated for any practical discharge scenario. While previous studies (e.g., [23, 108]) have modeled the small-scale fluid mechanics near the injection point and found impact levels well above this low threshold, these did not consider the discharge methods proposed herein (descending hydrate particles or rising, non-interacting droplet plumes from a bottom manifold). It is therefore difficult to extrapolate their findings to the present case. While violations within the dynamic mixing zone are likely to occur, we note that the design flexibility offered by the towed pipe hydrate plume and the bottom manifold in particular suggest that such violations could be limited to small volumes over short durations for moderate loadings of 10-100 kg/s. As noted previously, future research aimed at bridging this gap in the present analysis would be helpful (fluid dynamics modeling, field verification, and design cost estimates).

Another major caveat is the notion that there exists a "safe" threshold at which no impact, be it acute, chronic, or ecosystem, could be expected. Pörtner et al. [100], after an extensive review and discussion of physiological effects across multiple tolerant and intolerant species, warns against this model on the basis that the responses vary dramatically across different types of organisms. While they suggest that the number of organisms likely to suffer from acute CO_2 toxicity is low, the long-term sub-lethal effects on deep-sea fauna may have a significant effect on population structure and

species distribution. In particular, the long-term response of calcifying organisms in the surface ocean to ΔpCO_2 of 200 μatm ($\approx$ 0.02 kPa) is provided as an example. It is beyond the scope of the present study to weigh these considerations with the notion that a "safe" threshold can be identified on the basis of natural pH variability, although the the latter argument is somewhat persuasive on the basis that the "business as usual" scenario of atmospheric emissions will cause a change of at least 0.1 pH units in the upper ocean within a century [55].

In light of the above considerations, the overall conclusion is restated in the following manner: *if* a "safe" threshold can be defined reasonably near the one considered herein, *then* the present study finds that discharge scenarios could likely be designed and sited to limit violation of the threshold to a small volume. Unfortunately, this leaves a large question unresolved.

If it is assumed that the threshold of a 0.1 decrease in pH (or one like it) can be confirmed, then two important conclusions would logically follow from the present analysis. First, present or near present (for hydrate formation) technology would allow ocean sequestration to meet a substantial part of the required emissions reductions in the short term. The analysis suggests that impacts near the injection points could be minimized by, for example, use of a towed pipe method with large hydrate diameters. If CO_2 can effectively be dispersed over large areas to mostly avoid adverse biological impacts, then the great capacity of the ocean to act as a sink for CO_2 can be exploited. For example, if the ocean is treated as well-mixed, it can be shown that the 175 GtC of required avoided emissions mentioned in Chapter 1 could in theory be stored in the ocean volume below 2,000 m without causing an average pH drop greater than 0.1, which is consistent with other similar calculations [55]. Second, ocean sequestration can only be regarded as a temporary solution to the carbon problem; for any reasonable threshold defined, the storage capacity of the ocean becomes finite if the threshold is to be respected. Ignoring any assimilative capacity on the part of marine organisms over multiple generations, the amount of dilution required of a particular discharge configuration to respect an absolute threshold increases as the background pCO_2 increases [61].

From a practical policy standpoint, it is noted that a safe threshold, if one exists, can likely not be confirmed *a priori*. Natural ecosystems are complex and difficult to model due to the interaction of many species of different trophic levels with each other and with their environment. Mild environmental perturbations affecting only a small fraction of species may alter the internal balance of the ecosystem in ways that are subtle and which take long periods of time to manifest themselves on a large scale. Given the escalating sense of urgency to curb atmospheric CO_2 emissions that pervades the scientific community, ocean sequestration schemes would have to be enacted on the basis of an incomplete understanding of the biological impacts.

The existence of some uncertainty prior to deployment does not, however, necessarily preclude the use of ocean sequestration as a mitigation strategy. Rather, it places constraints on the implementation of the technology. Widespread deployment would be infeasible until small-scale demonstration projects of substantial duration could be completed to establish the ability of a regional ecosystem to withstand the perturbation, at least on a macroscopic level. Such projects could be implemented with minimal long-term risk since the effectiveness of a dilution strategy is relatively easy to measure and could be determined quickly after discharge is initiated, thus allowing water quality standards based on present-day biological data to be met while the longer term response of the ecosystem is monitored. Maximum flexibility in modifying the discharge configuration and location to find a suitable combination would be important, which further underscores the advantages offered by the towed pipe scenario (even if a stationary hydrate plume were pursued, a ship at rest would be a desirable test apparatus because discharge location could be easily changed). Flexibility would have to be built into the permitting process as well to allow for tweaking of the discharge configuration along the way. Nonetheless, the time to permit a discharge could be lengthy, making the time to large scale deployment lengthy as well.

As a climate change mitigation strategy, ocean sequestration is not presently in favor. Experience has shown opposition to the idea both in the U.S. and in Europe, largely rooted in concern over perceived biological impacts. The effect is highly

pronounced in the US, where government funded research into ocean sequestration has dwindled; for example, the National Energy Technology Laboratory's Program on Carbon Sequestration is no longer actively investigating ocean sequestration [90, 91]. Rather, focus has shifted toward geologic sequestration. Perceived advantages of this storage medium include its lower potential for ecosystem disruption, potentially longer sequestration times, an existing infrastructure with proven economic viability (e.g., enhanced oil recovery projects), and potential for disposal on a regional scale instead of in a global commons (thus reducing the need for multilateral agreements).

Despite the numerous advantages which at present favor geologic sequestration, this strategy is not without problems. First, it is only possible in places with geologic formations favorable for CO_2 storage. As an example, a lack of suitable geology appears to be one contributing factor to Japan's continued research on ocean sequestration [118], as evidenced by the heavy representation of Japanese studies in the recent literature (see Chapter 2). Second, and perhaps most importantly, future leakage of stored CO_2 to potable aquifers, to the ocean (if stored beneath the ocean floor), or to the atmosphere is a major concern, meaning that geologic storage implies monitoring indefinitely. As such, the responsibility and risk of adverse impacts of sequestration sites is inherited by future generations. Indeed, in this regard geologic sequestration faces some of the same challenges as nuclear waste storage, albeit to a lesser degree since CO_2 is considerably more benign and may be contained by a variety of geochemical trapping mechanisms (see [55]). Unlike ocean sequestration, which can be stopped at any time if it proves undesirable, the consequences of a geologic sequestration can persist long after injection has ceased. Since we, as a society, presumably wish to avoid passing our problems to our descendants, it follows that geologic sequestration is appropriately regarded as a short-term solution to mitigating climate change, and not as a "blank check" to consume the remaining fossil fuel resources on the planet.

While the present study does not take a stand for or against ocean sequestration, it finds that ocean sequestration should not be dismissed on the basis of environmental impact alone and, in fact, it could be quite benign. No sequestration alternative

to "business as usual" is perfect, but they do offer a practical way to curb the buildup of atmospheric CO_2 in the short term while long-term, sustainable energy solutions are developed. Sequestration inherently involves an acceptance of increased risk associated with the storage (e.g., damage to a deep-ocean ecosystem or harm caused by leakage from a geologic formation) so that consequences that are deemed worse can be reduced (e.g., severe climate shifts and the acidification of the surface oceans). In the absence of more definitive evidence of irreparable impacts, no viable sequestration alternatives should be abandoned. As a society, we may need all the options we can muster.

Bibliography

[1] E.E. Adams and E.J. Wannamaker. Dilution strategies for direct ocean carbon sequestration. *Journal of Marine Environmental Engineering*, 8:95–109, 2005.

[2] G. Alendal and H. Drange. Two-phase, near-field modeling of purposefully released co_2 in the ocean. *Journal of Geophysical Research*, 106(C1):1085–1096, 2001.

[3] D.A. Auerbach, J. Caulfield, H. Herzog, and E.E. Adams. Environmental impacts of ocean disposal of CO_2. In *Ocean Storage of CO_2, Workshop 2, Environmental Impact*. IEA Greenhouse Gas R and D Programme, 1996.

[4] D.I. Auerbach. Climate change mitigation via ocean disposal of power-plant-generated CO_2: a comprehensive environmental and political analysis. Master's thesis, Massachusetts Institute of Technology, 1996.

[5] D.I Auerbach, J.A. Caulfiled, E. E. Adams, and H.J. Herzog. Impacts of ocean CO_2 disposal on marine life: I. a toxicological assessment integrating constant-concentration laboratory assay data with variable-concentration field exposure. *Environmental Modeling and Assessment*, 2:333–343, 1997.

[6] R.N. Bamber. The effects of acidic sea water on young carpet-shell clams *Venerupis decussata* (L.) (*Mollusca: Veneracea*). *Journal of Experimental Marine Biology and Ecology*, 108:241–260, 1987.

[7] R.N. Bamber. The effects of acidic seawater on three species of lamellibranch mollusc. *Journal of Experimental Marine Biology and Ecology*, 143:181–191, 1990.

[8] J. Barry, E. Adams, R. Bleck, K. Caldeira, K. Carman, D. Erickson, J. Kennett, C. McLain, J Sarmiento, and C. Tsouris. Ecosystem and societal consequences of ocean versus atmospheric carbon storage. In *Presentation to the American Physical Union*, San Francisco, CA, December 2005.

[9] James P. Barry, Kurt R. Buck, Chris F. Lovera, L. Kuhnz, P.J. Whaling, E.T. Peltzer, P. Walz, and P. Brewer. Effects of direct ocean CO_2 injection on deep-sea meiofauna. *Journal of Oceanography*, 60:759–766, 2004.

[10] N.J. Bernier and D.J. Randall. Carbon dioxide anaesthesia in rainbow trout: effects of hypercapnic level and stress on induction and recovery from anaesthetic treatment. *Journal of Fish Biology*, 52:621–637, 1998.

[11] M. Bevelhimer and A. Fortner. Stress and recovery in fish exposed intermittently to near-lethal temperatures: a model based on laboratory results. In *EPRI's Second Thermal Ecology and Regulation Workshop*. EPRI, 2007.

[12] C.L. Brownell. Water quality requirements for first-feeding in marine fish larvae. II. pH, oxygen, and carbon dioxide. *Journal of Experimental Marine Biology and Ecology*, 44:285–298, 1980.

[13] M.L. Burleson and N.J. Smatresk. Branchial chemoreceptors mediate ventilaroty responses to hypercapnic acidosis in channel catfish. *Comparative Biochemistry and Physiology*, 98A:403–414, 2000.

[14] A. Calabrese and H.C. Davis. The pH tolerance of embryos and larvae of *Mercenaria mercenaria* and *Crassostrea virginica*. *Biological Bulletin*, 131(3):427–436, 1966.

144

[15] K. Caldeira and M.E. Wickett. Ocean model predictions of chemistry changes from carbon dioxide emissions to the atmosphere and ocean. *Journal of Geophysical Research*, 110(C09S04), 2005.

[16] J.N. Cameron and D.J. Randall. The effect of increased ambient CO_2 on arterial CO_2 tension, CO_2 content and pH in rainbow trout. *Journal of Experimental Biology*, 57:673–680, 1972.

[17] K.B. Carman, D. Thistle, J.W. Fleeger, and J.P. Barry. Influence of introduced CO_2 on deep-sea metazoan meiofauna. *Journal of Oceanography*, 60:767–772, 2004.

[18] J.A. Caulfield. Environmental impacts of carbon dioxide ocean disposal: plume predictions and time dependent organism experience. Master's thesis, Massachusetts Institute of Technology, 1996.

[19] J.A. Caulfiled, E. E. Adams, D.I Auerbach, and H.J. Herzog. Impacts of ocean CO_2 disposal on marine life: II. probabilistic plume exposure model used with a time-varying dose-response model. *Environmental Modeling and Assessment*, 2:345–353, 1997.

[20] B. Chen, Y. Song, M. Nishio, and M. Akai. Large-eddy simulation of double-plume formation induced by CO_2 dissolution in the ocean. *Tellus*, 55B:723–730, 2003.

[21] B. Chen, Y. Song, M. Nishio, and M. Akai. A eulerian-eulerian physical-biological impact model of zooplankton injury due to CO_2 ocean sequestration. *Journal of Oceanography*, 60:797–806, 2004.

[22] B. Chen, Y. Song, M. Nishio, M. Akai, and T. Ohsumi. A hybrid numerical model of LCO_2 and CO_2 enriched seawater dynamics in the ocean induced by moving-ship releasing. In *Proceedings of the Sixth International Conference on Greenhouse Gas Control Technologies*, 2002.

145

[23] B. Chen, Y. Song, M. Nishio, S. Someya, and M. Akai. Modeling near-field dispersion from direct injection of carbon dioxide into the ocean. *Journal of Geophysical Research*, 110(C09S15):1–13, 2005.

[24] N. Chen, M. Nishio, A. Sohma, and M. Akai. On injection parameters in the view of near-field bio-impacts and long-term efficiencies of CO_2 ocean seques- tration. In *Proceedings of the Eighth International Conference on Greenhouse Gas Control Technologies*, 2006.

[25] J.B. Claiborne and D.H. Evans. Acid-base balance and ion tranfers in the spiny dogfish (*Squalus acanthias*) during hypercapnia: a role for ammonia excretion. *Journal of Experimental Zoology*, 107:9–20, 1983.

[26] J.B. Claiborne and N. Heisler. Acid-base regulation and ion transfers in the carp (*Cyprinus carpio*): pHcompensation during graded long- and short-term environmental hypercapnia, and the effect of bicarbonate infusion. *Journal of Experimental Biology*, 126:41–61, 1986.

[27] C.E. Crocker and J.J. Cech Jr. Effects of hypercapnia on blood-gas and acid- base status in the white sturgeon, *Acipenser transmontanus*. *Journal of Com- parative Physiology*, 168B:50–60, 1998.

[28] C.E. Crocker, A. Farrell, A.K. Gamperl, and J.J. Cech Jr. Cardiorespiratory responses of white sturgeon to environmental hypercapnia. *American Journal of Physiology: Regulatory, Integrative and Comparative Physiology*, 279:R617– R628, 2000.

[29] C.E. Cross, B.S. Packer, J.M. Linta, H.V. Murdaugh Jr, and E.D. Robin. H^+ buffering and excretion in response to acute hypercapnia in the dogfish (*Squalus acanthias*). *American Journal of Physiology*, 216:440–452, 1969.

[30] A.P. Cruz-Neto and J.F. Steffensen. The effects of acute hypoxia and hyper- capnia on oxygen consumption of the freshwater european eel. *Journal of Fish Biology*, 50:759–769, 1997.

[31] R. Dewey and G. Stegen. The dispersion of CO_2 in the ocean: consequences of basin-scale variations in turbulence levels. In *Proceedings of the Fourth International Conference on Greenhouse Gas Control Technologies*, 1998.

[32] R. Dewey, G. Stegen, and M. Ozaki. Ocean dispersion of CO_2 from a moving ship source. In *Proceedings of the Fifth International Conference on Greenhouse Gas Control Technologies*, 2000.

[33] R.K. Dewey, G.R. Stegen, and R. Bacastow. Far-field impacts associated with ocean disposal of co2. *Energy Convers. Mgmt.*, 38S:S349–S354, 1997.

[34] A.G. Dickson and C. Goyet. Handbook of methods for the analysis of the various parameters of the carbon dioxide system in sea water (version 2). Technical Report ORNL/CDIAC-74, U.S. Department of Energy, 1994.

[35] H. Drange, G. Alendal, and O.M. Johannessen. Ocean release of fossil fuel co2: a case study. *Geophysical Research Letters*, 28(13):2637–2640, 2001.

[36] I. Fer and P.M. Haugan. Dissolution from a liquid CO_2 lake disposed in the deep ocean. *Limnology and Oceanography*, 48(2):872–883, 2003.

[37] D.J. Finney. *Probit analysis*. Cambridge University Press, 1971.

[38] S. Fivelstad, H. Haavik, G. Lovik, and A.B. Olsen. Sublethal effects and safe levels of carbon dioxide in seawater for atlantic salmon postsmolts (*Salmo salar* L.) smolts: ion regulation and growth. *Aquaculture*, 160(3):305–316, 1998.

[39] S. Fivelstad, A.B. Olsen, H. Ski, and Stefansson S. Effects of carbon dioxide on atlantic salmon (*Salmo salar* L.) smolts at constant pH in bicarbonate rich freshwater. *Aquaculture*, 178(1):171–187, 1999.

[40] M.J. Follows, T. Ito, and S. Dutkiewicz. On the solution of the carbonate chemistry system in ocean biogeochemistry models. *Ocean Modelling*, 12:290–301, 2006.

[41] A. Foss, B.A. Rosnes, and V. Oiestad. Graded environmental hypercapnia in juvenile spotted wolffish (*Anarhichas minor* olafsen): effects on growth, food conversion efficiency and nephrocalcinosis. *Aquaculture*, 220(1):607–617, 2003.

[42] C.W. Gardiner. *Handbook of Stochastic Methods for Physics, Chemistry and the Natural Sciences*. Springer-Verlag, 1985.

[43] D.S. Golomb, S.G. Zemba, J.W.H. Dacey, and A.F. Michaels. The date of CO_2 sequestered in the deep ocean. *Energy Convers. Mgmt.*, 33(5-8):675–683, 1992.

[44] GG. Goss, G.P. Laurent, and S.F. Perry. Evidence for a morphological component in acid-base regulation during environmental hypercapnia in the brown bullhead (*Ictalurus nebulosus*). *Cell and Tissue Research*, 268:539–552, 1992.

[45] M.S. Graham, Turner J.D., and C.M. Wood. Control of ventilation in the hypercapnic skate *Raja ocellata*: I. blood and extradural fluid. *Respiration Physiology*, 80:259–277, 1990.

[46] G.D. Grice, P.H. Wiebe, and E. Hoagland. Acid-iron waste as a factor affecting the distribution and abundance of zooplankton in the New York Bight. I. laboratory studies on the effects of acid waste on copepods. *Estuarine and coastal marine sciences*, 1:45–50, 1973.

[47] J.A. Grø ttum and T. Sigholt. Acute toxicity of carbon dioxide on european seabass (*Dicentrarchus labrax*): mortality and effect on plasma ions. *Comparative Biochemistry and Physiology*, 4:323–327, 1996.

[48] P.M. Haugan and G. Alendal. Turbulent diffusion and transport from a CO_2 lake in the deep ocean. *Journal of Geophysical Research*, 110(C09S14), 2005.

[49] P.M. Haugan, F. Thorkildsen, and G. Alendal. Dissolution of CO_2 in the ocean. *Energy Convers. Mgmt.*, 36(9):461–466, 1995.

[50] M. Hayashi, J. Kita, and A. Ishimatsu. Acid-base responses to lethal aquatic hypercapnia in three marine fishes. *Marine Biology*, 144:153–160, 2004.

[51] M. Hayashi, J. Kita, and A. Ishimatsu. Comparison of the acid-base responses to CO_2 and acidification in japanese flounder (*Paralichthys olivaceus*). *Marine Pollution Bulletin*, 49:1062–1065, 2004.

[52] N. Heisler. Acid-base regulation in fishes. In N. Heisler, editor, *Acid-base regulation in animals*, pages 309–356. Elsevier Science Publishers, Amsterdam, 1986.

[53] H. Herzog and D. Golomb. Carbon and storage from fossil fuel use. *Encyclopedia of Energy*, 1:277–287, 2004.

[54] S. Hirai, S. Tsushuma, R. Muraoka, H. Sanda, and M. Ozaki. Evaluation of advanced CO_2 dilution technology in ocean sequestration. In *Proceedings of the Seventh International Conference on Greenhouse Gas Control Technologies*, 2004.

[55] Intergovernmental Panel on Climate Change (IPCC). *Special report on Carbon Dioxide Capture and Storage*. Cambridge University Press, 2005.

[56] H. Ishida, T. Fukuhara, Y. Watanabe, Y. Shirayama, L. Golmen, J. Kita, M. Magi, and T. Ohsumi. Assessing the effect of high concentration of CO_2 on deep-sea benthic microorganisms using a benthic chamber system. In *Proceedings of the Eighth International Conference on Greenhouse Gas Control Technologies*, 2006.

[57] H. Ishida, Y. Watanabe, T. Fukuhara, S. Kaneko, K. Furusawa, and Y. Shirayama. In situ enclosure experiment using a benthic chamber system to assess the effect of high concentration of CO_2 on deep-sea benthic communities. *Journal of Oceanography*, 61:835–843, 2005.

[58] A. Ishimatsu, M. Hayashi, K.S. Lee, T. Kikkawa, and J. Kita. Physiological effects of fishes in a high-CO_2 world. *Journal of Geophysical Research*, 110(C09S09), 2005.

[59] A. Ishimatsu, T. Kikkawa, M. Hayashi, K.S. Lee, K. Murata, E. Kumagai, and J. Kita. Acute physiological impacts of CO_2 ocean sequestration on marine animals. In *Proceedings of the Seventh International Conference on Greenhouse Gas Control Technologies*, 2004.

[60] A. Ishimatsu, Kikkawa T., M. Hayashi, and K.S. Lee. Effects of CO_2 on marine fish: larvae and adults. *Journal of Oceanography*, 60:731–741, 2004.

[61] P.H. Israelsson, A.C. Chow, and E.E. Adams. Near and far field considerations regarding the viability of ocean carbon sequestration. In *Presentation to the Fifth Annual Conference on Carbon Capture and Sequestration*, Alexandria, VA, May 2006.

[62] P.H. Israelsson, Y.D. Kim, and E.E. Adams. A comparison of three Lagrangian approaches for extending near field mixing calculations. *Environmental Modelling and Software*, 21:1631–1649, 2006.

[63] G.K. Iwama and N. Heisler. Effect of environmental water salinity on acid-base regulation during environmental hypercapnia in the rainbow trout (*Oncorhynchus mykiss*). *Journal of Experimental Biology*, 158:1–18, 1991.

[64] R.G. Janssen and D.J. Randall. The effects of changes in pCO_2 in blood and water on breathing in rainbow trout *Salmo gairdneri*. *Respiration Physiology*, 25:235–245, 1975.

[65] F.B. Jensen and R.E. Weber. Kinetics of the acclimational responses of tench to combined hypoxia and hypercapnia. I and II. *Journal of Comparative Physiology*, 156B:197–211, 1985.

[66] S.M. Jeong, T. Sato, and B. Chen. Numerical study of co2 ocean sequestration in middle scale ocean by using moving/nesting grid methods. In *Proceedings of the Eighth International Conference on Greenhouse Gas Control Technologies*, 2006.

[67] T. Kikkawa, K. Hasegawa, Y. Minowa, T. Setoguma, and J. Kita. CO_2 tolerance of tomato clownfish (*Amphiprion frenatus*). In *Report to the Marine Ecology Research Institute (No. 9)*, pages 47–54. Marine Ecology Research Institute, 2006.

[68] T. Kikkawa, A. Ishimatsu, and J. Kita. Acute CO_2 tolerance during the early developmental stages of four marine teleosts. *Environmental Toxicology*, 18(6):375–382, 2003.

[69] T. Kikkawa, A. Ishimatsu, and J. Kita. Comparison of the lethal effect of CO_2 and acidification on red sea bream (*Pagrus major*) during the early developmental stages. *Marine Pollution Bulletin*, 48:108–110, 2004.

[70] T. Kikkawa, T. Sato, J. Kita, and A. Ishimatsu. Acute toxicity of temporally varying seawater CO_2 conditions on juveniles of japanese sillago (*Sillago japonica*). *Marine Pollution Bulletin*, 52:621–625, 2006.

[71] J. Kita and T. Ohsumi. Perspectives on biological research for CO_2 sequestration. *Journal of Oceanography*, 60:695–703, 2004.

[72] J. Kita and Y. Watanabe. Impact assessment of high-CO_2 environment on marine organisms. In *Proceedings of the Eighth International Conference on Greenhouse Gas Control Technologies*, 2006.

[73] H. Kurihara, S. Shimode, and Y. Shirayama. Effects of raised CO_2 concentration on the egg production rate and early development of two marine copepods (*Acartia steueri* and *Acartia erythraea*). *Marine Pollution Bulletin*, 49:721–727, 2004.

[74] H. Kurihara, S. Shimode, and Y. Shirayama. Sub-lethal effects of elevated concentrations of CO_2 on planktonic copepods and sea urchins. *Journal of Oceanography*, 60:743–750, 2004.

[75] H. Kurihara and Y. Shirayama. Effects of increased atmospheric CO_2 on sea urchin early development. *Marine Ecology Progress Series*, 274:161–169, 2004.

[76] M. Langenbuch and H.O. Portner. High sensitivity to chronically elevated CO_2 levels in a eurybathic marine sipunculid. *Aquatic Toxicology*, 70:55–61, 2004.

[77] B.K. Larsen, H.O. Portner, and F.B. Jensen. Extra- and intracellular acid-base balance and ionic regulation in cod (*Gadus morhua*) during combined and isolated exposures to hypercapnia and copper. *Marine Biology*, 128:337–346, 1997.

[78] K.S. Lee, J. Kita, and A. Ishimatsu. Effects of lethal levels of environmental hypercapnia on cardiovascular and blood-gas status in yellowtail, *Seriola quinqueradiata*. *Zoological Science*, 20:417–422, 2003.

[79] E. Lewis and D. W. R. Wallace. *Program Developed for CO_2 System Calculations, ORNL/CDIAC-105*. USDOE.

[80] C. Liro, E. Adams, and H. Herzog. Modelling the releases of CO_2 in the deep ocean. *Energy Convers. Mgmt.*, 33(5-8):667–674, 1992.

[81] Murai S. Sorai M. Magi, M. and T. Oshumi. A study of effectiveness of co2 ocean sequestration for mitigation of the ocean acidification. In *Proceedings of the Eighth International Conference on Greenhouse Gas Control Technologies*, 2006.

[82] Y. Masuda, Y. Yamanaka, Y. Sasai, M. Magi, and T. Ohsumi. A numerical study with an eddy-resolving model to evaluate chronic impacts in CO_2 ocean sequestration. In *Proceedings of the Eighth International Conference on Greenhouse Gas Control Technologies*, 2006.

[83] J.E. McKendry, W.K. Milsom, and S.F. Perry. Branchial CO_2 receptors and cardiorespiratory adjustments during hypercarbia in pacific spiny dogfish (*Squalus acanthias*). *Journal of Experimental Biology*, 204:1519–1527, 2001.

[84] D.J. McKenzie, E.W. Taylor, A.Z. Dalla Valle, and Steffenson J.F. Tolerance of acute hypercapnic acidosis by the european eel (*Anguilla anguilla*). *Journal of Comparative Physiology*, 172B:339–346, 2002.

[85] B. Michaelidis, C. Ouzounis, A. Paleras, and H.O. Portner. Effects of long-term moderate hypercapnia on acid-base balance and growth rate in marine mussels (*Mytulis galloprovincialis*). *Marine Ecology Progress Series*, 293:109–118, 2005.

[86] J. Minamiura, H. Suzuki, B. Chen, M. Nishio, and M. Ozaki. CO_2 release in deep ocean by moving ship. In *Proceedings of the Seventh International Conference on Greenhouse Gas Control Technologies*, 2004.

[87] F.M.M. Morel and J. Hering. *Principles and applications of aquatic chemistry*. John Wiley and Sons, Inc., 1993.

[88] N. Nakashiki and T. Ohsumi. Dispersion of CO_2 injected into the ocean at the intermediate depth. *Energy Convers. Mgmt.*, 38S:S355–S360, 1997.

[89] G.C. Nihous, L. Tang, and S.M. Masutani. A sinking plume model for deep CO_2 discharge. In *Proceedings of the Sixth International Conference on Greenhouse Gas Control Technologies*, 2002.

[90] U.S. Department of Energy: National Energy Technology Laboratory. Carbon sequestration program environmental reference document, August 2007.

[91] U.S. Department of Energy: National Energy Technology Laboratory. Carbon sequestration technology roadmap and program plan, August 2007.

[92] A. Okubo. Oceanic diffusion diagrams. *Deep-Sea Research*, 18:789–802, 1971.

[93] J.C. Orr. Modelling of ocean storage of CO_2 - the GOSAC study (report ph4/37). Technical report, International Energy Agency, Greenhouse Gas R&D Programme, 2004.

[94] M. Ozaki, T. Ohsumi, and S. Masuda. Dilution of released CO_2 in mid-ocean depth by moving ship. In *Proceedings of the Fourth International Conference on Greenhouse Gas Control Technologies*, 1998.

[95] S. Pacala and R. Socolow. Stabilization wedges: solving the climate problem for the next 50 years with current technologies. *Science*, 305:968–972, 2004.

[96] S.F. Perry. The regulation of hypercapnic acidosis in two salmonids, the freshwater trout (*Salmo gairdneri*) and the seawater salmon (*Onchorynchus kisutch*). *Marine Behavior and Physiology*, 9:73–79, 1987.

[97] S.F. Perry, R. Fritsche, T.M. Hoagland, D.W. Duff, and K.R. Olson. The control of blood pressure during external hypercapnia in the rainbow trout (*Oncorhynchus mykiss*). *Journal of Experimental Biology*, 202:2177–2190, 1999.

[98] S.F. Perry, S. Malone, and D. Ewing. Hypercapnic acidosis in rainbow trout (*Salmo gairdneri*). I. branchial ionic fluxes and blood acid-base status. *Canadian Journal of Zoology*, 65:888–895, 1987.

[99] J.E. Portmann. Results of acute toxicity tests with marine organisms, using a standard method. *Marine biology*, pages 212–217, 1970.

[100] H.O. Pörtner, M. Langenbuch, and B. Michaelidis. Synergistic effects of temperature extremes, hypoxia, and increases in CO_2 on marine animals: From earth history to global change. *Journal of Geophysical Research*, 62(C09S10), 2005.

[101] H.O. Pörtner, M. Langenbuch, and A. Reipschläger. Biological impact of elevated ocean CO_2 concentrations: Lessons from animal physiology and earth history. *Journal of Oceanography*, 60(4):705–718, 2004.

[102] D.J. Randall, N. Heisler, and F. Drees. Ventilatory responses to hypercapnia in the larger spotted dogfish *Scyliorhinus stellaris*. *American Journal of Physiology*, 230:590–594, 1976.

[103] L.F. Richardson. Atmospheric diffusion shown on a distance-neighbor graph. *Royal Soc. of London Proc., Ser. A*, 110:709–737, 1926.

[104] D.E. Riestenberg, C. Tsouris, P.G. Brewer, E.T. Peltzer, P. Walz, A.C. Chow, and E.E. Adams. Field studies on the formation of sinking CO_2 particles for ocean carbon sequestration: Effects of injector geometry on particle density

and dissolution rate and model simulation of plume behavior. *Environmental Science and Technology*, 39(18):7287 – 7293, 2005.

[105] C.D. Rose, W.G. Williams, T.A. Hollister, and P.R. Parrish. Method for determining acute toxicity of an acid waste and limiting permissible concentration boundaries of an oceanic mixing zone. *Environmental Science and Technology*, 11(4):367–371, 1977.

[106] E. Sandblom, A.P. Farrell, J. Altimiras, M. Axelsson, and G. Claireaux. Cardiac preload and venous return in swimming sea bass (*Dicentrarchus labrax* L.). *Journal of Experimental Biology*, 208:1927–1935, 2005.

[107] T. Sato. Modelling of biological impact in direct injection of carbon dioxide in the ocean. In *Proceedings of the Sixth International Conference on Greenhouse Gas Control Technologies*, 2002.

[108] T. Sato. Numerical simulation of biological impact caused by direct injection of carbon dioxide in the ocean. *Journal of Oceanography*, 60:807–816, 2004.

[109] T. Sato and T. Hama. Numerical simulation of dilution process in CO_2 ocean sequestration. In *Proceedings of the Fifth International Conference on Greenhouse Gas Control Technologies*, 2000.

[110] T. Sato and K. Sato. Numerical prediction of the dilution process and its biological impacts in CO_2 ocean sequestration. *Journal of Marine Science and Technology*, 6:169–180, 2002.

[111] T. Sato, Y. Watanabe, K. Toyota, and J. Ishizaka. Extended probit mortality model for zooplankton against transient change of pCO_2. *Marine Pollution Bulletin*, 50:975–979, 2005.

[112] Y. Shirayama and H. Thornton. Impacts of increased atmospheric CO_2 on shallow water marine benthos. *Journal of Geophysical Research*, 110(C09S08):1–7, 2005.

[113] B.A. Siebel and P.J. Walsh. Potential impacts of CO_2 injections on deep-sea biota. *Science*, 294, 2001.

[114] G.R. Smart, D. Knox, J.G. Harrison, J.A. Ralph, R.H. Richard, and C.B. Cowey. Nephrocalcinosis in rainbow trout *Salmo gairdneri* richardson; the effect of exposure to elevated CO_2. *Journal of Fish Diseases*, 2:279–289, 1979.

[115] S. A. Socolofsky and E. E Adams. Multi-phase plumes in uniform and stratified crossflow. *Journal of Hydraulic Research*, 40(6):661–672, 2002.

[116] G. Stegen, K. Cole, and R. Bacastow. Biogeochemical impacts of co2 storage in the ocean. *Energy Convers. Mgmt.*, 36(6-9):497–500, 1995.

[117] C.E. Stephan. Method for calculating an LC_{50}. In *Aquatic Toxicology and Hazard Evaluation: Proceedings of the First Annual Symposium on Aquatic Toxicology*. American Society for Testing and Materials, 1977.

[118] J.C. Stephens. Growing interest in carbon capture and storage (ccs) for climate change mitigation. *Sustainability: Science, Practice and Policy*, 2(2):4–13, 2006.

[119] M. Sugimori, K. Takeuchi, S. Furukawa, H. Ishida, and Y. Shirayama. Effects of CO_2 on deep-sea floor microbial communities. In *Proceedings of the Seventh International Conference on Greenhouse Gas Control Technologies*, 2004.

[120] M. Sugimori, K. Takeuchi, M. Ozaki, Y. Fujioka, and J. Ishizaka. Responses of marine biological communities to different concentrations of CO_2 in a mesocosm experiment. In *Proceedings of the Fifth International Conference on Greenhouse Gas Control Technologies*, 2000.

[121] A. Sundfjord, G. Alendal, P.M. Haugan, and L. Golmen. Oceanographic criteria for selecting future sites for CO_2 sequestration. In *Proceedings of the Fifth International Conference on Greenhouse Gas Control Technologies*, 2000.

[122] T. Takeda. Regulation of blood oxygenation during short-term hypercapnia in the carp, *Cyprinus carpio. Comparative Biology and Physiology*, 98A:517–521, 1997.

[123] T. Takeda and Y. Itazawa. Possibility of applying anesthesia by carbon dioxide in the transportation of live fish. *Nippon Suisan Gakkaishi*, 49:725–731, 1983.

[124] K. Takeuchi, Y. Fujioka, Y. Kawasahi, and Y. Shirayama. Impacts of high concentration of CO_2 on marine organisms; a modification of CO_2 sequestration. *Energy Conversion and Management*, 38 Suppl.:S337–S341, 1997.

[125] K. Takeuchi, M. Sugimori, S. Furukawa, and J. Ishizaka. Impacts of CO_2 on microbial communities in a mesocosm experiment. In *Proceedings of the Sixth International Conference on Greenhouse Gas Control Technologies*, 2002.

[126] M.N. Tamburri, E.T. Peltzer, G.E. Friederich, I. Aya, K. Yamane, and P. Brewer. A field study of the effects of CO_2 ocean disposal on mobile deep-sea animals. *Marine Chemistry*, 72:95–101, 2000.

[127] D. Thistle, K.R. Carman, L. Sedlacek, P.G. Brewer, J.W. Fleeger, and J.P. Barry. Deep-ocean, sediment-dwelling animals are sensitive to sequestered carbon dioxide. *Marine Ecology Progress Series*, 289:1–4, 2005.

[128] A.F.B. Thompson and L.W. Gelhar. Numerical simulations of solute transport in three-dimensional randomly heterogeneous porous media. *Water Resources Research*, 26:2541–2562, 1990.

[129] F. Thorkildsen and G. Alendal. Les study of flow around a CO_2-droplet plume in the ocean. *Energy Convers. Mgmt.*, 38S:S361–S366, 1997.

[130] D.P. Toews, G.F. Holeton, and N. Heisler. Regulation of the acid-base status during environmental hypercapnia in the marine teleost fish *Conger conger*. *Journal of Experimental Biology*, 107:9–20, 1983.

[131] C. Tsouris, P.G. Brewer, E. Peltzer, P. Walz, D. Riestenberg, L. Liang, and O.R. West. Hydrate composite particles for ocean carbon sequestration: field verification. *Environmental Science and Technology*, 38(8):2470–2475, 2004.

[132] C. Tsouris, P. Szymcek, P. Taboada-Serrano, S. D. McCallum, P. Brewer, E. Peltzer, P. Walz, E. Adams, A. Chow, W. K. Johnson, and J. Summers. Scaled-up ocean injection of CO_2-hydrate composite particles,. *Energy and Fuels*, 2007 (Accepted).

[133] S. Tsushima, S. Hirai, and M. Ozaki. Evaluation of advanced CO_2 dilution technology in ocean sequestration. In *Proceedings of the Eighth International Conference on Greenhouse Gas Control Technologies*, 2006.

[134] E.W. Vetter and C.R. Smith. Insights into the ecological effects of deep ocean CO_2 enrichment: the impacts of natural CO_2 venting at loihi seamount on deep sea scavengers. *Journal of Geophysical Research*, 110(C09S13), 2005.

[135] T. Volk and M.I. Hoffert. Ocean carbon pumps: analysis of relative strengths and efficiencies in ocean-driven atmospheric CO_2 changes. In E.T. Sundquist and W.S. Broecker, editors, *Geophysical Monograph 32, The Carbon Cycle and Atmospheric CO_2: Natural Variations Archean to Present*, pages 99–110. American Geophysical Union, Washington, D.C., 1985.

[136] E.J. Wannamaker. Modeling carbon dioxide hydrate particle releases in the deep ocean. Master's thesis, Massachusetts Institute of Technology, 2002.

[137] E.J. Wannamaker and E.E. Adams. Modeling descending carbon dioxide injection in the ocean. *Journal of Hydraulic Research*, 44(3):324–337, 2006.

[138] Y. Watanabe. Annual technical report Kansai Environmental Engineering Center Co. Ltd. Japan. (in Japanese). Technical report, 2001.

[139] Y. Watanabe, A. Yamaguchi, H. Ishida, T. Harimoto, S. Suzuki, Y. Sekido, T. Ikeda, Y. Shirayama, Ohsumi T. Takahashi, M.M., and J. Ishizaka. Lethality of increasing CO_2 levels on deep-sea copepods in the western north pacific. *Journal of Oceanography*, 62:185–196, 2006.

[140] R.F. Weiss. Carbon dioxide in water and seawater: the solubility of a non-ideal gas. *Marine Chemistry*, 2:203–215, 1974.

[141] O. R. West, C. Tsouris, L. Liang, S. Y Lee, and S. D McCallum. Negatively buoyant CO_2-hydrate composite for ocean carbon sequestration. *AIChE Journal*, 49:283–285, 2003.

[142] M.E. Wickett, K. Caldeira, and P.B. Duffy. Effect of horizontal grid resolution on simulations of oceanic cfc-11 uptake and direct injection of anthropogenic CO_2. *Journal of Geophysical Research*, 108(C6):3189, 2003.

[143] Y. Xu, J. Ishizaka, and S. Aoki. The behavior of sequestered CO_2 in a model of the north pacific. In *Proceedings of the Fourth International Conference on Greenhouse Gas Control Technologies*, 1998.

[144] Y. Yamada and T. Ikeda. Acute toxicity of lowered pH to some oceanic zooplankton. *Plankton Biology & Ecology*, 46(1):62–67, 1999.

[145] H. Yoshikawa, F. Kawai, and M. Kanamori. The relationship between the eeg and brain pH in carp, *Cyprinus carpio*, subjected to environmental hypercapnia at an anesthetic level. *Comparative Biochemistry and Physiology*, 107A(2):307–312, 1994.

[146] H. Yoshikawa, Y. Yokoyama, S. Ueno, and H. Mitsuda. Changes of blood gas in carp, *Cyprinus carpio*, anesthetized with carbon dioxide. *Comparative Biochemistry and Physiology*, 98A(4):431–436, 1991.

[147] R.E. Zeebe, D.A. Wolf-Gladrow, and H. Jansen. On the time fo establish chemical and isotropic equilibrium in the carbon dioxide system. *Marine Chemistry*, 65:135–153, 1999.